DEVELOPMENT AND EVALUATION OF NEW STRATEGIES FOR RETINAL GENE THERAPY USING CRISPR-MEDIATED TRANSCRIPTIONAL ACTIVATION

Klara Sonnie Hinrichsmeyer

Dissertation der Fakultät für Biologie
der Ludwig-Maximilians-Universität München

09 June 2022

Erster Gutachter:	Prof. Dr. Martin Biel
Zweiter Gutachter:	Prof. Dr. Christof Osman

Tag der Abgabe:	09.06.2022
Tag der mündlichen Prüfung:	27.10.2022

Eidesstattliche Erklärung

Ich versichere hiermit an Eides statt, dass die vorgelegte Dissertation von mir selbständig und ohne unerlaubte Hilfsmittel angefertigt ist. Hiermit erkläre ich, dass die vorgelegte Dissertation nicht ganz oder in wesentlichen Teilen einer anderen Prüfungskommission vorgelegt worden ist. Ich habe nicht anderweitig versucht eine Dissertation einzureichen oder mich der Doktorprüfung zu unterziehen.

München, den 02.06.2022 Klara Sonnie Hinrichsmeyer

Contents

List of Abbreviations

AAV	adeno-associated virus
AON	antisense oligonucleotide
APP	amyloid precursor protein
Cap	open reading frame encoding for AAV capsid proteins
Cas	CRISPR-associated
Cas9	CRISPR-associated protein 9
cDNA	complementary DNA
cGMP	cyclic guanosine monophosphate
CMV	cytomegalovirus
CNG	cyclic nucleotide-gated
COL1A1	collagen α1(I) chain
CRISPR	clustered regularly interspaced short palindromic repeats
CRISPRa	CRISPR-Cas mediated transactivation
DD	differentiation day
DNA	deoxyribonucleic acid
DSB	DNA double-strand break
dCas9	nuclease deficient Cas9
ERG	electroretinogram
FITC	fluorescein isothiocyanate
g	standard gravity (9.80665 m/s^2)
GC	guanylate-cyclase
GCN4	epitope of yeast general control nonderepressible 4 protein
GRK	G protein-coupled receptor kinase 1

G_T	transducin
GTP	guanosine triphosphate
h	hours
HEK293	human embryonic kidney 293
HEK293T	HEK293 expressing the simian virus 40 large T antigen
HSF1	activation domain from human heat-shock factor 1
HRP	horse radish peroxidase
indel	insertions or deletions
IRD	inherited retinal dystrophies
ITR	inverted terminal repeat
LB	lysogeny broth
L-cones	long wavelength (red) sensitive cones
m	minutes
M-cones	medium-long wavelength (green) sensitive cones
MS2	MS2 bacteriophage coat protein
MYO7A	myosin VIIA
MYO7A	human myosin VIIA gene
Myo7a	mouse myosin VIIA gene
MYO7B	myosin VIIB
MYO7B	human myosin VIIB gene
Myo7b	mouse myosin VIIB gene
n	sample size
NHEJ	non-homologous end joining
NRL	neural retina-specific leucine zipper
Nrl	murine neural retina-specific leucine zipper gene

Nxnl1	murine nucleoredoxin like 1 gene
NXNL1	human nucleoredoxin like 1 gene
Nxnl2	murine nucleoredoxin like 2 gene
NXNL2	human nucleoredoxin like 2 gene
OCT	optical coherence tomography
OD	*Oculus dexter* (right eye)
OS	*Oculus sinister* (left eye)
Otx2	mouse orthodenticle homeobox 2 gene
ONL	outer nuclear layer
Opn1mw	mouse M-opsin gene
p65	subunit of the human nuclear factor-κB transcription factor
pAdhelper	adenovirus helper plasmid
PAM	protospacer adjacent motif
PB	phosphate buffer
PBS	phosphate-buffered saline
PDE6	phosphodiesterase 6
Pde6b	murine phosphodiesterase 6 b gene
PEG	polyethylene glycol
PEI	polyethyleneimine
PES	polyethersulfone
PFA	paraformaldehyde
PCR	polymerase chain reaction
qPCR	quantitative real-time PCR
qRT-PCR	quantitative reverse transcription PCR
rAAV	recombinant adeno-associated virus

RdCVF	rod-derived cone viability factor
RdCVFL	long isoform of RdCVF
Rep	open reading frame encoding proteins for AAV replication
RHO	short rhodopsin promoter
Rho	mouse rhodopsin gene
RIPA	radio-immunoprecipitation assay
RNA	ribonucleic acid
RNA-seq	RNA sequencing
RP	retinitis pigmentosa
RPE	retinal pigment epithelium
Rta	replication and transcription activator of Epstein-Barr virus
RyR2	ryanodine receptor type 2
SAM	synergistic activation mediator
S-cones	short wavelength (blue) sensitive cones
scFv	single chain variable fragment antibodies
SDS	sodium lauryl sulfate
sgRNA	single guide RNA
shRNA	short hairpin RNA
*Sp*Cas9	*Streptococcus pyogenes* Cas9
SV40	simian virus 40
SV40polyA	SV40 polyadenylation signal
synpA	synthetic polyadenylation signal
TAL	transcription activator-like
TALEN	TAL effector nuclease
TBST	Tris-buffered saline with Tween 20

transactivation	transcriptional activation
Trβ2	mouse thyroid hormone receptor beta 2 gene
Tris	tris(hydroxymethyl)aminomethane
TSS	transcriptional start site
USH2A	Usher syndrome type 2A gene
UV	ultraviolet
vg	vector genomes
VP64	tetramer of the Herpes simplex virus transcription activator viral protein 16
VPR	VP64-p65-Rta
WT	wild-type
ZFN	zinc finger nuclease

Abstract

Inherited retinal dystrophies (IRDs) comprise a large and heterogeneous group of inherited blinding disorders characterised by loss of retinal structure and function. For the vast majority of these disorders including those caused by mutations in large genes or by gain-of-function mutations, no therapy exists. The gene replacement approach with recombinant adeno-associated viral (rAAV) vectors is currently the gold standard for (retinal) gene therapy. However, the rAAV genome packaging capacity (4.7 kb) impedes the delivery of large genes. Moreover, the gene replacement strategy is insufficient for the treatment of gain-of-function mutations which require simultaneous repression of the diseased allele. There is thus a high unmet medical need for the development of new strategies which are suited to overcome the limitations of current gene replacement approaches designed to treat IRDs.

Clustered regularly interspaced short palindromic repeats (CRISPR)-mediated transcriptional activation (CRISPRa) is independent of the target gene size and can also be modified to allow for treatment of more complex diseases or even to develop gene-independent gene therapy approaches. Nevertheless, CRISPRa modules exceed the genome packaging capacity of rAAVs and require dual rAAV vectors for *in vivo* expression.

In this study, I developed innovative CRISPRa-based gene therapy strategies in combination with dual AAV vectors designed to reconstitute split genes at the transcript level. This dual AAV vector strategy termed REVeRT (reconstitution via mRNA trans-splicing) was used to activate the MYO7B gene *in vivo*. MYO7B is a functional equivalent of MYO7A whose defects are associated with the Usher syndrome, the most frequent type of inherited deafblindness. The MYO7B gene could be efficiently activated in the murine retina and various other organs upon different routes of administration.

Furthermore, using a modified multiplexed CRISPRa system that allows concurrent gene activation and knockdown I tested a new approach for the treatment of gain-of-function mutations in the most common mouse model for autosomal dominant retinitis pigmentosa caused by the Pro23His mutation in the rod photoreceptor-specific rhodopsin gene (*Rho*) ($Rho^{P23H+/-}$). Although a proof-of-principle for simultaneous activation of the M-Opsin gene (*Opn1mw*), a cone-specific photopigment that can functionally compensate for the missing rhodopsin function, and repression of *Rho* were successful in the $Rho^{P23H+/-}$ retina, the retinal phenotype could not be improved in this mouse model.

Finally, the strategy of concurrent gene activation and knockdown was also evaluated to develop a new gene-independent gene therapy strategy in the $Rho^{P23H/+}$ mouse model. For this purpose, the *Nrl* gene was repressed to reprogramme diseased rod photoreceptors into less degeneration prone cone-like cells combined with transcriptional activation of the neuroprotective *Nxnl1* gene. This approach could ameliorate retinal degeneration four weeks after treatment.

In conclusion, the new strategies and techniques developed in this study show great potential for the treatment of IRDs and can be modified to treat a variety of other inherited and acquired diseases in different tissues and organs.

1. Introduction

1.1 CRISPR-Cas – Simplifying Genome Editing

1.1.1 Brief History of Genome Editing

Performing precise changes in the genome quickly became a desired goal after the discovery of deoxyribonucleic acid (DNA) as the genetic code. First edits of mammalian genomes were facilitated by homologous recombination in the 1980s. Here, DNA fragments containing the desired insert flanked by sequences complementary to the mammalian DNA were introduced into mammalian cells to enable specific insertions in the mammalian genome (Smithies et al., 1985; Thomas et al., 1986). While these were remarkable results opening the field of genome editing, low editing efficiency and incorporation outside of the target region were emerging as the major drawbacks of this technique. A breakthrough was the discovery of targeted DNA double-strand breaks (DSBs) as a necessity for an increased editing outcome (Rouet et al., 1994). DSBs are caused by different natural processes and, if not repaired, are lethal to mammalian cells. To repair these breaks, mammalian cells use mostly two different techniques. The predominant pathway is non-homologous end joining (NHEJ) which leads to a re-joining of the broken DNA ends. This process is error-prone and can lead to small insertions or deletions (indels) at the repair site (Chang et al., 2017). DNA repair can also occur based on a homologous DNA template, in most cases the sister chromatid. The homology-directed repair pathway possesses a higher fidelity and allows insertion of a synthetic repair template (Wright et al., 2018). In summary, DSBs in the context of genome editing are tolerated by mammalian cells, increase the editing efficiency of homologous recombination, and harbour the potential for gene knockout by insertion of indels in the coding sequence (Rouet et al., 1994; Urnov, 2018).

While the introduction of DSBs is a key component of an efficient genome editing tool, performing site-specific edits can only be achieved by a nuclease system that allows the recognition of a specific DNA locus. The first engineered system widely used for genome editing was based on the fusion of zinc finger DNA-binding proteins to the sequence-independent cleavage domain of the FokI endonuclease (Zink finger nucleases (ZFN), Figure 1) (Kim et al., 1996). The system consists of two zinc fingers each fused to FokI because FokI DNA cleavage demands dimerisation of the nuclease. (Bibikova et al., 2003; Bibikova et al., 2002). The DNA recognition of zinc fingers is based on interactions of a

protein α-helix with a DNA base triplet in the major groove of the DNA double helix making the design and validation of zinc fingers for a specific DNA locus rather complicated (Durai et al., 2005; Miller et al., 1985; Pavletich & Pabo, 1991).

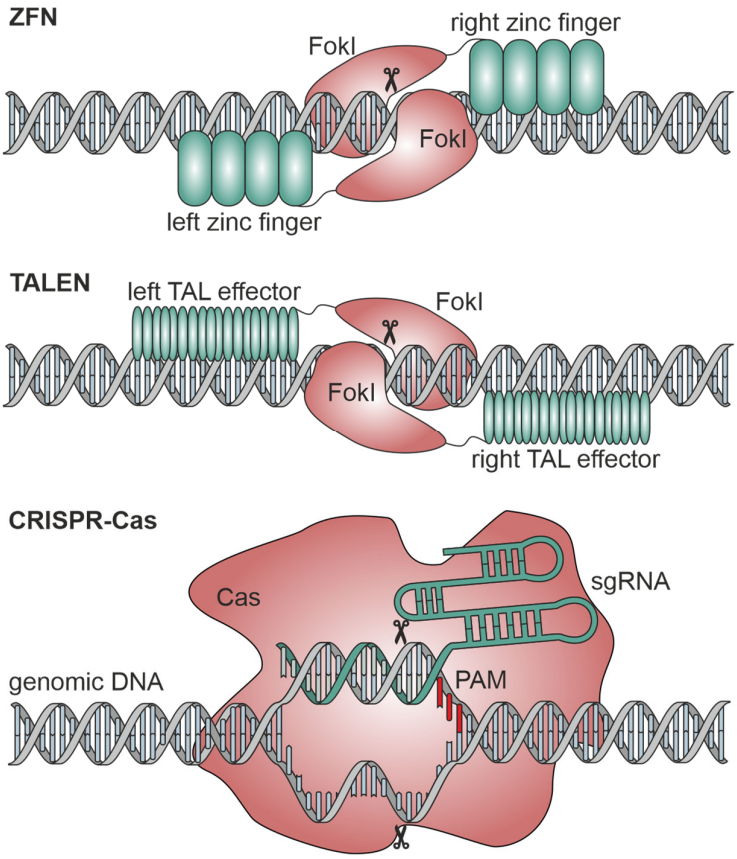

Figure 1: Nuclease systems used for genome editing. ZFN, TALEN and CRISPR-Cas are all based on the combination of a motif able to recognise a specific DNA locus (zinc finger, TAL effector, or sgRNA) with a nuclease able to perform DNA DSBs (FokI, Cas).

Another DNA binding protein which can be used in combination with the FokI cleavage domain is the transcription activator-like (TAL) effector (TAL effector nuclease (TALEN), Figure 1) (Christian et al., 2010). TAL effectors found in plant pathogenic bacteria simplified the design of new specific DNA targeting proteins. The recognition of a specific DNA by TAL effectors is based on the interaction of one protein repeat with one DNA base pair: Decryption of the TAL effector-DNA recognition code made the targeting of new DNA sites possible (Boch et al., 2009; Moscou & Bogdanove, 2009). Although this robust recognition code enabled an uncomplicated design to a specific locus, protein synthesis and validation of new TALEN systems remained problematic (Doudna & Charpentier, 2014).

Synthesis and validation of new sequence-specific nuclease systems were greatly simplified with the discovery of clustered regularly interspaced short palindromic repeats (CRISPR)-CRISPR-associated (Cas) system, in which DNA recognition is based on base pairing (Cong et al., 2013; Jinek et al., 2012; Mali et al., 2013). The CRISPR-Cas gene editing system

consists of a Cas nuclease and a single guide ribonucleic acid (sgRNA) harbouring a spacer sequence for DNA recognition (Figure 1). Compared to the ZFN or TALEN systems the design and synthesis of new sgRNAs targeting specific DNA loci are considerably easier. For binding to the target sequence in the genome, CRISPR-Cas systems only require a short sequence (protospacer adjacent motif, PAM) next to the sgRNA spacer sequence (Jinek et al., 2012; Sternberg et al., 2014).

1.1.2 Discovery of the CRISPR-Cas Systems

CRISPR were first described in 1987 in *Escherichia coli*, but the function of these uncommon repeats remained a mystery for a long time (Ishino et al., 1987). Later studies revealed that the spacers within the repetitive sequences of CRISPR loci are of plasmid or viral origin (Bolotin et al., 2005; Mojica et al., 2005; Pourcel et al., 2005). Together with sequence analysis of CRISPR associated genes (Bolotin et al., 2005; Jansen et al., 2002) (Haft et al., 2005; Makarova et al., 2006), these findings concluded with the uncovering of CRISPR-Cas as part of the bacterial immune system (Barrangou et al., 2007). Furthermore, CRISPR-Cas systems were classified into three types based on the employment of different Cas proteins, today the most relevant are type II systems using the nuclease Cas9 (Makarova et al., 2011). Upon invasion of foreign DNA, Cas proteins cleave the DNA and incorporate the short sequences in between the repeats of a CRISPR locus (Figure 2) (Barrangou et al., 2007; Garneau et al., 2010). After transcription and processing, the CRISPR RNA (crRNA) assembles with the complementary recognition site of a trans-encoded crRNA (tracrRNA) (Deltcheva et al., 2011). Cas9 can capture the crRNA:tracrRNA complex, enabling the CRISPR-Cas system to recognise foreign DNA by complementary base pairing, and perform DSBs if the spacer binds next to a specific PAM (Brouns et al., 2008; Garneau et al., 2010; Makarova et al., 2011).

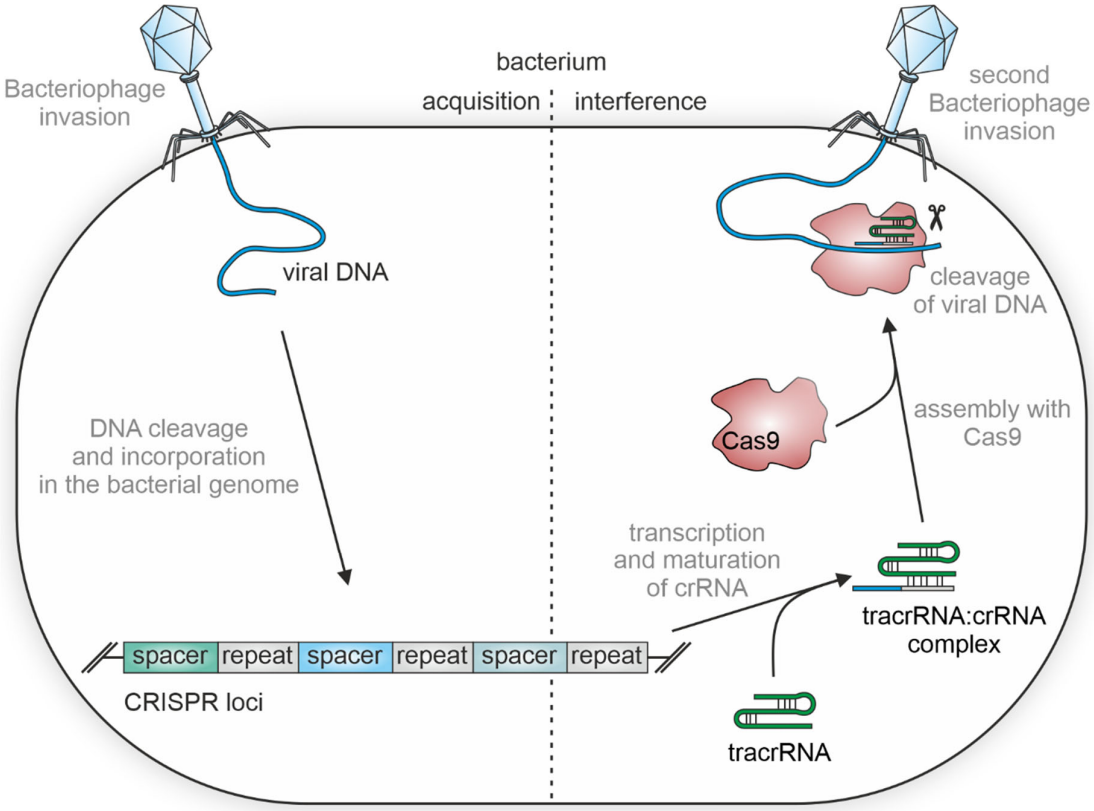

Figure 2: Type II CRISPR-Cas mediated immunity as part of the bacterial immune system. CRISPR-Cas mediated immunity can be divided into different stages. First, the acquisition of a new resistance after the first infection with a virus (bacteriophages), the viral DNA is cleaved and incorporated into a CRISPR locus (left side). Transcription from the CRISPR locus, maturation of a crRNA, and assembly with the complementary recognition site of a tracrRNA. The tracrRNA then enables the recognition of the tracrRNA:crRNA complex by a Cas nuclease (e.g., Cas9). The final stage is the interference (right side). After a second invasion of the same bacteriophage DNA, the spacer enables CRISPR-Cas9 to recognise and cleave the viral DNA.

For the first gene editing experiments *Streptococcus pyogenes* Cas9 (*Sp*Cas9) was used (Cong et al., 2013; Jinek et al., 2013; Mali et al., 2013). As a type II CRISPR system, it requires only one enzyme to perform DSBs in comparison to other CRISPR systems (Sapranauskas et al., 2011). Furthermore, *Sp*Cas9 needs a short NGG (N: A, G, C or T) PAM sequence for target recognition, which is found on average every 8 bp in the human genome (Cong et al., 2013; Mojica et al., 2009). For efficient protein expression and localisation in human cells, the *Sp*Cas9 was codon-optimised and fused to a nuclear localisation signal (Cong et al., 2013; Jinek et al., 2013; Mali et al., 2013). To further decrease the components necessary for CRISPR-Cas gene editing the tracrRNA:crRNA complex was shortened and fused into one sgRNA (Jinek et al., 2012; Mali et al., 2013). Moreover, it was shown that

CRISPR-Cas can also be employed for simultaneous editing of different target sites using multiple sgRNAs (Cong et al., 2013; Mali et al., 2013).

DNA DSBs are mediated by the HNH- and RuvC-like nuclease domains within the Cas9 enzyme, which cleave the complementary and noncomplementary strands, respectively (Jinek et al., 2012). A nuclease-deficient ("dead") Cas9 (dCas9) was developed shortly after the discovery of the CRISPR-Cas9 system by introducing point mutations in the nuclease domains (Qi et al., 2013). dCas9 was fused to effector domains to enable a plethora of different functions, e.g., gene activation (Gilbert et al., 2013; Maeder et al., 2013; Perez-Pinera et al., 2013), gene repression (Gilbert et al., 2013; Lawhorn et al., 2014; Qi et al., 2013), base editing (Gaudelli et al., 2017; Komor et al., 2016; Nishida et al., 2016), histone modification (Cheng et al., 2016; Hilton et al., 2015; Kearns et al., 2015), and alteration of DNA methylation (McDonald et al., 2016; Vojta et al., 2016; Xu et al., 2016).

1.1.3 Transcriptional Activation with CRISPR-Cas9

Artificial control of transcription enables a wide range of applications such as the study of gene functions or the reprogramming of cells. Transcriptional gene activation (transactivation) can be performed by recruiting transactivation domains fused to dCas9 to the promoter region of the gene of interest (Bikard et al., 2013; Gilbert et al., 2013). The first transactivation module used for the activation of endogenous genes in human cells was a tetramer of the Herpes simplex virus transcription activator viral protein 16 (VP64), fused to the C-terminal site of dCas9 (Maeder et al., 2013). Over time several transactivation modules have been developed. The three most efficient and widely used transactivation modules are dCas9 fused to the transactivation domains VP64, p65 and Rta (dCas9-VPR), synergistic activation mediator (SAM), and dCas9-Suntag (Figure 3) (Chavez et al., 2015; Chavez et al., 2016; Konermann et al., 2015; Tanenbaum et al., 2014). While dCas9-VPR is a single fusion protein, the SAM and Suntag system rely on the expression of additional transcription activator complexes and their recruitment based on RNA aptamers or antibodies, respectively. The three modules operate with similar efficiency in different cell types and species. If necessary, the efficiency of these modules can be further increased by adding additional sgRNAs, binding to a neighbouring site of the target sequence (usually the promoter region of the gene to be activated) (Chavez et al., 2016).

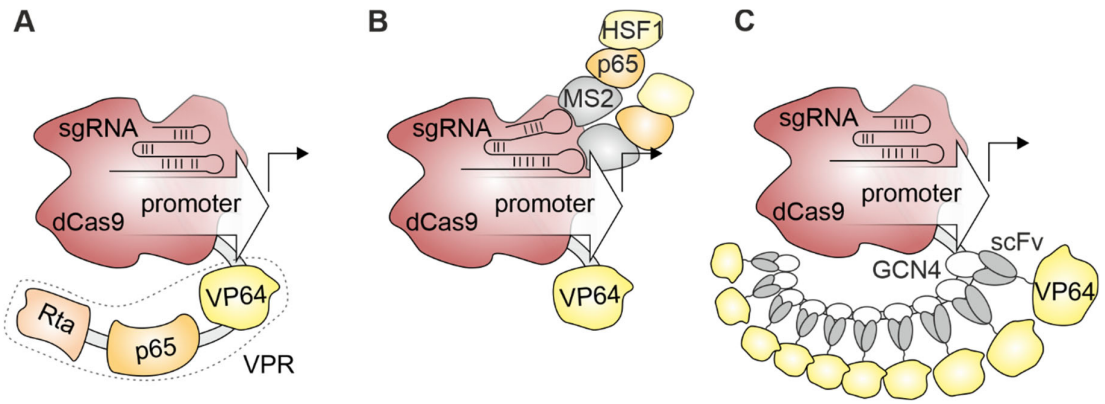

Figure 3: Most potent transactivation modules. A, dCas9-VPR is a fusion protein of dCas9 and the transcription factor VP64 (Beerli et al., 1998), the human nuclear factor-κB transcription factor (p65) (Schmitz & Baeuerle, 1991), and the replication and transcription activator of the Epstein-Barr virus (Rta) (Gwack et al., 2003). **B**, The SAM system consists of the dCas9-VP64 fusion protein and additional activator complexes containing the MS2 bacteriophage coat protein (MS2). The activator complexes employ the activation domain from human heat-shock factor 1 (HSF1) (Marinho et al., 2014) and p65. They are recruited to MS2-binding RNA aptamers at the tetra-loop and stem-loop 2 of the modified sgRNAs. **C**, The dCas9-Suntag system uses a chain of ten epitopes of the yeast general control nonderepressible 4 protein (GCN4), that is fused to the C-terminus of dCas9. GCN4-targeting single-chain variable fragment antibodies (scFv) fused to the transcription factor VP64 are used as transcriptional activators.

1.1.4 CRISPR-Cas9 for Gene Therapy

Gene therapy is the treatment of diseases by supplementation or manipulation of the genetic code. Both gene editing and transcriptional activation mediated by CRISPR-Cas9 have already been used for therapeutic applications. The use of catalytically active Cas9 in gene therapy largely focuses on *ex vivo* gene editing of T-cells or haematopoietic stem cells, correction of mutations by homology-directed repair, abolishing of splice signals or total gene expression, or silencing of dominant-negative alleles (Amoasii et al., 2017; Bailey & Maus, 2019; Bakondi et al., 2016; Ding et al., 2014; Maeder et al., 2019; Wang et al., 2020; Wu et al., 2019; Yin et al., 2014). Despite safety concerns about introducing DSBs (Haapaniemi et al., 2018) and permanent changes into the genomic DNA (Kang et al., 2020; Schaefer et al., 2017) as well as the bacterial Cas9 protein itself (Charlesworth et al., 2019), clinical trials for *in vivo* genome editing with CRISPR-Cas9 have already been approved by the FDA for the treatment of Leber Congenital Amaurosis (ClinicalTrials.gov Identifier: NCT03872479). In this context, Cas9 is used to excise a splice site mutation from an intronic region (Maeder et al., 2019). Further clinical studies for the *in vivo* treatment of other genetic

diseases (i.e., transthyretin amyloidosis (NCT04601051), and hereditary angioedema (NCT05120830)) are currently running.

In comparison to approaches utilizing catalytically active Cas9, CRISPR-Cas mediated transactivation (CRISPRa) does not introduce DSBs into the genome. Thus, the risk of generating off-target effects is considerably reduced (Kemaladewi et al., 2019; Liao et al., 2017; Matharu et al., 2019). So far, CRISPRa has been therapeutically used to activate disease modifier genes, cell-protective genes, and differentiation factors in the context of genetic and acquired diseases or to increase the activation of the remaining healthy gene copy in cases of heterozygous loss-of-function mutations (Colasante, Lignani, et al., 2020; Colasante, Qiu, et al., 2020; Kemaladewi et al., 2019; Liao et al., 2017; Matharu et al., 2019; Yamagata et al., 2020). Another interesting target for CRISPRa is the transactivation of genes functionally equivalent to the mutated gene (Becirovic, 2022; Bohm et al., 2020; Kemaladewi et al., 2019; Liao et al., 2017; Riedmayr et al., 2022). These functional counterparts are often expressed in specific cell types but show strong structural and functional similarities. Furthermore, activation can also be combined with the simultaneous knockout of another gene. This multiplexing approach is based on the observation that sgRNAs with shortened spacer sequences (<16 nt) abolish the nuclease activity of Cas9 (Dahlman et al., 2015; Kiani et al., 2015). Such a system could allow for more sophisticated strategies, for example, to treat gain-of-function mutation where gene supplementation must be combined with simultaneous gene knockout of the mutated allele (Becirovic, 2022).

In conclusion, the CRISPR-Cas family holds great therapeutic potential and has already demonstrated high efficiency in the treatment of many different genetic diseases.

1.2 The Retina – a Window to the World

1.2.1 Structure and Development

The retina is a remarkable neuronal tissue of the human body that even allows the detection of single photons. The retina lines the back of the eye, shows high similarity in structure and function across species, and the retinal cells can be subdivided into five classes of neurons (Figure 4) (Hoon et al., 2014).

The main light-sensitive cells of the retina are the photoreceptors. They can be subdivided into rod and cone photoreceptors. Cones are responsible for daylight and colour vision and

are, in most mammals, outnumbered approximately 20-fold by rods, which mediate dim-light vision (Masland, 2012). The cell bodies of photoreceptors form the outer nuclear layer. The region where the synaptic endings of photoreceptors connect to bipolar cells is named the outer plexiform layer. Bipolar cells are responsible for signal transmission to the inner retina. Depending on the type of bipolar cell the retinal signal is further processed at this step. Bipolar cells differ by the speed of their response, the type and amount of cells in their receptive field, and the type of electrical response that they create after the light-mediated stimulation of photoreceptors (Euler et al., 2014). ON bipolar cells are depolarised while OFF bipolar cells show a hyperpolarisation upon the glutamate release originating from the synapses of light-stimulated photoreceptors. In addition to bipolar cells, the outer plexiform layer also includes the synapses of horizontal cells. Their main function is to adjust the photoreceptor signal based on the average level of illumination falling into the region of the photoreceptors to which the horizontal cell is connected. This allows for a better vision in an environment with different levels of brightness (Masland, 2012). Another class of neurons that further refines the signal coming from bipolar cells are amacrine cells. They can be divided into about 30 different types with specific functions such as detection of object motion or combining ON and OFF bipolar cell signals (Masland, 2012). In the inner plexiform layer, the endings of bipolar and amacrine cells meet ganglion cells. The axons of ganglion cells form the optic nerve, which transports the retinal signal to the brain.

Besides the retinal neurons, also non-neuronal cells are important for retinal structure and function. Müller Glia cells are the main glial cell type in the retina and maintain retinal integrity and homeostasis. The retina is additionally protected by the retinal pigment epithelium which plays a key role in the renewal of photoreceptor outer segments.

Although they serve different functions, all retinal neurons and Müller glial cells have been shown to derive from the same progenitors (Turner & Cepko, 1987). During differentiation, neuronal cells lose their ability to divide and become post-mitotic. The fate of photoreceptors is determined during this step.

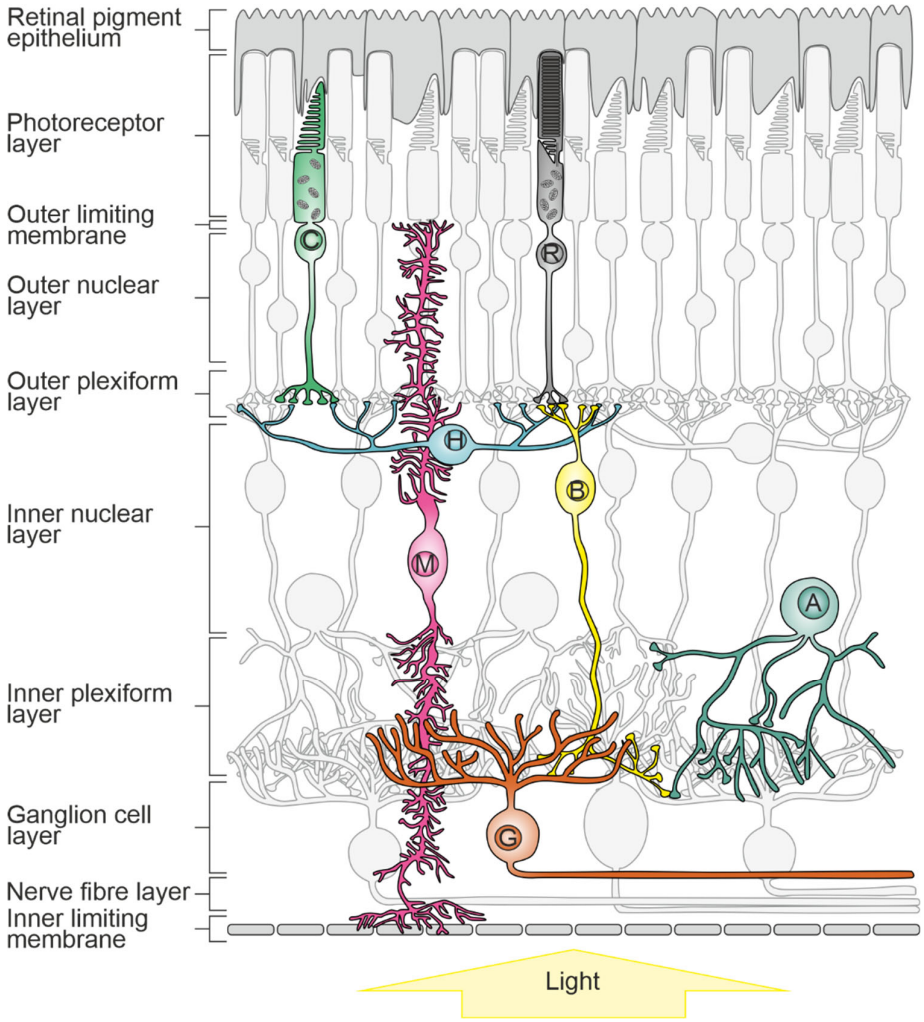

Figure 4: Structure and organisation of the retinal cells. When light enters the retina, photons are captured and translated into a neural signal by cone and rod photoreceptors. Processing and refinement of the visual signal start already in the retina by horizontal and amacrine cells interacting with bipolar and ganglion cells that transmit the retinal signal from the photoreceptors to the brain. Retinal homeostasis and integrity are maintained by Müller glial cells. C, cone. R, rod photoreceptor. H, horizontal cell. B, bipolar cell. A, amacrine cell. G, ganglion cell. M, Müller glial cell. Adapted from Swaroop et al. (2010).

To perceive different colours at least two types of cones with peak sensitivity for different wavelengths are needed. Most mammals possess at least two types of cones, short-wavelength sensitive (S)-cones and medium-long wavelength (green) sensitive (M)-cones, that express different types of photoreceptor pigments (opsins). To be able to perceive a wider range of colours, humans additionally possess L-cones expressing a long-wavelength (red) sensitive opsin (Nathans et al., 1986). During development, the fate of multipotent progenitor cells is determined by different transcription factors (Figure 5). The future role of a photoreceptor precursor is mainly determined by the presence of the neural retina leucine

zipper (NRL) protein. This transcription factor leads to the activation of rod-specific genes and represses genes required for cone-specific development (Mears et al., 2001).

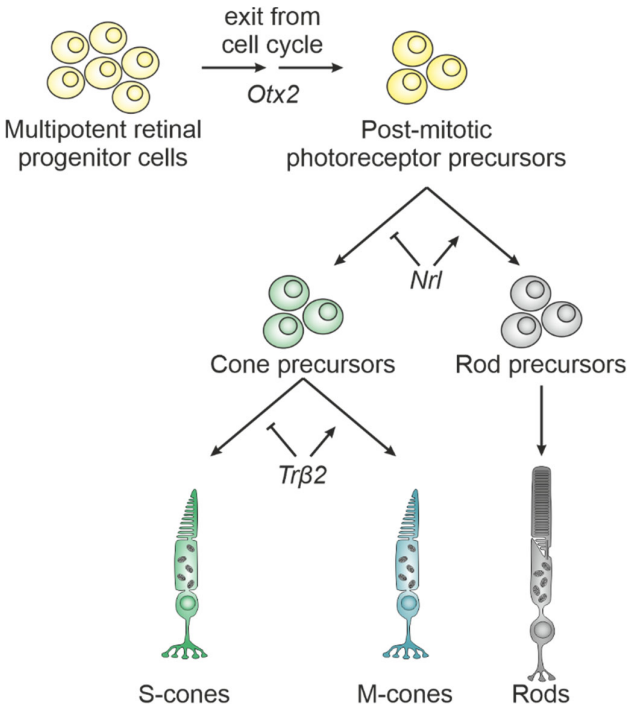

Figure 5: Differentiation of photoreceptor cells in the murine retina. A key factor in the differentiation of multipotent retinal progenitors into photoreceptor precursors is the expression of the orthodenticle homeobox 2 gene (*Otx2*). Expression of the neural leucine zipper gene (*Nrl*) determines the developmental pathway of rods. The further development of cone precursors is regulated by the expression of the thyroid hormone receptor beta 2 gene (*Trβ2*) (Swaroop et al., 2010).

1.2.2 The Phototransduction Cascade

To enable vision, the light captured by photoreceptors must be translated into a signal readable to the neurons of the visual cortex. The first step of this translation is mediated by the phototransduction cascade. The opsins are photopigments which are responsible for the detection of photons in rods and cones. During the phototransduction cascade, the energy of photons is converted into a chemical and finally into an electric signal that causes the transmitter release to the synapses of bipolar cells. (Figure 6).

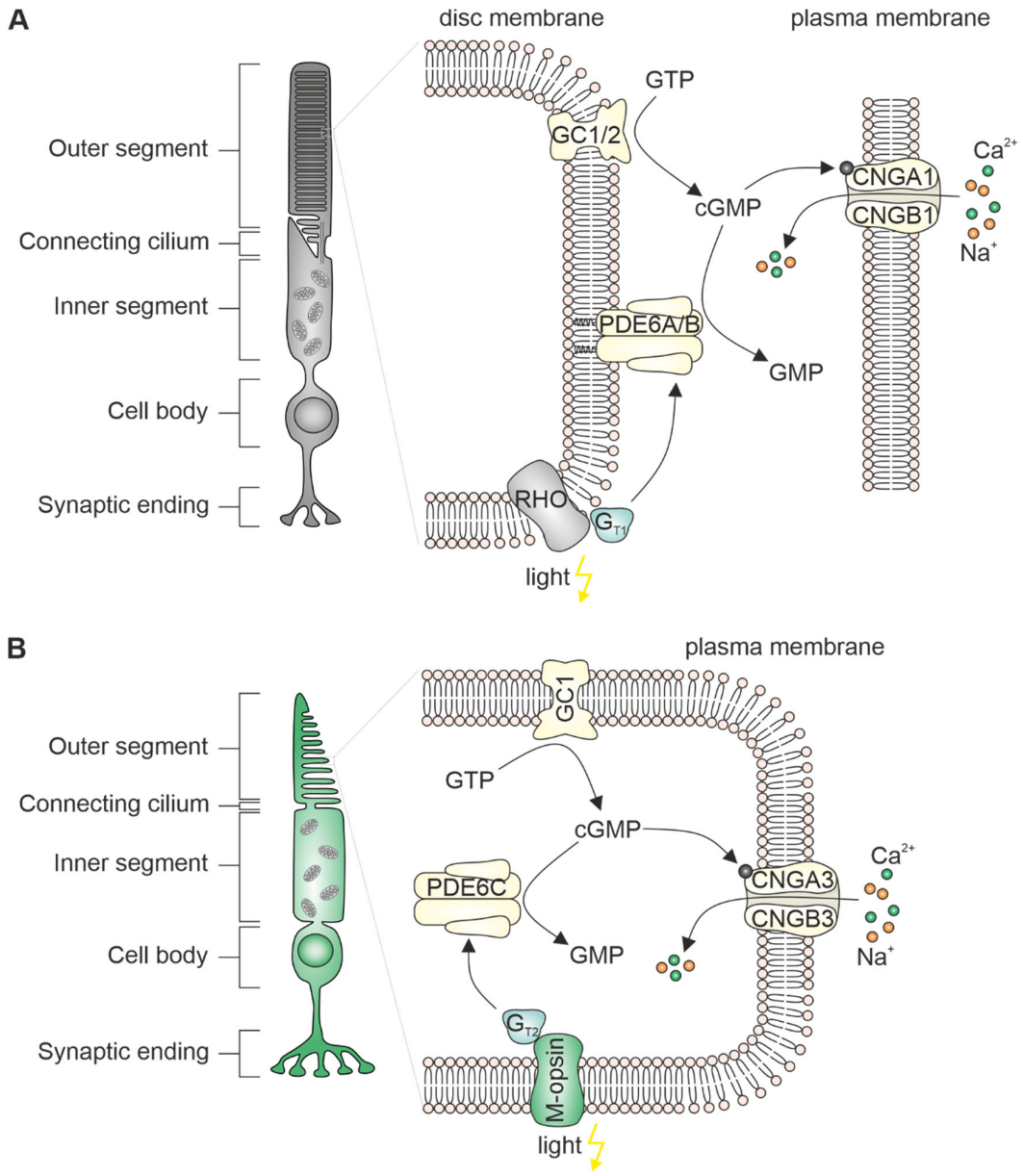

Figure 6: Phototransduction cascade in rod and cone photoreceptors. Photons activate the visual pigments in rod (**A**) or cone (**B**) photoreceptors. This activation leads to the hydrolysis of cyclic guanosine monophosphate (cGMP) by phosphodiesterase 6 (PDE6). The decrease in cGMP concentration causes the closing of cyclic nucleotide-gated (CNG) channels responsible for the depolarising dark current in photoreceptors. RHO, rhodopsin. G_T, transducin. GC, guanylate-cyclase. GTP, guanosine triphosphate. GMP, guanosine monophosphate.

The major steps of the phototransduction cascade in rods and cones are very similar and involve many proteins that are not identical in the two cell types but are structurally and functionally strongly related. If no light is present, photoreceptors are depolarised by the steady influx of calcium (Ca^{2+}) and sodium cations (Na^{+}) through cyclic nucleotide-gated (CNG) channels, consisting of the subunits CNGA1/CNGB1 in rods and CNGA3/CNGB3

in cones. This steady inward current of cations is called dark current and is specific for photoreceptors. CNG channels are dependent on cyclic guanosine monophosphate (cGMP), which is constantly produced from guanosine triphosphate (GTP) by guanylate-cyclase (GC) 1 or 2 (GC2 is only expressed in rods). Photons activate the visual pigments, rhodopsin in rods, and opsins in cones, by photoisomerisation. This leads to further activation of the G-protein transducin (G_T), which stimulates phosphodiesterase 6 (PDE6). Upon stimulation, the membrane bound PDE6A/B dimer in rods or the soluble PDE6C homodimer in cones catalyses the hydrolysis of cGMP. The light-induced decline in cGMP concentration closes CNG channels, which leads to a decreased cation influx. The resulting hyperpolarisation reduces the release of glutamate containing vesicles at the synaptic ending of the photoreceptors (Yau & Hardie, 2009).

The differences in rod- and cone-specific proteins result in an up to 100-fold higher light sensitivity of rods. By comparison, cone photoreceptors exhibit faster response kinetics, allowing higher acuity of their signal (Baylor, 1987). Despite their differences, some functionally equivalent rod and cone proteins have already been proven to be interchangeable. Shi et al. generated a transgenic mouse line in which rhodopsin was replaced by S-opsin. They were able to show that S-opsin generates a similar response to rhodopsin when expressed in rods and interacts with all rod-specific proteins necessary for signal creation. Furthermore, S-opsin expression in rods enhances cell survival and restores the formation of rod-outer segments, which are missing in mouse models lacking rhodopsin (Shi et al., 2007). The ectopic expression of the rod α subunit of transducin in cones or the cone α subunit of transducin in rods in mouse models lacking the cone or rod α subunit, respectively, showed that both subunits enable identical response characteristics in the other photoreceptor type (Deng et al., 2009). In addition, it has been shown that the expression of a cone PDE6C transgene in rods of a PDE6B-deficient mouse model could restore light sensitivity in rods (Deng et al., 2013).

1.2.3 Inherited Retinal Diseases

Inherited retinal dystrophies (IRDs) comprise a large and heterogeneous group of dystrophies linked to genetic mutations. To this point, mutations in 280 genes have been identified to be associated with IRDs (RetNet, https://sph.uth.edu/RetNet/). Depending on the affected gene and the specific mutation, IRDs show a high variation in the manifestation of associated symptoms and can also be accompanied by symptoms present in other tissues

and organs (syndromic IRDs). Furthermore, all patterns of inheritance can be found in the heterogeneous group of IRD-causing mutations.

With 1:4000 non-syndromic retinitis pigmentosa (RP) has the highest prevalence of all IRDs (Verbakel et al., 2018). RP is characterised by a progressive loss of vision. In most cases, RP starts in adolescence with night-blindness and a progredient restriction of peripheral vision caused by continuous degeneration of rod photoreceptors. In later stages, the secondary cone degeneration impairs day-light vision and leads to the eventual loss of total vision. While autosomal-recessive inheritance is most common for RP, autosomal-dominant and X-linked inheritance can also occur. Some forms of RP can be caused by the combination of mutations in different genes (di- or polygenic). Mutations in rhodopsin are the most frequent cause of autosomal-dominant RP. Among the rhodopsin mutations, the proline to histidine substitution at amino acid position 23 (P23H) alone causes 10 % of all autosomal-dominant RP cases in North America (Meng et al., 2020). Usher syndrome (USH) is a syndromic type of autosomal-recessive IRDs and is the leading cause of inherited deafblindness worldwide. The retinal phenotype in USH patients is caused by RP with variable disease onset. USH can be divided into three clinical types (USHI-III) based on the severity and onset of symptoms. The most severe USHI form is predominantly caused by mutations in the myosin VIIA gene (*MYO7A*) (Delmaghani & El-Amraoui, 2022; Whatley et al., 2020).

Retinal degeneration in IRD patients can be measured by optical coherence tomography (OCT). In the early stages, shortening of the photoreceptor outer segments becomes visible and after progressive degeneration of photoreceptors, a reduction in the thickness of the outer nuclear layer (ONL) can be measured. The retinal function can be assessed by electroretinogram (ERG) measurements. A decreased ERG signal in the rod photoreceptors can be detected even before the first appearance of symptoms, while a reduction of the cone ERG occurs only in the later stages of the disease (Verbakel et al., 2018).

1.2.4 Retinal Gene Therapy

The concept of gene therapy was first introduced in 1972 by Friedmann and Roblin. Since then, the eye has been one of the first targets for translational gene therapy as it offers several advantages over other tissues. The eye can be reached locally, reducing the required dose and the risk of systemic complications. In addition, the lower maximum immune response

and the protection by the blood-retinal barrier represent an immunologic privilege (Willett & Bennett, 2013). In 2017, the US Food and Drug Administration approved Luxturna, the first gene therapy treatment for an IRD. The therapeutic strategy of Luxturna is based on the supplementation of the coding sequence of the gene of interest as a replacement for the diseased gene (Fenner et al., 2021). For gene replacement therapy, a transgene containing a promoter, the desired coding sequence and a polyadenylation signal are needed (Figure 7). To reach the target cells the transgene can be packaged in different vector types.

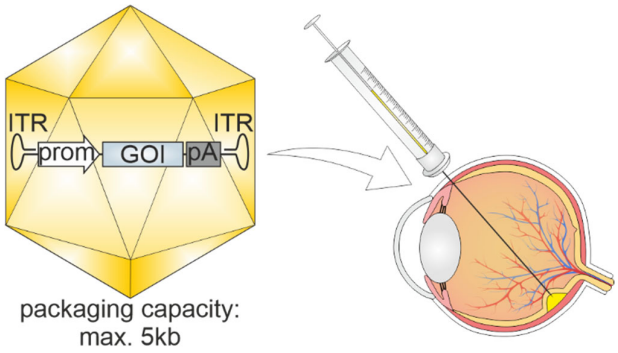

Figure 7: Retinal gene replacement therapy with rAAV vectors. Left panel, recombinant AAV (rAAV) vector for gene therapy. The packaged transgene consists of inverted terminal repeats (ITRs), a promoter, the coding sequence of the gene of interest (GOI), and a polyadenylation signal (pA). The packaging capacity is limited to <5 kB. Right panel, the rAAVs are administered between the retina and the RPE (subretinally). Successful injection can be confirmed by the formation of a subretinal bleb.

The current gold standard for *in vivo* gene therapy are adeno-associated virus (AAV) vectors due to their low immunogenicity, high transduction rates, and long-term expression in post-mitotic cells (High & Roncarolo, 2019; D. Wang et al., 2019; Wang et al., 2020). Other viral vectors used for gene therapy are lenti- and adenoviruses. Both offer a less favourable safety profile, due to insertional mutagenesis or high immunogenicity, respectively. Nevertheless, lentiviruses are predominantly used for *ex vivo* transgene delivery applications (Bulcha et al., 2021). The development of non-viral vector delivery platforms based on nanoparticles is currently ongoing (Chen et al., 2020). Unresolved problems with low transduction efficiency and no long-term expression, which would make multiple dose applications necessary, leave them unfavourable for gene replacement (Wang et al., 2020).

Transduction of cells with AAV vectors starts with the interaction of the AAV with cell surface receptors. This interaction facilitates their uptake by endocytosis and initiates the AAV transduction cycle (Figure 8) (D. Wang et al., 2019). Natural occurring AAV serotypes show high variability in tissue tropism, which is caused by differences in their performance during AAV trafficking in the body and all stages of the transduction process (Nonnenmacher & Weber, 2012). Based on these findings, engineered AAV serotypes with

enhanced retinal tropism have been developed such as the AAV2/8Y733F variant (Petrs-Silva et al., 2009).

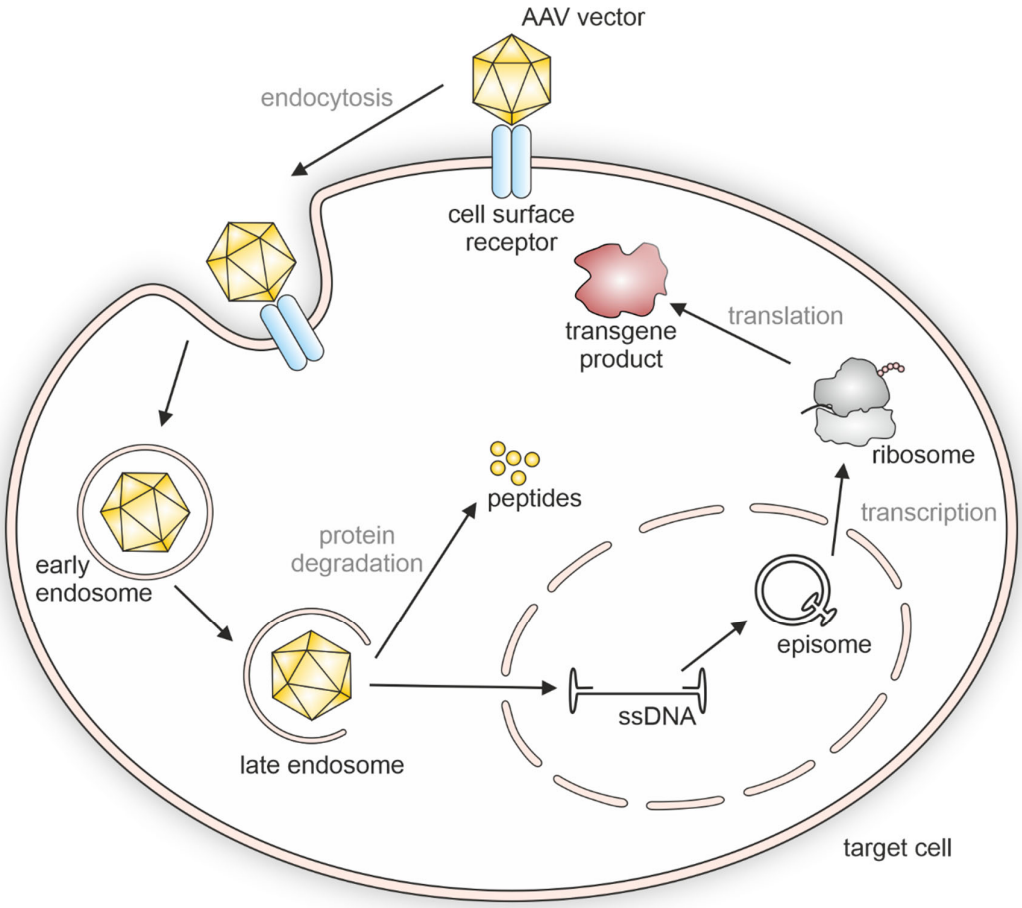

Figure 8: AAV transduction cycle. Transduction of cells by AAV vectors proceeds in several steps. Interaction of the AAV with cell surface receptors initiates the uptake by endocytosis. A conformational change of AAV viral capsid proteins induced by the low endosomal pH leads to escape from the endosome. At this point, the AAV can be degraded by proteosomes or transported through the nuclear pore complex into the nucleus. Uncoating of the AAV releases the viral single-stranded DNA. After second-strand synthesis, concatemerisation of the AAV ITRs results in the formation of a double-stranded episome. Transcription and translation by natural cellular processes lead to the expression of the desired transgene product (D. Wang et al., 2019).

One substantial drawback of rAAVs as gene therapy vectors is their limited packaging capacity. The packaging of transgenes over 5 kB including the AAV inverted terminal repeats leads to fragmentation of the provided transgene (Wu et al., 2010). The ITRs and other regulatory elements required for transgene transcription (e.g., promoter or polyadenylation signal) limit the maximal coding sequence of a gene that can be packaged into an rAAV to approximately 4 kB if a short promoter (<300 bp) is used. To extend their range of application, several strategies based on the reconstitution of two separate gene

halves packaged into different rAAV vectors have been developed (Figure 9) (Tornabene & Trapani, 2020; Trapani et al., 2021; Wang et al., 2020). The first dual rAAV strategies were based on gene reconstitution at the AAV genome level and can be divided into three strategies: overlapping vectors, DNA *trans*-splicing vectors, and hybrid vectors (Figure 9A) (Patel et al., 2019). For overlapping vectors reconstitution is facilitated by homologous recombination based on overlapping regions in the coding sequence of the gene of interest (Duan et al., 2000). DNA *trans*-splicing vectors use the introduction of a splice donor site after the 5' part of the gene of interest and a splice acceptor site before the 3' part, to enable correct splicing of the full-length coding sequence after concatemerisation based on the ITRs (Nakai et al., 2000; Sun et al., 2000; Yan et al., 2000). To increase reconstitution efficiency, combinations of both techniques have been developed. These hybrid vectors possess elements necessary for splicing as well as complementary binding domains (BD) to facilitate homologous recombination (Ghosh et al., 2008). But even with the hybrid vectors, reconstitution efficiency remained comparatively low (Carvalho et al., 2017; Levy et al., 2020; Tornabene et al., 2019; Trapani et al., 2014). The discovery of split inteins as protein sequences that can mediate a scarless and highly efficient reconstitution of two protein halves has advanced the field of dual rAAV vectors (Wu et al., 1998). Since then, split-inteins have been widely used for the reconstitution of various transgenes (Figure 9B) (Bohm et al., 2020; Chew et al., 2016; Levy et al., 2020; Lim et al., 2020; Tornabene et al., 2019; Truong et al., 2015; Villiger et al., 2018). While these vectors show high reconstitution efficiencies, they also harbour two key drawbacks which limit their use for translational purposes. I) Low flexibility in split site selection. Successful reconstitution relies on the presence of cysteine, serine, or threonine at the split site and the position of the split site to be outside of structural domains to enable proper protein folding (Muralidharan & Muir, 2006; Shah & Muir, 2014). II) Decreased safety. Split inteins create inteins in an equimolar ratio to the reconstituted proteins. As inteins are of bacterial origin they are potentially immunogenic. The reconstitution at the mRNA level via mRNA trans-splicing represents another possibility for dual rAAV vectors (Figure 9C) (Pergolizzi et al., 2003; Song et al., 2009). In contrast to the more common *cis*-splicing, *trans*-splicing is performed between two different mRNA transcripts (Pergolizzi et al., 2003). Therefore, *trans*-splicing vectors in contrast to DNA splicing vectors need a promoter and polyadenylation signal present in both rAAV vectors for the efficient expression of the respective transcripts. Recently, new dual rAAV vector technology based on reconstitution via mRNA trans-splicing (REVeRT) has

been developed by our group and shows high reconstitution efficiency for reporter genes *in vivo* (unpublished data, manuscript submitted).

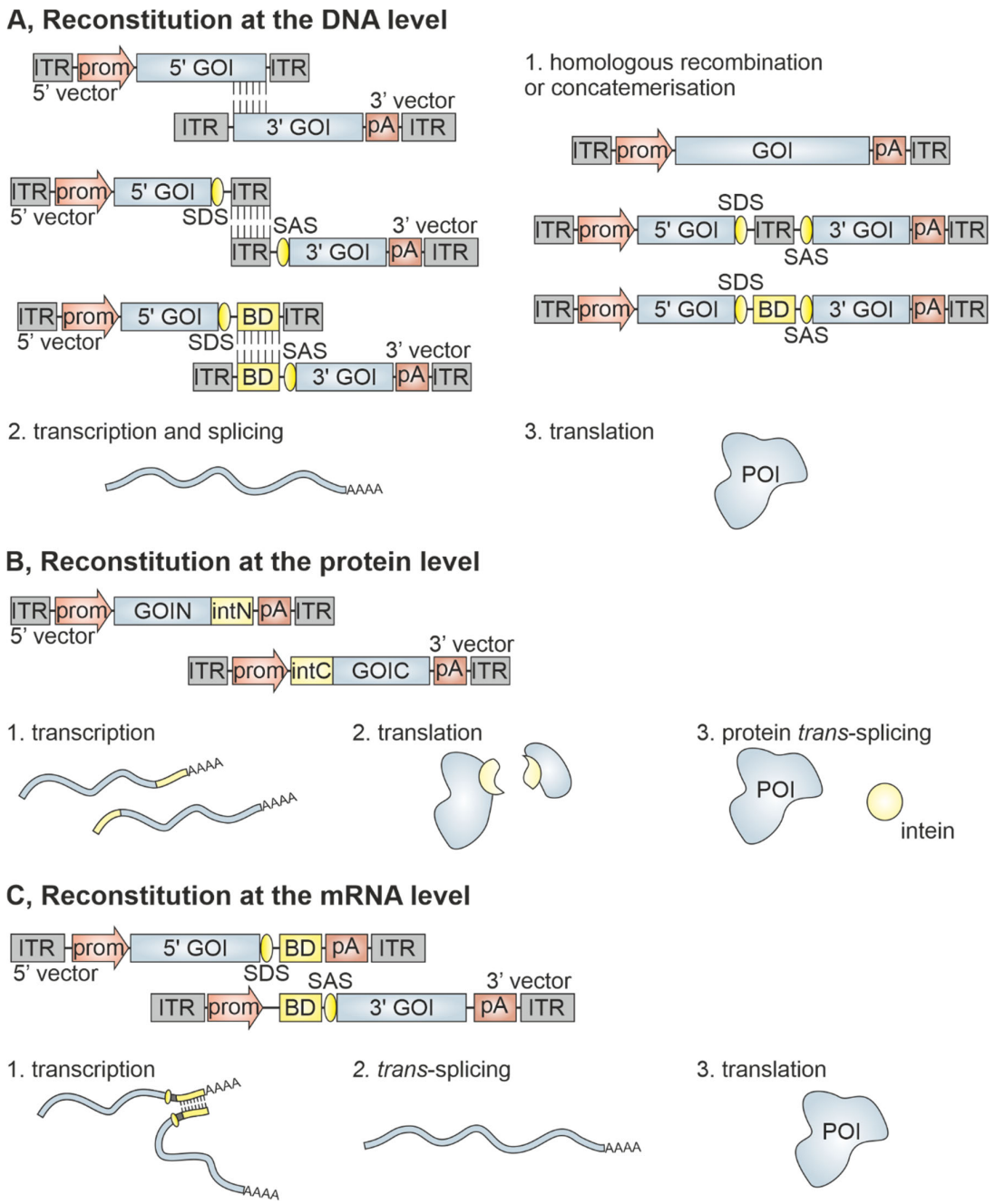

Figure 9: Dual rAAV strategies. For dual rAAV strategies, the gene of interest (GOI) is split into two fragments and each of them is packaged into one separate rAAV vector. After cotransduction of dual rAAVs split gene fragments can reconstitute at the DNA, protein, or mRNA level. A, At the DNA level, reconstitution is facilitated by homologous recombination or concatemerisation based on complementary sequences. Reconstitution based on ITR concatemerisation or homologous binding domains (BD) needs the presence of a splice donor (SDS) and splice acceptor site (SAS). B, Split inteins can catalyse a scarless reconstitution of two protein fragments while excising themselves. C, mRNA trans-splicing is used to combine two mRNA fragments. For a successful reconstitution, complementary

BDs, a strong SDS and SAS are needed. prom, promoter. POI, protein of interest. intN, N-terminal intein. intC, C-terminal intein.

Besides being limited by the AAV packaging capacity, gene replacement therapy comes with other disadvantages. Gene replacement strategies are less suitable for diseases caused by gain-of-function mutations, polygenic diseases, or diseases caused by mutations in genes encoding multiple splice isoforms each fulfilling different functions. There is thus a high unmet medical need to develop more advanced gene therapy strategies for the treatment of IRDs. One attractive solution is the transactivation of functionally equivalent genes by CRISPR-Cas (Bohm et al., 2020; Kemaladewi et al., 2019). This transactivation strategy is gene size-independent and well suited to circumvent the aforementioned drawbacks of classical gene replacement. Moreover, it also offers a decisive advantage over CRISPR-Cas-based gene-editing approaches designed to correct specific mutations (Maeder et al., 2019). Compared to CRISPRa, these personalised medicine approaches are associated with a significantly higher expenditure of time and effort and thus also with higher development costs.

As IRDs are a highly heterogeneous group of rare diseases, the development of gene independent strategies would benefit a high number of patients. As some IRD-associated genes are expressed in rod or cone photoreceptors only, reprogramming strategies that reduce the expression of these genes in the affected cell type could be beneficial. The reprogramming of rods into cone photoreceptors can be facilitated by the knockout of *NRL*, which encodes for the main transcription factor responsible for determining rod fate and rod homeostasis (Figure 5). A CRISPR-Cas based knockout of *Nrl* in mice has already been proven useful in mouse models carrying mutations in rod-specific genes encoding for rhodopsin (*Rho*) or phosphodiesterase 6 b (*Pde6b*) (W. Yu et al., 2017). Another gene independent strategy is the supplementation with neuroprotective factors. The rod-derived cone viability factor (RdCVF) is a trophic factor expressed by rods that promotes cone survival by stimulation of aerobic glycolysis (Figure 10) (Ait-Ali et al., 2015; Leveillard et al., 2004). Aerobic glycolysis in photoreceptors is hypothesised to be needed for the renewal of the photoreceptor outer segment (Casson et al., 2013). Gene supplementation with the RdCVF encoding nucleoredoxin like 1 gene (*Nxnl1*) enhances cone photoreceptor survival (Ait-Ali et al., 2015; Byrne et al., 2015; Yang et al., 2009). Interestingly, the additional supplementation with the long isoforms of RdCVF (RdCVFL), a thioredoxin enzyme, shows a complementary protective effect on cones and might be necessary for optimal treatment effects (Byrne et al., 2015; Cronin et al., 2010). A drawback of RdCVF supplementation is

that it relies on the presence of rod photoreceptors to express sufficient amounts of the trophic factor, which causes the treatment effect to diminish as the degeneration progresses. A combination of the rod reprogramming approach and the RdCVF(L) supplementation strategy could increase the therapeutic potential by ensuring the survival of reprogrammed rods and preventing degeneration by enhanced RdCVF(L) expression.

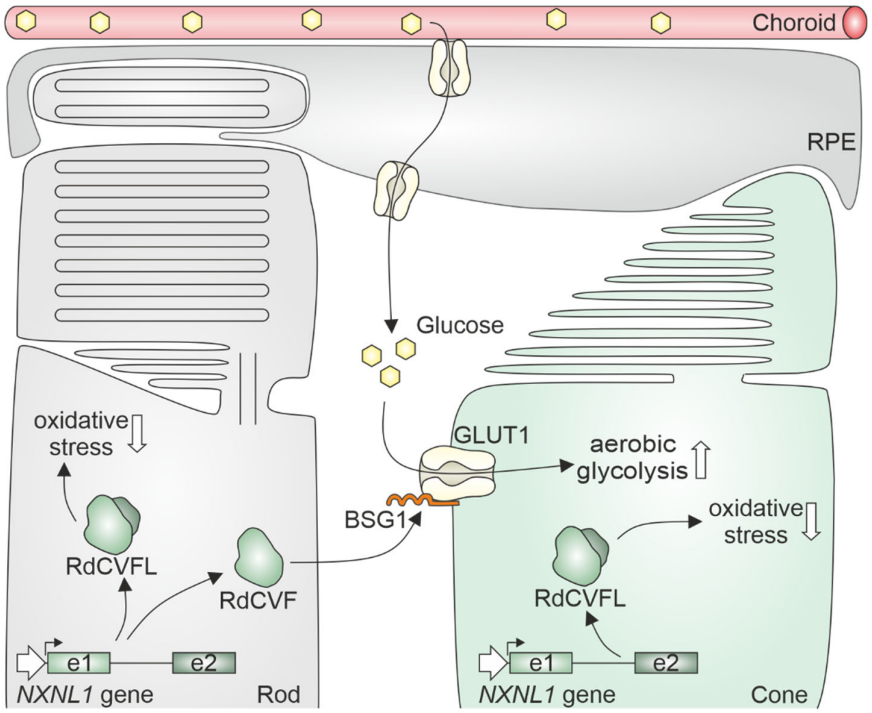

Figure 10: RdCVF and RdCVFL in photoreceptors. In rod photoreceptors, both transcript variants of the nucleoredoxin like 1 gene (*NXNL1*) are expressed. Rod-derived cone viability factor (RdCVF) binds to basigin 1, (BSG1) enhancing glucose uptake through glucose transporters (GLUT1) into cone photoreceptor cells. Increased glucose enhances aerobic glycolysis, necessary for photoreceptor outer segment renewal. Cone photoreceptors themselves only express the long splice isoform of *NXNL1* (RdCVFL). RdCVFL is a thioredoxin enzyme and leads to the reduction of oxidative stress in photoreceptors. e1, exon 1. e2, exon 2. RPE, retinal pigment epithelium.

2. Aim of the Study

Gene replacement is currently the most advanced strategy in gene therapy. However, it is limited by target gene size, is not efficient for the treatment of gain-of-function mutations and can only be used for the treatment of a specific gene deficiency. This study was set out to develop and evaluate new strategies that overcome these limitations.

In the first part of the study, the transactivation of functionally equivalent genes with the dual REVeRT rAAV technology was evaluated. This included the principal evaluation of the transcriptional activation of *Myo7b* in the retina and the evaluation of the transcriptional activation approach in non-retinal murine tissues or organs.

The goal of the second part of this study was to develop a treatment strategy for gain-of-function mutation. This included i) providing a proof-of-principle for simultaneous transactivation and knockout of two different genes with Cas9-VPR in the murine retina, ii) optimising the transactivation efficiency of the sgRNAs, and iii) establishing a gene therapy in a gain-of-function $Rho^{P23H/+}$ mouse model using the optimised strategy.

The last part of the study aimed at the development of a gene independent therapy approach based on cellular reprogramming by gene knockdown and neuroprotection by transactivation of trophic factors. This strategy is to be optimised *in vitro* and to be applied to the $Rho^{P23H/+}$ mouse model.

3. Materials and Methods

3.1 Materials

All chemicals used in this study were obtained in "pro analysis" or "for molecular biological use" quality by VWR, Sigma-Aldrich, Merck, Bio-Rad, or Roth if not stated otherwise. Water was either obtained highly pure and deionised from the Milli-Q Plus System (Merck Millipore) purified with 18.2 MΩ x cm (25 °C) (ultra-pure water) or by distillation of deionised water with a distillation apparatus (Schott) followed by autoclaving (Vakulab PL, MMM Group) (sterile ultra-pure water). Solutions and buffers were sterilised by autoclaving or filtering through a 0.22 µm sterile syringe filter (VWR).

3.2 Cloning

3.2.1 Expression Vectors

For this study, the pAAV2.1 expression vector (Michalakis et al., 2010) was used for *in vitro* experiments and the production of rAAV vectors. The pAAV2.1 expression vector contains two AAV2 ITRs enclosing the desired transgene and a β-lactamase coding sequence for ampicillin resistance. In this study gene expression was driven by the cytomegalovirus promoter (CMV) for ubiquitous expression, a short rhodopsin promoter (RHO, Wagner et al. (2021)) for specific expression in rod photoreceptors and a short rhodopsin kinase promoter also known as G protein-coupled receptor kinase 1 promoter (GRK, Khani et al. (2007)) for photoreceptor-specific expression. As a termination signal, the simian virus 40 polyadenylation signal (SV40polyA) or a short synthetic polyadenylation signal (synpA) were used for efficient polyadenylation and increased transcript stability.

For efficient rAAV production, an additional plasmid containing the coding sequence for proteins necessary for replication (Rep) and packaging (Cap) of rAAVs in trans and an adenovirus helper plasmid (pAdhelper) are essential. The pAAV2/8Y733F plasmid was used for the expression of the AAV2 Rep and the AAV8 Cap for enhanced photoreceptor-specific transduction (Petrs-Silva et al., 2009). As an adenovirus helper the pAdDeltaF6 plasmid was used, a gift from James M. Wilson (Addgene plasmid # 112867).

The transactivation efficiency of the sgRNAs targeting the *Opn1mw* promoter region was tested in combination with the SP-dCas9-VPR plasmid, a gift from George Church (Addgene plasmid #63798, Chavez et al. (2015)).

Table 1: List of plasmids used in this study.

Plasmid name
pAAV2.1-3xsgMyo7b-CMV-5'dCas9-BDlacZ-SV40polyA
pAAV2.1-CMV-BDlacZ-3'dCas9-VPR-synpA
pAAV2/8Y733F
pAdhelper (pAdDeltaF6, Addgene plasmid #112867)
pAAV2.1-3xsgMYO7B-CMV-5'dCas9-BDlacZ-SV40polyA
pAAV2.1-3xsgMYO7B-GRK-5'dCas9-BDlacZ-SV40polyA
pAAV2.1-GRK-BDlacZ-3'dCas9-VPR-synpA
pAAV2.1-sgRho-2xsgOpn1mw(1-2)-RHO194-5'Cas9-BDlacZ-SV40polyA
pAAV2.1-sgRho-3xsgOpn1mw(1-3)-RHO194-5'Cas9-BDlacZ-SV40polyA
pAAV2.1-sglacZ-RHO194-5'Cas9-BDlacZ-SV40polyA
pAAV2.1-3xsgOpn1mw(1-3)-RHO194-5'Cas9-BDlacZ-SV40polyA
pAAV2.1-2xsgOpn1mw(1-2)-RHO194-5'Cas9-BDlacZ-SV40polyA
pAAV2.1-RHO194-BDlacZ-3'Cas9-VPR-synpA
SP-dCas9-VPR (Addgene plasmid #63798)
pAAV2.1-3xsgOpn1mw(1-3, 20 nt)-RHO194-dCas9N-IntN -SV40polyA
pAAV2.1-sgOpn1mw(1)-RHO194-5'Cas9-BDlacZ-SV40polyA
pAAV2.1-sgOpn1mw(2)-RHO194-5'Cas9-BDlacZ-SV40polyA
pAAV2.1-sgOpn1mw(3)-RHO194-5'Cas9-BDlacZ-SV40polyA
pAAV2.1-sgOpn1mw(4)-RHO194-5'Cas9-BDlacZ-SV40polyA
pAAV2.1-sgOpn1mw(5)-RHO194-5'Cas9-BDlacZ-SV40polyA
pAAV2.1-sgOpn1mw(6)-RHO194-5'Cas9-BDlacZ-SV40polyA
pAAV2.1-sgOpn1mw(1a)-RHO194-5'Cas9-BDlacZ-SV40polyA
pAAV2.1-sgOpn1mw(1b)-RHO194-5'Cas9-BDlacZ-SV40polyA
pAAV2.1-sgOpn1mw(1c)-RHO194-5'Cas9-BDlacZ-SV40polyA
pAAV2.1-sgOpn1mw(2a)-RHO194-5'Cas9-BDlacZ-SV40polyA
pAAV2.1-sgOpn1mw(2b)-RHO194-5'Cas9-BDlacZ-SV40polyA
pAAV2.1-sgOpn1mw(2c)-RHO194-5'Cas9-BDlacZ-SV40polyA
pAAV2.1-sgOpn1mw(3a)-RHO194-5'Cas9-BDlacZ-SV40polyA

Plasmid name
pAAV2.1-sgOpn1mw(3b)-RHO194-5'Cas9-BDlacZ-SV40polyA
pAAV2.1-sgOpn1mw(3c)-RHO194-5'Cas9-BDlacZ-SV40polyA
pAAV2.1-sgRho-3xsgOpn1mw(1,2,3a)-RHO194-5'Cas9-BDlacZ-SV40polyA
pAAV2.1-sgNrl(1)-RHO194-5'Cas9-BDlacZ-SV40polyA
pAAV2.1-sgNrl(2)-RHO194-5'Cas9-BDlacZ-SV40polyA
pAAV2.1-sgNxnl1(1)-CMV-5'Cas9-BDlacZ-SV40polyA
pAAV2.1-sgNxnl1(2)-CMV-5'Cas9-BDlacZ-SV40polyA
pAAV2.1-sgNxnl1(3)-CMV-5'Cas9-BDlacZ-SV40polyA
pAAV2.1-sgNxnl1(4)-CMV-5'Cas9-BDlacZ-SV40polyA
pAAV2.1-2xsgNxnl1(2-3)-CMV-5'Cas9-BDlacZ-SV40polyA
pAAV2.1-2xsgNxnl1(3-4)-CMV-5'Cas9-BDlacZ-SV40polyA
pAAV2.1-sgNxnl2(1)-CMV-5'Cas9-BDlacZ-SV40polyA
pAAV2.1-sgNxnl2(2)-CMV-5'Cas9-BDlacZ-SV40polyA
pAAV2.1-CMV-BDlacZ- 3'Cas9-VPR-synpA
pAAV2.1-sgNrl(1)-2xsgNxnl1(3-4)-sgNxnl2(1)-GRK-5'Cas9-BDlacZ-SV40polyA
pAAV2.1-GRK-BDlacZ- 3'Cas9-VPR-synpA

3.2.2 Standard Cloning Techniques

Cloning was either performed using classical restriction cloning or the restriction site-independent Gibson assembly (Gibson et al., 2009). Genes of interest e.g., inserts, were obtained by restriction digest, PCR, oligo annealing, or synthesised by commercial providers (e.g., Integrated DNA technologies IDT, eurofins genomics, or BioCat GmbH). For restriction digest, fast digest restriction enzymes (Thermo Fisher Fermentas) were used to obtain insert and vector (see table below for reaction mix).

Thermo Fisher Fast Digest restriction mix	
Plasmid	3 µg
FD Green Buffer	2 µl
FD Restriction enzyme	each 0.5 µl
Ultra-pure water	to 20 µl

The different fragments were separated by gel electrophoresis using 0.7 – 2 % agarose gels. The desired band was excised from the gel and purified using the QIAquick gel extraction kit (Qiagen). DNA concentration was determined using the NanoDrop 2000c spectrophotometer (Thermo Fisher Scientific). For ligation, either the T4 Ligase (Thermo Fisher Scientific) or the Rapid DNA Dephosphorylation and Ligation Kit (Roche) were used.

For Gibson cloning the insert and vector were designed to contain 15 – 25 bp overhangs complementary to the vector backbone. For the reaction, a self-made Gibson reaction mix was used. The vector, obtained by restriction digest, and the inserts were added to 15 µl of Gibson reaction mix in a 1:1-10 ratio (preferably 1:5) and incubated for 1 h at 50 °C.

Gibson reaction mix

1M Tris-HCl, pH 7.5	160 µl
1M $MgCl_2$	16 µl
dNTP Mix, 10 mM each	32 µl
1M DTT	16 µl
PEG-8000	80 mg
Nicotinamide adenine dinucleotide	1.06 mg
T5 Exonuclease	1.2 µl
Phusion polymerase	20 µl
Taq ligase	160 µl
Ultra-pure water	to 700 µl

For transformation 5 µl ligation mix or 4 µl Gibson cloning mix were added to 100 µl freshly thawed suspension of competent 10-beta Escherichia coli K12 bacterial cells (New England BioLabs) and incubated for 30 min on ice. Heat shock was performed by 30 s incubation at 42 °C in a Thermomixer compact (Eppendorf) followed by 2 min incubation on ice. The bacteria were then plated onto an LB(+)-agarose plate containing 100 µg/ml of ampicillin. The plates were incubated overnight in a 37 °C incubator (Heraeus, Thermo Fisher Scientific) or for 2 days at room temperature (21 °C).

For mini plasmid DNA preparation single bacteria colonies were inoculated in 5 ml LB(+)-medium supplemented with 100 µg/ml ampicillin at 37 °C in a shaking incubator (Certomat IS, B. Braun Biotech International) overnight. Plasmid DNA was extracted using a protocol

based on alkaline lysis. Correct plasmids were identified by restriction digest followed by gel electrophoresis and sequenced to confirm the correct incorporation of the insert.

LB(+) medium	
Peptone	10 g
Yeast extract	5 g
NaCl	5 g
D-(+)-Glucose	1 g
Ultra-pure water	to 1000 ml

LB(+) agar plate	
Agar	7.5 g
Ampicillin (added after autoclaving)	50 mg
LB(+) medium	to 500 ml

For midi and maxi preparation, the desired bacterial colonies were incubated in 100 ml or 200 ml LB(+) medium containing 100 µg/ml ampicillin, respectively. The plasmid DNA was isolated and purified using the PureLink™ HiPure Plasmid Midiprep or Maxiprep Kit (Invitrogen, Thermo Fisher Scientific).

The correct sequences for all plasmids were verified using sanger sequencing (eurofins genomics). The ITR integrity of pAAV2.1 plasmids was checked by two restriction digests with Eam1105I or SmaI (Thermo Fisher Scientific). The correct band pattern was identified by gel electrophoresis with 0.7 % agarose gels.

ITR integrity restriction digest	
Plasmid	2 µl
FD Green Buffer	2 µl
FD Eam1105I or FD SmaI	0.3 µl
Ultra-pure water	to 20 µl

3.3 Single Guide RNA Design

Single guide RNAs were designed with help of the CRISPOR software (crispor.tefor.net) for *Sp*Cas9. For gene activation sgRNAs were designed to target the region from -300 bp to 0 bp relative to the transcriptional start site (TSS) of the gene of interest. For gene activation with a catalytically active Cas9-VPR a spacer length of 14-15 nt was used otherwise the spacer length was 20 nt. The first three sgRNAs targeting the *Opn1mw* promoter region were shortened versions of the sgRNAs published in Bohm et al. (2020). The first sgRNA spacer for the knockout of *Nrl* was already tested and published in W. Yu et al. (2017). The second

was designed with help of the VBC score software (Ulrich Elling - Institute of Molecular Biotechnology).

The expression of the sgRNAs was driven by a human U6 promoter. If the spacer sequence did not start with Guanine, it was added in front of the spacer sequence to the final construct as a transcriptional start site for the U6 promoter.

Table 2: sgRNA spacer sequences

sgRNA	**Spacer sequence**	**Target and purpose**
sgMyo7b(1)	AGACTCCAAGAACGCCAGTC	Transcriptional activation of *Myo7b* with dCas9-VPR
sgMyo7b(2)	GGGCACCATTAACCACTGCT	Transcriptional activation of *Myo7b* with dCas9-VPR
sgMyo7b(3)	GGAAGGGCTCCAAGCGGAAC	Transcriptional activation of *Myo7b* with dCas9-VPR
sgRho	GTACGGTGACGTAGAGCGTG	*Rho* exon 1, Knockout of *Rho* with Cas9-VPR
sgOps(1)	GGGGCCTTTAAGGTA	Transcriptional activation of *Opn1mw* with Cas9-VPR
sgOps(2)	GCCACCCCTGTGGAT	Transcriptional activation of *Opn1mw* with Cas9-VPR
sgOps(3)	CTTGCTTGTTTACAA	Transcriptional activation of *Opn1mw* with Cas9-VPR
sgOps(4)	GTCCTGTAACCCCAT	Transcriptional activation of *Opn1mw* with Cas9-VPR
sgOps(5)	GATGATCTAAGTCCT	Transcriptional activation of *Opn1mw* with Cas9-VPR
sgOps(6)	CTGCAGGATCAGCCC	Transcriptional activation of *Opn1mw* with Cas9-VPR
sgOps(1a)	TCTTAATTGGGCCC	Transcriptional activation of *Opn1mw* with Cas9-VPR
sgOps(1b)	GGTGAAGGGTTTGG	Transcriptional activation of *Opn1mw* with Cas9-VPR

sgRNA	Spacer sequence	Target and purpose
sgOps(1c)	AGATCAGATGGTGA	Transcriptional activation of *Opn1mw* with Cas9-VPR
sgOps(2a)	TGGACTCAGAAACA	Transcriptional activation of *Opn1mw* with Cas9-VPR
sgOps(2b)	CTGAGCCACCCCTG	Transcriptional activation of *Opn1mw* with Cas9-VPR
sgOps(2c)	CACAGGGGTGGCTC	Transcriptional activation of *Opn1mw* with Cas9-VPR
sgOps(3a)	CTGCAAGCCAGGAA	Transcriptional activation of *Opn1mw* with Cas9-VPR
sgOps(3b)	CCCTACTGCAAGCC	Transcriptional activation of *Opn1mw* with Cas9-VPR
sgOps(3c)	TCCTGGCTTGCAGT	Transcriptional activation of *Opn1mw* with Cas9-VPR
sgNrl(1)	GTATGGTGTGGAGCCCAACG	*Nrl* exon 3, Knockout of *Nrl* with Cas9-VPR
sgNrl(2)	GATGAAGTTCGAAATAAAGC	*Nrl* exon 3, Knockout of *Nrl* with Cas9-VPR
sgNx1(1)	CAGAGCCAGAATTG	Transcriptional activation of *Nxnl1* with Cas9-VPR
sgNx1(2)	GGTATTATTCTTGG	Transcriptional activation of *Nxnl1* with Cas9-VPR
sgNx1(3)	TCACTGCAAGACCC	Transcriptional activation of *Nxnl1* with Cas9-VPR
sgNx1(4)	GTTGAAGGTTCATG	Transcriptional activation of *Nxnl1* with Cas9-VPR
sgNx2(1)	AGTCCGGACATCCG	Transcriptional activation of *Nxnl2* with Cas9-VPR
sgNx2(2)	AGATTCTCCAAGGG	Transcriptional activation of *Nxnl2* with Cas9-VPR

3.4 Cell Culture and Transfection

3.4.1 HEK293 and HEK293T Cells

Human embryonic kidney 293 (HEK293) (DMSZ) were maintained in DMEM culture medium (1 g/l glucose + GlutaMAX supplement + pyruvate, Gibco) + 10 % FBS + 1 % penicillin/streptomycin (Biochrom) and HEK293T cells (DMSZ) in DMEM culture medium (4.5 g/l glucose + GlutaMAX supplement, Gibco) + 10 % FBS + 1 % penicillin/streptomycin (Biochrom) in a CO_2 incubator (Heraeus, Thermo Fisher Scientific) at 10 % CO_2 and 37 °C. The cells were passaged twice per week before they reached 100 % confluency.

Transient transfection of HEK293 cells was performed using the calcium phosphate technique (Kingston et al., 2003). The following reagents were added in the indicated order. 2x BBS was added while vortexing.

Transfection mix	**6-well plate**	**6 cm dish**
Plasmid DNA	3 µg	6 µg
2.5 M $CaCl_2$	30 µl	60 µl
Sterile ultra-pure water	to 300 µl	to 600 µl
2x BBS	300 µl	600 µl

The transfection mix was incubated for 3 min at room temperature before the reaction mix was added dropwise to the cells. To distribute the transfection mix, the plates were gently rocked back and forth. Afterwards, the cells were placed into a CO_2 incubator at 5 % CO_2 and 37 °C for 4 – 16 h. The transfection media was removed and replaced by fresh medium. The cells were placed back into a CO_2 incubator at 10 % CO_2 and 37 °C. The cells were harvested 48-72 h after transfection.

3.4.2 661W Cells

661W cells, an immortalised cone photoreceptor cell line, were kindly provided by M. Al-Ubaidi, University of Houston, Houston, TX. 661W cells were used to evaluate sgRNAs *in vitro*. The cells were maintained in DMEM culture medium (1 g/l glucose + GlutaMAX supplement + pyruvate, Gibco) + 10 % FBS + 1 % antibiotic/antimycotic (Thermo Fisher Scientific) in a CO_2 incubator (Heraeus, Thermo Fisher Scientific) at 5 % CO_2 and 37 °C and passaged twice per week before they reached 100 % confluency.

For transfection of 661W cells, the Xfect transfection reagent (Takara Bio) was used. Cells were seeded at a density of 2 x 10^5 cells per well in a 6-well plate. The culture media was reduced to 1 ml in each well before transfection. The plasmid DNA was first diluted in Xfect transfection buffer and then thoroughly vortexed Xfect reagent was added. The mix was vortexed for 10 s and incubated for 10 min at room temperature.

Xfect transfection mix	
Plasmid DNA	7.5 µg
Xfect transfection buffer	to 100 µl
Xfect transfection reagent	2.25 µl

100 µl of transfection mix were added dropwise to the cells and the plates were rocked back and forth to distribute the transfection mix evenly in the culture medium. Subsequently, the plate was put back in the 5 % CO_2 incubator. Transfection medium was replaced by fresh medium after 4 – 16 h. The cells were harvested 48-72 h after transfection.

3.4.3 Mouse Embryonic Fibroblasts

Mouse embryonic fibroblasts (MEF) were isolated according to a previously described protocol (Jat et al., 1986; Xu, 2005). MEFs were maintained in DMEM culture medium (1 g/l glucose + GlutaMAX supplement + pyruvate, Gibco) + 10 % FBS + 1 % antibiotic/antimycotic (Thermo Fisher Scientific) in a CO_2 incubator (Heraeus, Thermo Fisher Scientific) at 5 % CO_2 and 37 °C. The cells were passaged twice per week before they reached 100 % confluency.

For transfection, the Xfect transfection reagent was used. MEFs were seeded at a density of 1.5 x 10^5 cells per well in a 6-well plate. The transfection was performed under the same conditions as described for the 661W cells.

3.4.4 Mouse Hippocampal Primary Neurons

Mouse hippocampal primary neurons were isolated according to the protocol described in Fath et al. (2009). The primary neurons were maintained in Neurobasal medium (Gibco)

supplemented with 2 % B27 (Gibco) and 0.25 % GlutaMAX supplement (Gibco) in a CO2 incubator (Heraeus, Thermo Fisher Scientific) at 5 % CO2 and 37 °C.

Transduction was performed after seven days in vitro by adding 7.5 x 10^{10} vector genomes (vg) rAAVs (MOI: 100,000) directly to the media in each well and the primary neurons were harvested seven days after transduction for RNA isolation.

3.4.5 Human Retinal Organoids

Human retinal organoids were differentiated and cultured according to the protocol described in Quinn et al. (2018) in the Wijnholds lab at Leiden University Medical Centre. Human retinal organoids after differentiation day 98 (DD98) were maintained in Retinal Lamination Medium 2 at 5 % CO2 and 37 °C.

Retinal Lamination Medium 2

DMEM culture medium (4.5 g/l glucose + GlutaMAX supplement + pyruvate, Gibco)	53.625 ml
DMEM/F12 (Gibco)	53.625 ml
embryonic stem cell qualified FBS (Gibco)	12.5 ml
50x B27 Supplement (Gibco)	2.5 ml
100x MEM Non-Essential Amino Acids (Gibco)	1.25 ml
100x antibiotic–antimycotic	1.25 ml
50 mM taurine	0.25 ml
10 mM all-trans retinoic acid	6.25 µl

For transduction, the retinal organoids were transferred into an agarose-coated 96-well plate. Transduction was performed at DD146 by reducing the culture medium to 25 µl and adding 1.09 x 10^{12} vg rAAVs in 25 µl culture medium to the retinal organoids. After 8 h 150 µl culture medium was added to each well. After 24 h the retinal organoids were transferred to an agarose-coated 24-well plate The medium was changed every 2-3 days. Human retinal organoids were harvested three weeks after transduction.

3.5 Recombinant Adeno-Associated Viral Vector Production

3.5.1 Transfection and Harvest

Recombinant adeno-associated viral vectors (rAAV) were produced by polyethyleneimine (PEI)-transfection of a pAAV2.1 plasmid containing the gene of interest, the pAAV2/8Y733F plasmid, and a pAdhelper plasmid into HEK293T cells. HEK293T cells were seeded one day before transfection at a density of 1.5 x 10^6 cells per plate to 15 x 15 cm plates (Greiner BIO-ONE). Before transfection, the FBS-containing medium was exchanged with 18 ml serum-free medium.

For transfection, the plasmid DNA was diluted in serum-free medium to obtain the DNA mix. The PEI 20-reagent (1 mg/ml polyethyleneimine hydrochloride (average M_n 20,000) in sterile ultra-pure water, pH 6.95) was vortexed thoroughly and added to serum-free medium. The PEI mix was vortexed for 5 s before it was added to the DNA mix. The transfection mix was vortexed again for 10 s. The transfection mix was incubated for 15 min before 900 µl of the mix were added dropwise to each 15 ml plate. Finally, the transfection mix was distributed equally by gently rocking the plates back and forth. The cells were put back into the 10 % CO_2 incubator.

DNA mix	
AAV2 vector plasmid	81 µg
pAAV2/8Y733F plasmid	X µg
pAdhelper plasmid	Y µg
Serum-free medium	to 6750 µl

PEI mix	
PEI 20-reagent	2 µl per µg total DNA
Serum-free medium	to 6750 µl

To calculate the acquired amounts of pAdhelper and AAV capsid plasmid the following calculations were used.

$$\text{X µg of AAV8Y733F plasmid} = \frac{81\ \text{µg x } 4522.84\ \text{g/mol}}{\text{Molar weigth AAV2 vector plasmid}}$$

$$\text{Y µg of pAdhelper plasmid} = \frac{81\ \text{µg x } 9509.36\ \text{g/mol}}{\text{Molar weigth AAV2 vector plasmid}}$$

The cells were harvested 72 h after transfection with a cell scraper (Sarstedt) and collected with the medium in a 500 ml centrifugation bottle (Nalgene™ Polycarbonate Centrifuge Bottles with Sealing Closure, Thermo Fisher Scientific). The cell-containing medium was

centrifuged at 4000 x *g* for 15 min at 4 °C to separate the cells from the medium. The supernatant was filtered through a 0.45 µm polyethersulfone (PES) filter (VWR) and a 40 % Polyethylene glycol 8000 (PEG) solution was added. The amount of PEG solution was calculated using the following formula:

$$\text{volume of 40 \% PEG solution} = \frac{\text{weight of supernatant [g] x 0.08}}{0.32}$$

Subsequently, the solution was incubated for 72 h at 4 °C to precipitate the containing rAAVs. The cell pellet was resolved in 7.5 ml lysis buffer, transferred into a 50 ml tube (Labcon), frozen in liquid nitrogen, and thawed again in a 37 °C water bath (Thermo Fisher Scientific). This freeze-thaw cycle was reaped twice. The frozen cell-pellet lysis buffer mix was stored at -80 °C until further processing.

Lysis buffer

5 M NaCl	1.5 ml
1 M Tris-HCl, pH 8.5	2.5 ml
Sterile ultra-pure H_2O	to 50 ml

After incubation, the PEG-medium mix was centrifuged at 4000 x *g* for 15 min at 4 °C. The supernatant was discarded, and the pellet was resuspended in the cell-pellet lysis buffer mix. To remove the contained plasmid DNA the solution was incubated with 50 U/ml Benzonase (Merck) for 30 min in a 37 °C water bath. After incubation, the solution was centrifuged at 4000 x *g* for 20 min at 4 °C. The supernatant was transferred into a new 50 ml tube and centrifuged again at 4000 x *g* for 20 min at 4 °C. The resulting supernatant was further proceeded by iodixanol gradient centrifugation.

3.5.2 Iodixanol Gradient Centrifugation

Iodixanol gradient centrifugation was performed to isolate the rAAV particles. The supernatant was transferred into a Quick-Seal Polypropylene tube (Beckman). Using a peristaltic pump (Miniplus3 peristaltic pump, Gilson) and a sterile long glass Pasteur pipette (VWR) a density gradient was established by carefully adding 7 ml 15 %, 5 ml 25 %, 5 ml 40 %, and 6 ml 60 % iodixanol solution below the rAAV containing solution. The Quick-seal polypropylene tubes were sealed with the Beckman tube topper (Beckman) and

centrifuged at 50,000 x *g* for 1 h 45 min at 17 °C in an optima LE-80K ultracentrifuge (Beckman Coulter) with the 70 Ti rotor (Beckman). Afterwards, the 40 % iodixanol phase containing the rAAV particles was collected by inserting a 20 ml syringe (B.Braun) with a 20-gauge cannula (VWR) into the 40 % iodixanol phase with the needle bevel facing upwards and collecting about 4 ml solution. The rAAV-containing solution was stored at 4 °C until further processing.

Iodixanol solutions	**15 %**	**25 %**	**40 %**	**60 %**
10x phosphate-buffered saline (PBS)	5 ml	5 ml	5 ml	-
1 M $MgCl_2$	50 µl	50 µl	50 µl	50 µl
2.5 M KCl	50 µl	50 µl	50 µl	50 µl
5 M NaCl	10 ml	-	-	-
OptiPrep™ (Progen)	10 ml	20.9 ml	33.3 ml	50 ml
Phenol red (1 %, w/v)	37.5 µl	50 µl	-	35.5 µl
Sterile ultra-pure H_2O	to 50 ml	to 50 ml	to 50 ml	-

3.5.3 Anion Exchange Chromatography

The rAAV-containing solution was further purified by anion exchange chromatography. For this purpose, a HiTrap QFF 5 ml anion exchange column (GE Healthcare) and the ÄKTAprime plus system (GE Healthcare) with loop injector (50 ml superloop, GE Healthcare) were used. After assembling the ÄKTA prime system the pressure limit was set to 0.5 MPa and the column was equilibrated using buffer A until the values for the ultraviolet (UV) absorbance at 280 nm and the conductivity coefficient were constant. The rAAV-containing solution was diluted with buffer A in a 1:1 ratio and added to the loop injector. The sample was then loaded onto the column with a flow rate of 1.0 ml/min and fractions of 1 ml were collected. The absorbance and conductivity were monitored. The fractions with high UV absorbance, indicating the presence of rAAV particles, were collected. After the UV absorbance and conductivity went down again, indicating that all rAAV particles passed through the system, the column was regenerated with 2.5 M NaCl solution. Before the next

rAAV-containing solution was loaded, the system was washed with sterile, ultra-pure water. The rAAV containing aliquots were combined and stored at 4 °C until further processing.

Buffer A, pH 8.5

Tris	1.2 g
NaCl	0.44 g
Sterile ultra-pure H_2O	to 500 ml

3.5.4 Increasing rAAV Concentration

Amicon Ultra-4 centrifugation filter units (Merck) were used to increase the rAAV concentration. These steps were performed under laminar airflow to avoid contamination of the rAAV solution. First, the rAAV solution obtained from Anion exchange chromatography was supplemented with 0.001 % Tween, to avoid adsorption of rAAV particles to the filter unit, and syringe filtered through a 0.2 µm sterile PES filter (VWR). 4 ml of the filtered rAAV solution were added on top of the Amicon filter unit and centrifuged at 3000 x *g* for 5 min at room temperature. The flow-through was discarded and equal amounts of rAAV solution were added again on top of the filter unit. This step was repeated until the volume of the rAAV solution was reduced to 500 µl. The filter was washed with 1 ml 0.001 % Tween/PBS-MK solution followed by centrifugation at 3000 x *g* for 1-2 min at room temperature until the volume was reduced to 100 µl. The rAAV solution was split up into 10 µl aliquots. The aliquots were stored at -80 °C.

0.001 % Tween/PBS-MK solution

10x PBS	5 ml
1 M $MgCl_2$	50 µl
2.5 M KCl	50 µl
Tween 20	0.5 µl
Sterile ultra-pure water	to 50 ml

3.5.5 rAAV Titer Determination

Quantitative real-time PCR (qPCR) was used to determine the rAAV titer. A standard curve was established based on a serial dilution of a fragment containing the AAV2 ITR. The fragment was obtained by restriction digest of a pAAV2.1 plasmid with the restriction

enzymes FD XhoI and AdeI (Thermo Fisher Scientific). The desired band was purified by gel electrophoresis and the concentration was obtained with a NanoDrop 2000c (Thermo Fisher Scientific). The DNA concentration necessary for the standard solutions, containing 10^9 - 10^5 copies of the AAV2 ITR fragment, was calculated using the following formula.

$$c(10^X \text{ copies})[\frac{\text{ng}}{\mu\text{l}}] = \frac{10^X \times 660 \times 10^9 \frac{\text{ng}}{\text{mol} \times \text{bp}} \times \text{fragment size [bp]}}{N_A \times 2.5\ \mu\text{l}}$$

$$N_A\ (Avogadro\ constant) = 6.022 \times 10^{23} \frac{1}{mol}$$

A qPCR was performed with triplicates of the standard solutions and a 1:100000 dilution of the rAAV sample. To set up the qPCR reaction MicroAmp™ Fast Optical 96-well Reaction Plate (Applied Biosystems, Thermo Fisher Scientific), the PowerUp™ SYBR™ Green Master Mix (Thermo Fisher Scientific) and primer amplifying a region of the AAV2 ITR were used.

ITR2 forward: 5' GGAACCCCTAGTGATGGAGTT3'

ITR2 reverse: 5' CGGCCTCAGTGAGCGA 3'

The reaction mix was prepared as follows.

qPCR reaction mix	
PowerUp™ SYBR™ Green Master Mix	5 µl
ITR2 forward (4 µM)	0.5 µl
ITR2 reverse (4 µM)	0.5 µl
rAAV dilution or standard solution	2.5 µl
Sterile ultra-pure H_2O	1.5 µl

The qPCR was run on the QuantStudio™ 5 Real-Time PCR system (Thermo Fisher Scientific) under the following conditions.

Step	Number of cycles	Temperature	Duration
Uracil-DNA Glycosylase activation	1	50 °C	2 min
Hot-Start DNA Polymerase activation	1	95 °C	5 min
Denaturation	40	95 °C	5 s
Annealing		58 °C	5 s
Elongation		60 °C	30 s
Melt curve acquisition	1	95 °C	15 s
	1	60 °C	1 min
	1	Ramp to 95 °C (+ 0.3 °C/s)	2 min
	1	95 °C	15 s

The data was analysed using the QuantStudio™ Design & Analysis software (Thermo Fisher Scientific) the number of vg contained in the dilution of the rAAV sample could be inferred from the obtained standard curve.

3.6 Animals

All animal experiments in this study were performed in accordance with the German laws on animal welfare (Tierschutzgesetz) and with the permission of the local authorities (District Government of Upper Bavaria). For this study C57BL/6J wild-type as well as *Rho*$^{P23H/+}$ mice (B6.129S6(Cg)-*Rho*$^{tm1.1Kpal}$/J, The Jackson Laboratory), a mouse model for autosomal dominant retinitis pigmentosa carrying the P23H mutation in rhodopsin, were used. Mice were bred in-house and maintained in a 12 h light/dark cycle. Food (Ssniff; regular feed: R/M-H; breeding feed: M-Z Extrudat) and water was provided ad libitum. Mice were anaesthetised with isoflurane and euthanised for retina and organ isolation by cervical dislocation and for hippocampi isolation by decapitation. P0 pups used for hippocampal primary neuron culture were euthanised by decapitation.

3.6.1 Subretinal Injection

Mice were anaesthetised by intraperitoneal injection of 0.01 mg/g body weight ketamine (Medistar) and 0.02 mg/g body weight xylazine (Xylariem, Ecuphar). During anaesthesia, they were kept on a 37 °C heating plate (Leica Biosystems). Pupils were dilated using 0.5 % tropicamide eye drops (Mydraticum Stulln, Pharma Stulln). After the total absence of the paw withdrawal reflex subretinal injection was performed. The virus was drawn into a Nanofil 10 µl syringe (World Precision Instruments) with a 34-gauge bevelled needle (World Precision Instruments). The fundus of the mouse eye was focused using a surgical microscope (OPMI 1 FR pro, Zeiss). The needle was held at a 30° angle with the needle bevel facing away from the eye while sclera, choroid, and pigment epithelium were penetrated. The correct needle position below the retina was confirmed using the surgical microscope. 1 µl of titer-matched viral solution ($4.71 \times 10^{10} – 6 \times 10^{11}$ vg/µl) was injected into the subretinal space. Successful injections were confirmed by the formation of a subretinal bleb. The needle was slowly removed from the eye. Afterwards, the eyes were treated with 0.3 mg/g dexamethasone and 5 mg/g gentamycin containing eye ointment (Dexamytrex, Bausch + Lomb). When the injections were performed with mice at postnatal day 21 (P21) or younger, the pups were put back into the parental cage after recovery from anaesthesia.

3.6.2 Stereotactic Injection

Mice at P30 were anaesthetised by intraperitoneal injection of 0.01 mg/g body weight ketamine (Medistar) and 0.02 mg/g body weight xylazine (Xylariem, Ecuphar). After the total absence of the paw withdrawal reflex, the mice were fixed in sternal recumbence in the stereotactic apparatus (Neurostar GmbH). Bregma and lambda were identified after uncovering the skull and used as a reference for the calibration of the Neurostar software (Neurostar GmbH). The coordinates used for inserting the needle into the hippocampi were ML ± 1.4, AP -2.06, and DV 1.4. Titer-matched rAAV vectors (3.77×10^{10} vg in 0.8 µl) were injected into the hippocampus at a flow rate of 0.3 µl/min. After the injection, the animals were removed from the stereotactic apparatus and the scalp was sutured. During anaesthesia, the eyes were covered with Bepanthen eye ointment (Bayer), and the mice were kept on a 37 °C heating plate. The hippocampi were harvested four weeks after injection.

3.6.3 Intraperitoneal Injection

C57BL/6J wild-type mice were injected at P7 with 10 µl titer-matched viral solution (4 x 10^{10} vg/µl). Organs were isolated 5 weeks after injection.

3.6.4 Electroretinogram Measurements

Full-field ERG measurements were performed using the Celeris system (Diagnosys LLC). For scotopic measurements, the mice were kept for 16 h under dark conditions. The mice were anaesthetised by intraperitoneal injection of 0.02 mg/g body weight ketamine and 0.04 mg/g body weight xylazine. After 5 min 0.5 % tropicamide eye drops were applied to dilate the pupils. ERG measurements were performed when the pupils were fully dilated (10 min after application of mydriatic eyedrops). To keep the eyes moist and ensure contact of the eye with the ERG stimulator containing the light-guided electrodes during the recordings 2 % Hypromellose eyedrops (Methocel, OmniVision) were applied. Scotopic responses were obtained for single light flashes at intensities of 0.003 (blue light, 455 nm), 0.01, 0.03, 0.1, 0.3, 1, 3 and 10 cd.s/m² (all remaining intensities 6500 K white light). For photopic measurements, the mice were light-adapted with 3 cd/m² for 5 min. Photopic responses were recorded for single light-flashes at intensities of 0.01, 0.03, 0.1, 0.3, 1, 3 and 10 cd.s/m². All photopic recordings were performed with constant 9 cd/m² background illumination. Measurements were recorded from 50 ms before stimulus onset to 300 ms post-stimulus and the voltage signals were sampled at 1 Hz. Flicker ERG recordings were recorded for single light flashes at 3 cd.s/m^2 with a frequency of 10 HZ and constant 9 cd/m² background illumination. Five (scotopic) or ten (photopic) sweeps were averaged for every recording. After the measurement, Bepanthen eye ointment (Bayer) was applied to the eyes and the mice were kept on a 37 °C heating plate until full recovery from anaesthesia. Analysis was performed using the Espion V6 software (Diagnosys LLC).

3.6.5 Optical Coherence Tomography

Retinal morphology was evaluated by OCT using a modified Spectralis HRA + OCT system (Heidelberg Engineering) in combination with contact lenses. Mice were anaesthetised by intraperitoneal injection of 0.02 mg/g body weight ketamine and 0.04 mg/g body weight xylazine and pupils were dilated using mydriatic eyedrops. 2 % Hypromellose eye drops were applied to keep the eyes moist during the experiments. 31 scans per eye were obtained

in high-resolution mode with a 30° angle. ONL thickness was measured between the outer plexiform layer and the external limiting membrane. Mean ONL thickness was calculated from six values from two different scans in the injection area.

3.7 RNA Isolation

For this study RNA was isolated from mouse and human cell lines, human retinal organoids as well as mouse tissue.

For RNA isolation from cells, transfected and control cells were harvested 48 to 72 h after transfection. Transduced mouse primary hippocampal neurons were harvested seven days after transduction. The cell media was removed, and the cells were washed with PBS. 350 µl or 600 µl RLT plus buffer (Qiagen) supplemented with 10 µl/ml β-mercaptoethanol was added to each well of a well plate or 6 cm dish, respectively. The cells were incubated for 2-3 min at room temperature while the plate was tilted from side to side to ensure even distribution of the lysis buffer. The cells were collected in the lysis buffer and transferred into safe-lock tubes (Eppendorf). They were disrupted in a mixer mill (Retsch) at 30 Hz for 1 min. The stainless-steel balls (Retsch) were removed, and the samples were centrifuged at 21,000 x *g* for 5 min. RNA was isolated using the RNeasy plus Mini Kit (Qiagen) according to the manufacturer's protocol.

For RNA isolation from human retinal organoids, harvested organoids were frozen in liquid nitrogen. 400 µl TRI reagent (Zymo) was added to two organoids into a safe-lock tube. The organoids were disrupted with stainless-steel balls in a mixer mill at 30 Hz for 1 min. The RNA was isolated using the Direct-zol™ DNA/RNA Miniprep (Zymo) according to the manufacturer's instructions. An on-column DNA digest using the DNase I Set (Zymo) was performed to ensure no contamination with genomic or AAV DNA.

For RNA isolation from murine tissue, mice were anaesthetised with isoflurane and sacrificed by cervical dislocation. Organs were isolated from the mice using surgical tools, washed with PBS, and subsequently frozen in liquid nitrogen. For retina isolation, the eyes were opened with a scalpel and the vitreous body was removed. Using blunt forceps, the retina was separated from the remaining eye cup and frozen in liquid nitrogen. RNA was isolated from the tissues using different RNA isolation kits (see Table 3). For disruption and homogenization of the tissues, the mixer mill with a stainless-steel ball in each tube was used. Heart, liver, and brain tissue were disrupted with the mixer mill at 30 Hz for 30 s before

the amount of tissue for RNA isolation was taken from the sample. After disruption, the stainless-steel ball was removed, and the RNA was isolated according to the manufacturer's protocol of the corresponding RNA isolation kit.

Table 3: RNA isolation from mouse tissue

Tissue	Kit used for RNA isolation	Amount tissue	Volume lysis buffer	Conditions mixer mill	Volume for RNA Isolation
Retina	RNeasy plus Mini Kit (Qiagen)	One retina (~ 30 mg)	350 µl	2 x 2 min, 20 Hz	350 µl
Hippocampus	RNeasy plus Mini Kit (Qiagen)	One hippocampus (~ 30 mg)	350 µl	2 x 2 min, 20 Hz	350 µl
Heart	RNeasy plus Mini Kit (Qiagen)	~ 30 mg	350 µl	2 x 2 min, 30 Hz	350 µl
Skeletal muscle	RNeasy Fibrous Tissue Mini Kit (Qiagen)	25 – 50 mg	300 µl	2 x 2 min, 30 Hz	300 µl
Liver	RNeasy plus Mini Kit (Qiagen)	~ 30 mg	600 µl	2 x 2 min, 30 Hz	600 µl
Brain	Direct-zol™ DNA/RNA Miniprep (Zymo)	25 mg	800 µl	2 x 1 min, 30 Hz	800 µl
Lung	RNeasy plus Mini Kit (Qiagen)	~ 150 mg	600 µl	2 x 2 min, 30 Hz	120 µl

After RNA isolation the RNA concentration was measured using the NanoDrop 2000c UV spectrophotometer (Thermo Fisher Scientific). RNA was kept on ice until further processing or stored at -80 °C.

3.8 cDNA Synthesis

cDNA synthesis was performed using the RevertAid First Strand cDNA Synthesis Kit (Thermo Fisher Scientific) according to the manufacturer's protocol. For the synthesis both Random Hexamer and Oligo(dT)$_{18}$ primers were added to the reaction. Between 17-5000 ng RNA were used for RNA obtained from cells and 200-5000 ng for RNA obtained from mouse tissue. A control without the reverse transcriptase was included for every experiment.

3.9 Quantitative Reverse Transcription PCR

To estimate the transactivation efficiency of the sgRNAs quantitative revere transcription PCR (qRT-PCR) was used. Primers for qRT-PCR were designed with the primer-BLAST software (U. S. National Centre for Biotechnology Information) (Ye et al., 2012) to generate a 90-150 bp amplicon and include an intron on the corresponding genomic DNA (gDNA), to prevent amplification of gDNA.

The qRT-PCR was performed with duplicates of each sample diluted with RNase-free water in a 1:5 ratio. To set up the qRT-PCR reaction MicroAmp™ Fast Optical 96-well Reaction Plate (Applied Biosystems, Thermo Fisher Scientific) and the PowerUp™ SYBR™ Green Master Mix (Thermo Fisher Scientific) were used. The reaction mix was prepared as follows.

qRT-PCR reaction mix

PowerUp™ SYBR™ Green Master Mix	10 µl
Primer forward (10 µM)	0.6 µl
Primer reverse (10 µM)	0.6 µl
Sample (diluted 1:5)	5 µl
RNase-free water	3.8 µl

The qRT-PCR was run on the QuantStudio™ 5 Real-Time PCR system (Thermo Fisher Scientific) under the following conditions.

Step	Number of cycles	Temperature	Duration
Uracil-DNA Glycosylase activation	1	50 °C	2 min
Hot-Start DNA Polymerase activation	1	95 °C	2 min
Denaturation	40	95 °C	3 s
Annealing		58 °C	5 s
Elongation		60 °C	25 s
Melt curve acquisition	1	95 °C	15 s
	1	60 °C	1 min
	1	Ramp to 95 °C (+ 0.3 °C/s)	2 min
	1	95 °C	15 s

The data was analysed using the QuantStudio™ Design & Analysis software (Thermo Fisher Scientific). The baseline and threshold settings were corrected if necessary. To evaluate the relative fold change in mRNA expression to the control group (e.g., untransfected cells) the comparative Ct method ($2^{-\Delta\Delta Ct}$ method) (Schmittgen & Livak, 2008) was used.

The Ct value was normalised to a housekeeping gene (i.e., *Alas*).

$$\Delta Ct = Ct_{target} - Ct_{housekeeping}$$

The fold changes were obtained with the following equation (delta delta Ct analysis).

$$\Delta\Delta Ct = \Delta Ct - \text{Mean}\ (\Delta Cts\ \text{of all replicates of control group})$$

$$\text{Relative expression to reference sample} = 2^{-\Delta\Delta Ct}$$

If no expression was measured by qRT-PCR the Ct values were set to 40, to enable the calculation of a fold change.

Table 4: Primer pairs used for qRT-PCR

Target	Forward primer (5' – 3')	Reverse Primer (5' - 3')
Alas	CAGGAGGACGTGCAGGAAAT	CGGCTTGGATCCTCTCCATC
ALAS	GATGTCAGCCACCTCAGAGAAC	CATCCACGAAGGTGATTGCTCC
(d)Cas9	AGTCTTCACGAGCACATCGC	CCTTCCCATTACTTTGACGAGTTC
Myo7b	GGGACACAAGTACAGGAAGGA	GCGTTCAAAGCCCACTAGG
MYO7B	AAGGACTACGCCCACATCCG	CTGAGGCGTCCAGGTTCTC
Nr2e3	CTTCATGGCTGTCAAATGGGC	AGCTCATTCCATGCCTCTTCC
Nxnl1	GAAAAATGGCTCTTCCTGCCG	GGGATGGCGGTGATTTCGTA
Nxnl2	TCGAGGTGGTTTTCGTGTCG	GACGGACAGAGAACTGGCG
Opn1mw	GGAGCAGGTACTGGCCTTATG	GGAGGTAGCAGAGCACGATG
Opn1sw	CATCCCCGCCTTCTTTTCCAA	CCTGCACACCATCTCCAGAAT
RdCVF	GAAAAATGGCTCTTCCTGCCG	ACCAGGACAGTAAACCTCCAG
RdCVF2	TCGAGGTGGTTTTCGTGTCG	CCTGGGTCCCCACTCACTG
Rho	GGATCATGGCGTTGGCCTGT	CCGCATGAACATTGCATGCCC

3.10 Protein Extraction

For protein extraction, radio-immunoprecipitation assay (RIPA) or Triton-X lysis buffer were used for MYO7B or NRL experiments, respectively.

RIPA lysis buffer	
10 x RIPA (Merck)	1 ml
50 % Glycerol	2 ml
Ultra-pure water	7 ml
cOmplete™ ULTRA Protease Inhibitor Cocktail tablets (Roche)	1 tablet

Triton-X lysis buffer	
Triton X-100	50 µl
5 M NaCl	0.3 ml
2.5 M $CaCl_2$	8 µl
Ultra-pure water	to 10 ml
cOmplete™ ULTRA Protease Inhibitor Cocktail tablets (Roche)	1 tablet

Protein was isolated from mouse retina or eyecup. For the isolation of the eyecup, the mice were anaesthetised with isoflurane and sacrificed by cervical dislocation and the eye was isolated by cutting the optical nerve with surgical scissors (KLS martin). The eye was punctured with a 21-gauge needle at the ora serrata and transferred into 4 %

paraformaldehyde (PFA) for 5 min. The eye was positioned under a stereomicroscope (Stemi 2000, Zeiss) on a filter paper drenched with 0.1 M phosphate buffer (PB). Surgical spring scissors (Fine Science Tools) were used to cut along the ora serrata to remove the cornea, iris, and lens. Using forceps (Fine Science Tools), the vitreous was removed from the eyecup. The eyecup was transferred into a safe-lock tube and frozen in liquid nitrogen.

0.1 M PB	
$Na_2HPO_4 \times 2H_2O$	28.48 g
$NaHPO_4 \times H_2O$	5.52 g
Ultra-pure water	to 2 l

4 % PFA	
Paraformaldehyde	6 g
0.1 M PB	to 150 ml

The retina was isolated as described for the RNA isolation. 50 or 100 µl lysis buffer was added to each frozen eyecup or retina in a safe-lock tube, respectively. After the addition of a stainless-steel ball, the samples were disrupted twice at 15 Hz for 30 s. Afterwards, the tubes were tumbled for 20 min at 4 °C in a tube rotator (VWR). The stainless-steel balls were removed, and the lysates were centrifuged for 10 min at 5000 x *g*, 4 °C. The protein-containing supernatant was transferred into new tubes. The samples were stored at -20 °C until further processing.

3.11 Western Blot

Protein lysates were prepared for Western Blot by incubation of 30 µl lysate with 6 µl Laemmli + DTT buffer for 10 min at 72 °C.

Laemmli + DTT buffer	
0.5 M Tris-HCl/SDS buffer	7 ml
Glycerol	3 ml
SDS	1 g
Bromophenol blue	1.2 mg
DTT	0.93 g

For the Western Blot 7 % and 15 % sodium lauryl sulfate (SDS)-polyacrylamide gels were used for the detection of MYO7B and NRL, respectively. SDS-polyacrylamide gels were cast with the Mini-Protean system (Biorad).

0.5 M Tris-HCl/SDS buffer, pH 6.8	
Tris-HCl	39.4 g
SDS	2.0 g
Ultra-pure water	to 500 ml

1.5 M Tris-HCl/SDS buffer, pH 8.8	
Tris-HCl	118.2 g
SDS	2.0 g
Ultra-pure water	to 500 ml

SDS-polyacrylamide gel	**7 %**	**15 %**	**4 % stacking gel**
Rotiphorese® Gel 30 (Carl Roth)	2.7 ml	5.7 ml	0.5 ml
0.5 M Tris-HCl/SDS buffer	2.8 ml	2.8 ml	-
1.5 M Tris-HCl/SDS buffer	-	-	0.95 ml
Ultra-pure water	5.8 ml	5.8 ml	2.3 ml
Ammonium persulphate	22.5 µl	22.5 µl	18.75 µl
Tetramethylethylenediamine	7.5 µl	7.5 µl	3.75 µl

After the addition of 36 µl sample and 8 µl Page Ruler (Thermo Fisher Scientific) to the gel, electrophoresis was performed with the Mini-Protean system (Biorad) at 140 V for 1 h 10 min in Electrophoresis buffer.

Electrophoresis buffer	
Tris	3 g
Glycine	14.4 g
SDS	1 g
Ultra-pure water	to 1 l

For Western blotting, a wet transfer was performed. The polyvinylidene fluoride blotting membrane (VWR Peqlab) was incubated for a few minutes in methanol and sponges and filter paper were drained in the blotting buffer. The blot was assembled in the following order: sponge, filter paper, gel, membrane, filter paper, and sponge and run at 100 V for 1 h 30 min.

Blotting buffer	
Tris	3 g
Glycine	14.4 g
Ultra-pure water	to 1 l

To inhibit the unspecific binding of the antibodies the membrane was incubated for 1 h at room temperature in 0.1 g/ml milk powder in Tris-buffered saline with Tween 20 (TBST) buffer on a roller mixer (SRT6, Stuart equipment).

TBST buffer	
Tris	1.2 g
NaCl	8.0 g
Tween 20	1 ml
Ultra-pure water	to 1 l

The primary antibody was diluted in an appropriate concentration (see table below) in 5 ml TBST buffer containing 0.01 g/ml milk powder. The membrane was added to the primary antibody solution and incubated for 16 h at 4 °C on a roller mixer.

Table 5: Primary antibodies for Western Blot

Primary antibody	**Target**	**Working dilution**	**Host**	**Source**	**Catalogue number**
Anti-MYO7B antibody	Myo7b	1:1000	rabbit	Sigma-Aldrich	HPA039131
Anti-β-Actin−Peroxidase antibody, clone AC-15	Beta-actin	1:3000	mouse	Sigma-Aldrich	A3854
Human NRL Antibody	Nrl	1:500	goat	R&D systems	AF2945
Histone H3 (D1H2) XP® Rabbit mAb	Histon H3	1:5000	rabbit	Cell Signaling Technology	4499S

If the primary antibody was not linked to horseradish peroxidase (HRP) a secondary antibody was used to enable detection. The membrane was incubated in 5 ml TBST buffer containing 0.01 g/ml milk powder and an appropriate dilution of the secondary antibody for 1.5 h at room temperature.

Table 6: Secondary antibodies for Western Blot

Secondary antibody	Target	Working dilution	Host	Source	Catalogue number
mouse anti-rabbit IgG-HRP	Rabbit IgG	1:2000	mouse	Santa Cruz	sc-2357
m-IgGκ BP-HRP	Mouse IgGκ	1:2000	N/A	Santa Cruz	sc-516102
mouse anti-goat IgG-HRP	Goat IgG	1:2000	mouse	Santa Cruz	sc-2354

Before detection, the membrane was washed three times in TBST buffer and with ultra-pure water. For detection, the ChemiDoc MP imaging system (Bio-Rad) and the ImmunoCruz western blotting luminol reagent (Santa Cruz) were used. The Image Lab 5.2 software (Bio-Rad) was used for the acquisition, processing, and analysis of the Western Blot image. The acquisition protocol was set to signal accumulation mode (setup: 3-360 s, 33 pictures).

3.12 Immunohistochemistry

For immunohistochemistry, cryosectioning of mouse retina was performed. The mice were anaesthetised with isoflurane and sacrificed by cervical dislocation and the temporal site of the eye was marked using a hot 20-gauge needle. The eye was isolated by cutting the optical nerve with surgical scissors. The eye was pierced with a 20-gauge needle at the ora serrata and transferred into 4 % PFA for 5 min. Then the eye was placed under a surgical microscope on a filter paper drenched with 0.1 M PB and surgical spring scissors were used to cut along the ora serrata to remove the cornea, iris, and lens. The temporal site of the eye was marked again by a small incision. Using forceps, the vitreous was removed from the eyecup. The eyecup was then fixated in 4 % PFA for 45 min. After fixation, the eyecup was washed three times in 0.1 M PB for 5 min on ice. For cryopreservation, the eyecup was placed in 0.1 M PB containing 30 % saccharose for at least 16 h. The eyecup was embedded in a tissue-freezing medium (Tissue-Tek O.C.T. compound, Sakura) and placed on dry ice until the

medium was solidified. The retina was sectioned into 10 µm-thick slices using a cryostat (Leica CM3050 S, Leica Biosystems) and the sections were collected on coated glass object slides (Thermo Fisher Scientific). Retinal sections were stored at -20 °C until further processing.

To perform the immunohistochemical staining the retinal sections were thawed at room temperature and transferred to a humidity chamber (Merck). The sections were encircled with a Super PAP pen liquid blocker (Science Services) and rehydrated by application of 150 µl of 0.1 M PB for 5 min and fixed with 50 µl of 4 % PFA for 10 min. The sections were washed three times for 5 min with 150 µl of 0.1 M PB. The primary antibodies or fluorescein isothiocyanate (FITC) conjugated lectin were diluted to an appropriate concentration with 0.1 M of PB containing 5 % ChemiBLOCKER (Merck) and 0.3 % Triton X-100. 25 µl of this solution was added to each section and the sections were incubated for 16 h at 4 °C. The primary antibody solution was removed, and the retinal sections were washed three times with 150 µl of 0.1 M PB for 5 min.

Table 7: Primary antibodies for IHC

Primary antibody	Target	Working dilution	Host	Source	Catalogue number
Anti-Rhodopsin Antibody, CT, last 9 amino acids, clone Rho 1D4	Rhodopsin	1:1500	mouse	Merck	MAB5356
Anti-Opsin Antibody, Red/Green	M-opsin	1:300	rabbit	Merck	AB5405
Lectin from Arachis hypogaea (peanut), FITC conjugate	Cone photoreceptors	1:100	Arachis hypogaea	Sigma-Aldrich	L7381

Secondary antibodies conjugated to fluorophores were used to make the signal detectable. Each section was incubated with 25 µl of a solution containing the secondary antibody in an appropriate dilution and 2 % ChemiBLOCKER in 0.1 M PB for 1.5 h at room temperature.

Table 8: Secondary antibodies for IHC

Secondary antibody	Target	Working dilution	Host	Source	Catalogue number
Cy™3 AffiniPure Donkey Anti-Rabbit IgG (H+L)	Rabbit IgG (H+L)	1:400	donkey	Jackson ImmunoResearch	711-165-152
Cy™5 AffiniPure Goat Anti-Mouse IgG (H+L)	Mouse IgG (H+L)	1:400	goat	Jackson ImmunoResearch	115-175-146

After the application of the secondary antibody, the samples were protected from light and the sections were washed again three times for 5 min with 150 µl of 0.1 M PB. To stain the nuclei, 50 µl of 5 µg/ml Hoechst solution (Thermo Fisher Scientific) was added to the sections and they were incubated for 10 min at room temperature. The sections were finally washed with 0.1 M PB, embedded using PermaFluor aqueous mounting medium (Thermo Fisher Scientific), and covered with a coverslip (Thermo Fisher Scientific). The immunolabeled retinal cryosections were imaged shortly after staining and stored at 4 °C protected from light.

3.13 Confocal Microscopy

Images of immunolabeled retinal cryosections were obtained with a Leica TCS SP8 spectral confocal laser scanning microscope (Leica Microsystems) equipped with lasers emitting at the wavelength 405 nm, 488 nm, 561 nm, and 633 nm, an HC PL APO CS2 40x/1.30 Oil objective (Leica Microsystems) and type F immersion liquid (Leica Microsystems). The images were acquired as z stacks using the Las X software (Leica Microsystems). Excitation wavelength and emission filter settings were chosen according to the used fluorescent dyes. The images consisting of multiple z-stacks were merged by maximum projection and further processed with the open-source ImageJ 1.52t software (National Institutes of Health, Schmittgen and Livak (2008)).

3.15 RNA Sequencing

Total RNA was sent to a commercial provider (Genewiz Germany GmbH) to perform RNA sequencing (RNA-seq) and analysis. mRNA was enriched by poly(A) selection. After preparation of the cDNA library, paired-end sequencing was performed on an Illumina HiSeq system (Illumina) with 150 bp read length and over 20 million reads per sample. Sequence reads were trimmed for adapter sequences and quality using Trimmomatic v.0.36 (Bolger et al., 2014) and mapped using the STAR aligner v.2.5.2b (Dobin et al., 2013) to the *Mus musculus* GRCm38 reference genome provided by ENSEMBL. FeatureCounts from the Subread package v.1.5.2 (Liao et al., 2014) was used to calculate unique gene hit counts; unique reads that fell outside of exon regions were excluded. The obtained gene hit counts were analysed using DESeq2 (Love et al., 2014). P-values and log2 fold changes were obtained using the Wald test. Differentially expressed genes were defined by an adjusted p-value < 0.05 and absolute log2 fold change > 1.

3.14 Statistics

Statistical analysis and graphical visualization were performed using Prism 9.3.1 software (GraphPad Software). The performed statistical test and sample size (n) are indicated in each figure legend. Values are shown as mean ± standard error of the mean.

4 Results

4.1 Evaluation of dCas9-VPR mediated Transactivation for Retinal Gene Therapy

4.1.1 Transactivation of *Myo7b* in the Murine Retina

The coding sequence of *MYO7A* (6.6 kb) exceeds the packaging capacity of one rAAV vector and requires dual rAAV vectors for gene supplementation. Moreover, different splice isoforms are expressed from the *MYO7A* locus and their contribution to the structure and function of photoreceptors is not clear yet. As gene supplementation using dual rAAV can cover only one of these isoforms, the therapeutic benefit might not be optimal using this approach. In an attempt to develop a new strategy for the therapy of mutations in *MYO7A*, transactivation of a functionally equivalent gene was evaluated. To identify functionally equivalent genes, criteria based on amino acid identity, conservation of functional domains and total length were applied (Riedmayr et al., 2022). This resulted in the identification of MYO7B as a highly promising candidate. MYO7B shows high similarity to MYO7A (Figure 11) and can form complexes with MYO7A interaction partners (I. M. Yu et al., 2017). These results suggest that the functionally related MYO7B has a high chance of compensating for the missing MYO7A function in the retina. Furthermore, also *MYO7B* expresses different splice isoforms that might have equal functionality to the *MYO7A* isoforms.

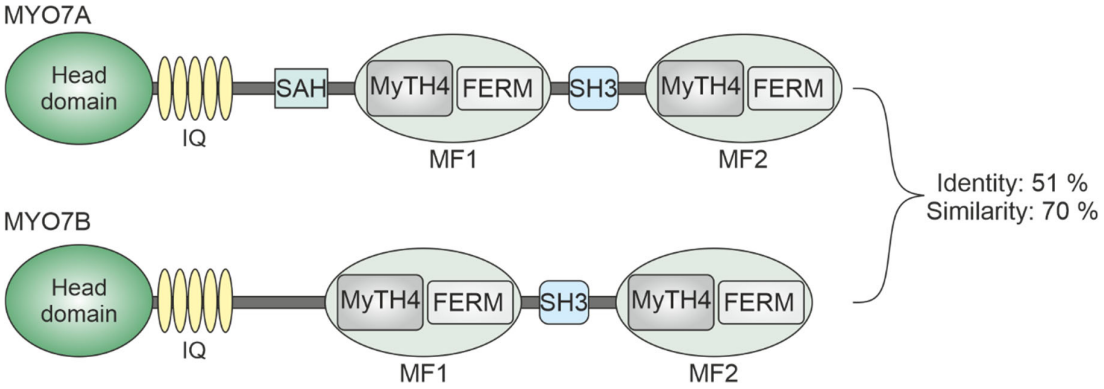

Figure 11: Structural similarity between MYO7A and MYO7B. Scheme comparing the structural domains of MYO7A and MYO7B. The amino acid identity and similarity of MYO7A and MYO7B are shown on the right. IQ, IQ calmodulin binding motive. SAH, single α helix. MyTH4, myosin tail homology 4 domain. FERM, four-point-one, ezrin, radixin, moesin domain. MF, MyTH4/FERM domain. SH3, Tyrosine-protein kinase CSK homology 3 domain. Adapted from I. M. Yu et al. (2017).

To identify a potent transactivating module targeting the murine *Myo7b* promoter region, a sgRNA array consisting of three sgRNAs to facilitate transactivation was designed. To this

end, the experiments were set out to test the efficiency of *Myo7b* promoter region-targeting sgRNAs in 661W cells, an immortalized derivative of cone photoreceptors. 661W cells were co-transfected with split dCas9-VPR expression cassettes equipped with all elements needed for the production of the rAAV vectors (Figure 12A, B). A split dCas9-VPR system is used because the coding sequence of dCas9-VPR (5.8 kb) exceeds the rAAV genome packaging capacity. The advantage of this approach is that the same expression cassettes can later be utilized to generate dual REVeRT rAAVs vectors for subsequent *in vivo* experiments. To exclude any effects caused by the dCas9-VPR system alone, the *Myo7b* promoter region-targeting sgRNAs were replaced by a control sgRNA targeting the bacterial *lacZ* gene. After cotransfection of 661W cells with plasmids encoding for split dCas9-VPR and sgRNAs (Figure 12A), a significant increase in *Myo7b* expression was observed by qRT-PCR (Figure 12C)

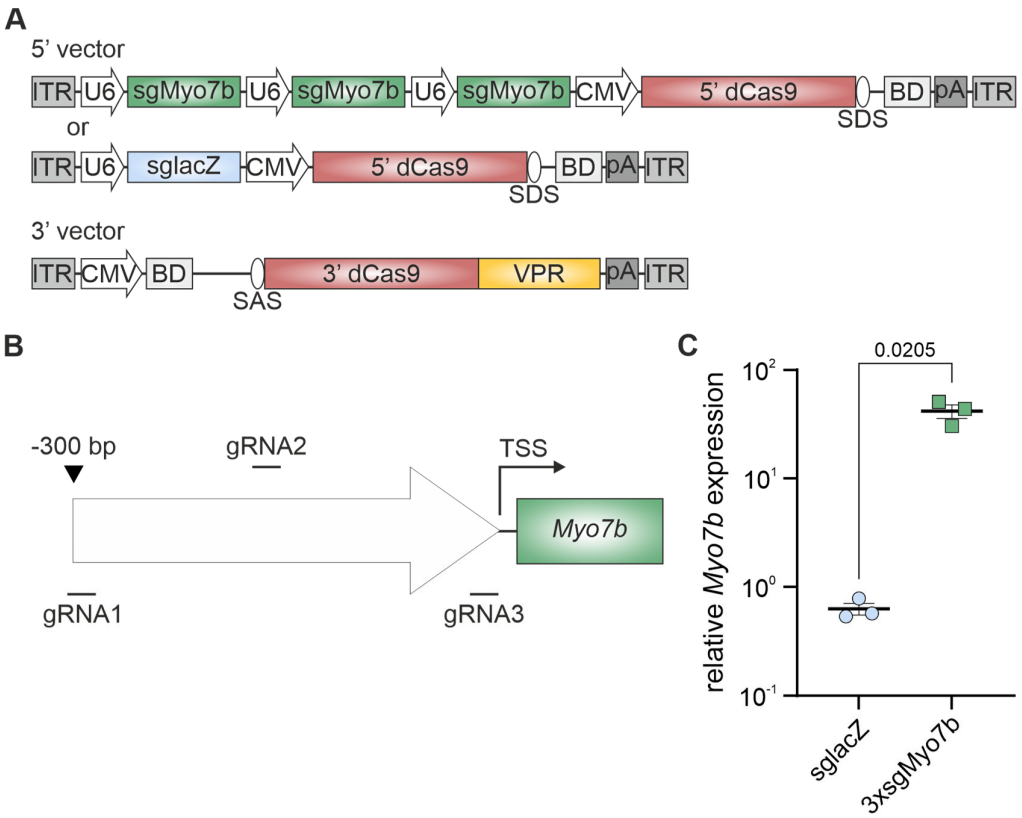

Figure 12: Transactivation of *Myo7b* in 661W cells. A, rAAV vector plasmids containing split dCas9-VPR and sgRNAs targeting the Myo7b promoter region (sgMyo7b). B, Binding position of different sgRNAs targeting the *Myo7b* promoter region. C, Relative *Myo7b* expression in 661W cells after cotransfection with the plasmids in A. The 5' vector contained either sgRNAs for *Myo7b* transactivation (3xsgMyo7b, n = 3) or a control sgRNA targeting the bacterial *lacZ* gene (sglacZ, n = 3). For statistical analysis, a two-tailed Welch's t-test was performed. U6, human U6 promoter. CMV, cytomegalovirus promoter. BD, binding

domain. SDS, splice donor site. SAS, splice acceptor site. pA, polyadenylation signal. *Myo7b*, murine myosin VII b gene. bp, base pairs. TSS, transcriptional start site.

To enhance the efficiency of retinal transduction, the rAAV vectors utilized for these and all following experiments were produced using the AAV2/8Y733F capsid (Petrs-Silva et al., 2009). The dual rAAVs were first validated in mouse hippocampal primary neurons. Reconstitution of dCas9-VPR mRNA and transactivation of *Myo7b* was confirmed by qRT-PCR seven days post transduction of these neurons (Figure 13A, B).

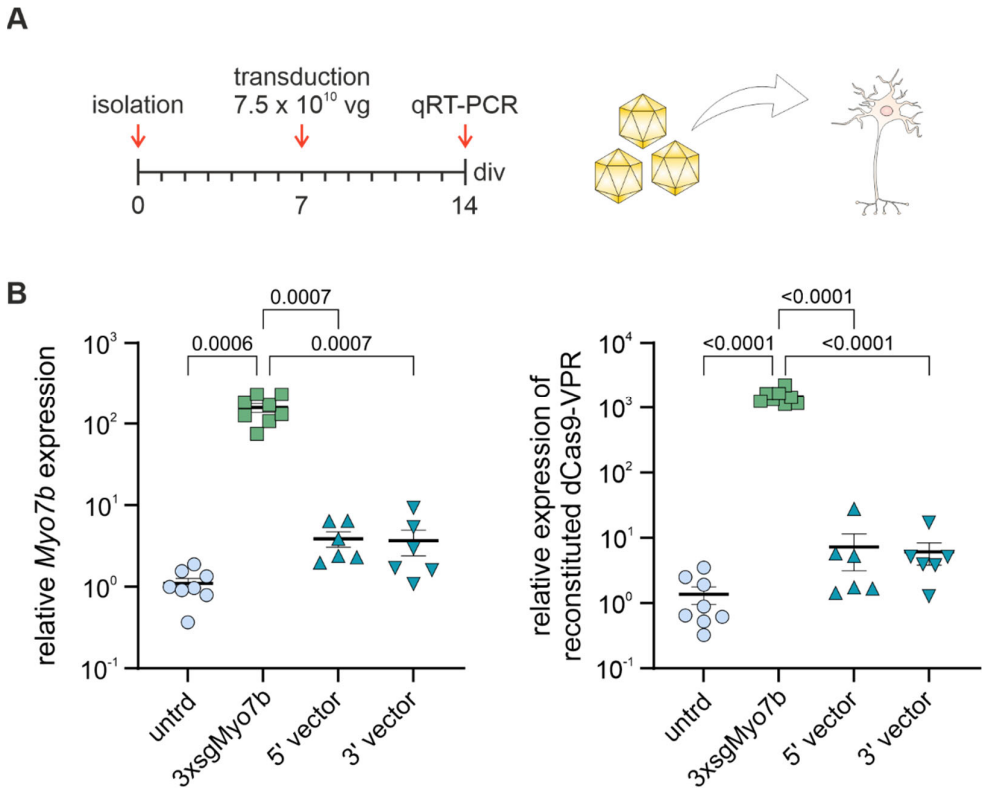

Figure 13: Transactivation of *Myo7b* in mouse primary neurons. A, Experimental design for the transduction of hippocampal mouse primary neurons with rAAV vectors generated from the plasmids depicted in Fig 12A. Hippocampal primary neurons were isolated and cultured by Manuela Brümmer. B, Relative expression of *Myo7b* (left panel) and reconstituted dCas9-VPR (right panel) in primary neurons transduced with an rAAV containing the 5' part of the dCas9 coding sequence and sgRNAs targeting the *Myo7b* promoter region (5' vector, n = 6), or the 3' part of the dCas9-VPR coding sequence (3' vector, n = 6) or both vectors (3xsgMyo7b, n= 8) compared to untransduced neurons (untrd, n = 8). For statistical analysis, Welch ANOVA with Dunnett's T3 multiple comparison test was performed. vg, vector genomes. div, days in vitro.

Following this validation, the dual REVeRT rAAV system for transactivation of *Myo7b* was applied to the murine retina. C57BL/6J wild-type (WT) mice were subretinally injected at postnatal day 21 (P21) (Figure 14A). Efficient reconstitution of dCas9-VPR and transactivation of *Myo7b* were observed four weeks after injection (Figure 14B, C). These

results provide a proof-of-principle for transactivation of *Myo7b* in the retina and demonstrate that the dual REVeRT rAAV system can reconstitute dCas9-VPR *in vivo*.

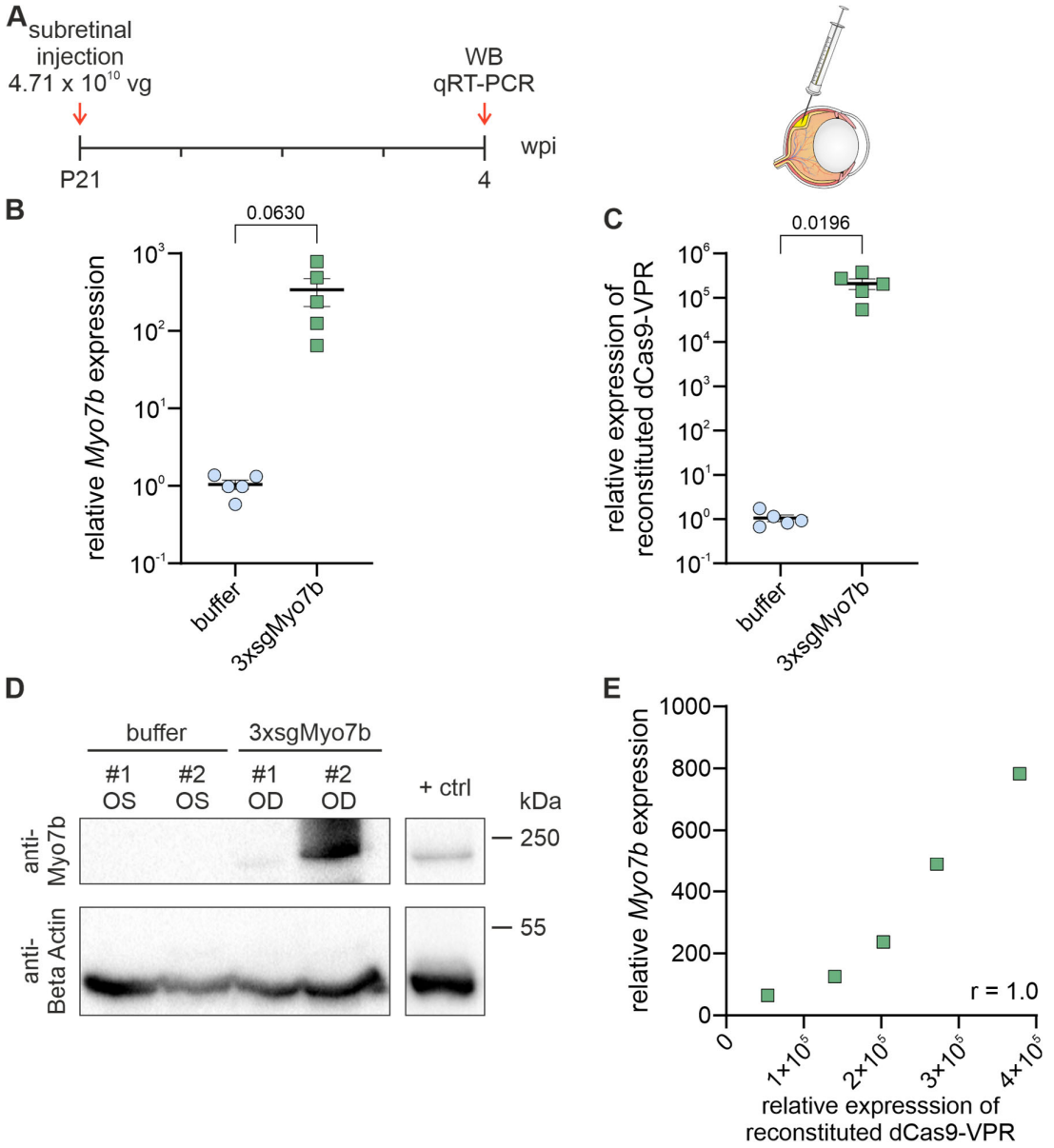

Figure 14: Transactivation of *Myo7b* in the murine retina. A, Experimental design for *Myo7b* transactivation upon subretinal injection. **B-C**, Relative expression of *Myo7b* (B) and reconstituted dCas9-VPR (C) in retinas four weeks after subretinal injection with rAAV vectors encoding split dCas9-VPR and three sgRNAs targeting the *Myo7b* promoter region (3xsgMyo7b, n= 5). The contralateral eye injected with rAAV formulation buffer served as a reference (buffer, n = 5). **D**, Western blot (WB) from lysates of retinas of two mice (#1 and #2) 4 weeks after subretinal injection (n = 2). For comparison, a positive control (+ ctrl) from a lysate obtained from 661W cells stably expressing Myo7b is shown. **E**, Scatter plot showing the correlation between the values for relative Myo7b expression and relative expression of reconstituted dCas9-VPR obtained from murine retinas four weeks after subretinal injection (n = 5). Spearman r is shown in the lower-right corner. For statistical

analysis in B, a two-tailed paired t-test was performed. P21, postnatal day 21. wpi, weeks post injection. kDa, kilo Dalton. OS, *oculus sinister*. OD, *oculus dexter*.

To determine whether *Myo7b* transactivation also leads to the expression of MYO7B protein, a western blot with retinal lysates was performed. The corresponding band could be detected for both eyes injected with the dual REVeRT rAAV for *Myo7b* transactivation and was absent in the buffer-injected control eyes (Figure 14D). The variance in *Myo7b* expression suggests that the transactivation efficiency might depend on the amount of reconstituted dCas9-VPR. In line with this hypothesis, plotting of *Myo7b* expression against the expression of reconstituted dCas9-VPR showed a high correlation between the amount of dCas9-VPR and the transactivation efficiency (Figure 14E).

4.1.2 Transactivation of *Myo7b* in Additional Tissues

CRISPR-mediated transactivation can also be used for diseases affecting other tissues (Kemaladewi et al., 2019). Therefore, the experiments were set out to evaluate whether the dual REVeRT rAAV vectors expressing split dCas9-VPR in combination with sgRNAs targeting the *Myo7b* promoter region can transactivate this gene in different non-retinal tissues. It appears conceivable that transactivation efficiency is dependent on the administration route. To address this question, intraperitoneal administration was chosen (Figure 15A). Compared to local administration such as subretinal injections, transduction of specific tissues upon intraperitoneal delivery of the dual rAAVs is more challenging. The dual rAAVs are diluted in the bloodstream and must cross multiple biological barriers to reach specific tissues. Five weeks after intraperitoneal injection of WT mice, successful transactivation of *Myo7b* and efficient reconstitution of dCas9-VPR were observed in the retina, heart, skeletal muscle, lung, and liver (Figure 15B, C). These data demonstrate that the dual REVeRT rAAV transactivation system is largely independent of the target tissue or route of administration. Nevertheless, no *Myo7b* transactivation could be detected in the brain upon intraperitoneal injection (Figure 15B). The most plausible explanation is that the injected rAAVs with serotype 8 could not cross the blood-brain-barrier. This is consistent with a previous study investigating the tissue tropism of different AAV serotypes upon systemic injection (Zincarelli et al., 2008).

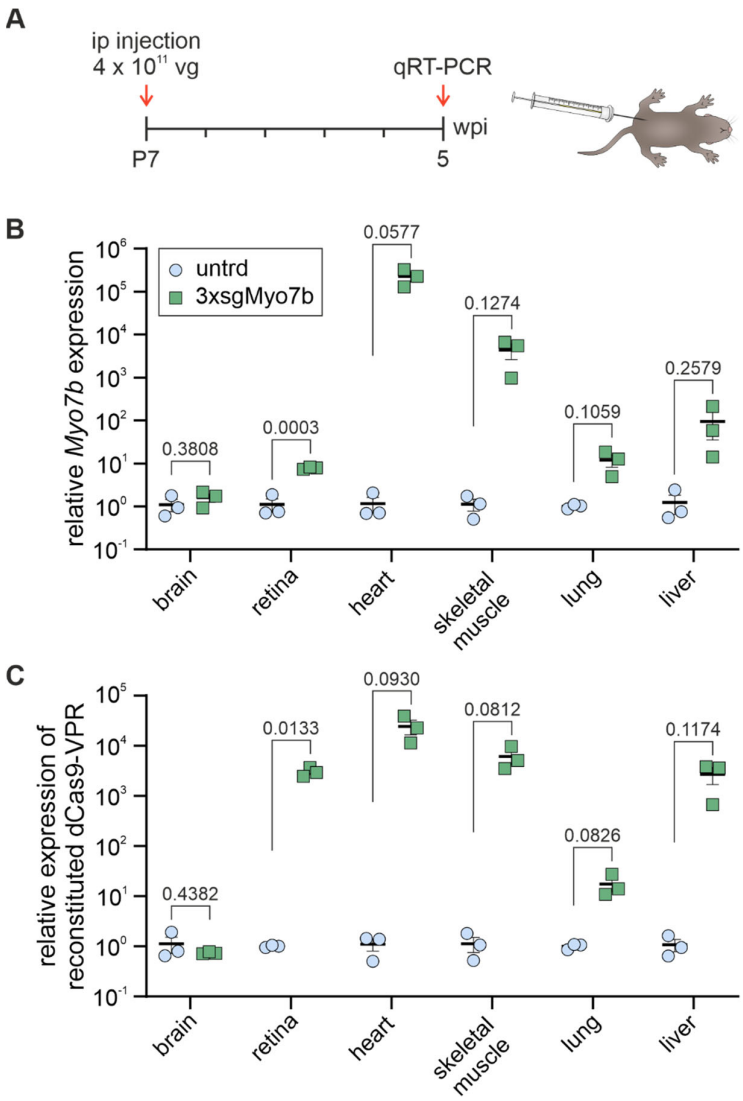

Figure 15: Transactivation of *Myo7b* in different tissues after intraperitoneal injection. **A**, Experimental design for the evaluation of *Myo7b* transactivation in different tissues after intraperitoneal (ip) injection of rAAV vectors containing split dCas9-VPR and three sgRNAs for *Myo7b* transactivation. Intraperitoneal injections were performed by Stefan Thalhammer. **B-C**, *Myo7b* expression (B) and expression of reconstituted dCas9-VPR (C) five weeks after injection with rAAV vectors for *Myo7b* transactivation (3xsgMyo7b, n = 3) compared to samples from untreated mice (untrd, n = 3). For statistical analysis, a two-tailed Welch's t-test was performed.

These results raised the question of whether local administration of the dual REVeRT rAAV vectors is capable of transactivating *Myo7b* in the brain. Hippocampal injection of the dual REVeRT rAAV transactivation vectors resulted in functional reconstitution of dCas9-VPR accompanied by transactivation of *Myo7b* in the hippocampus (Figure 16A, B). Analogous to the subretinal injections a strong correlation between *Myo7b* transactivation and the amount of reconstituted dCas9-VPR was observed (Figure 16C).

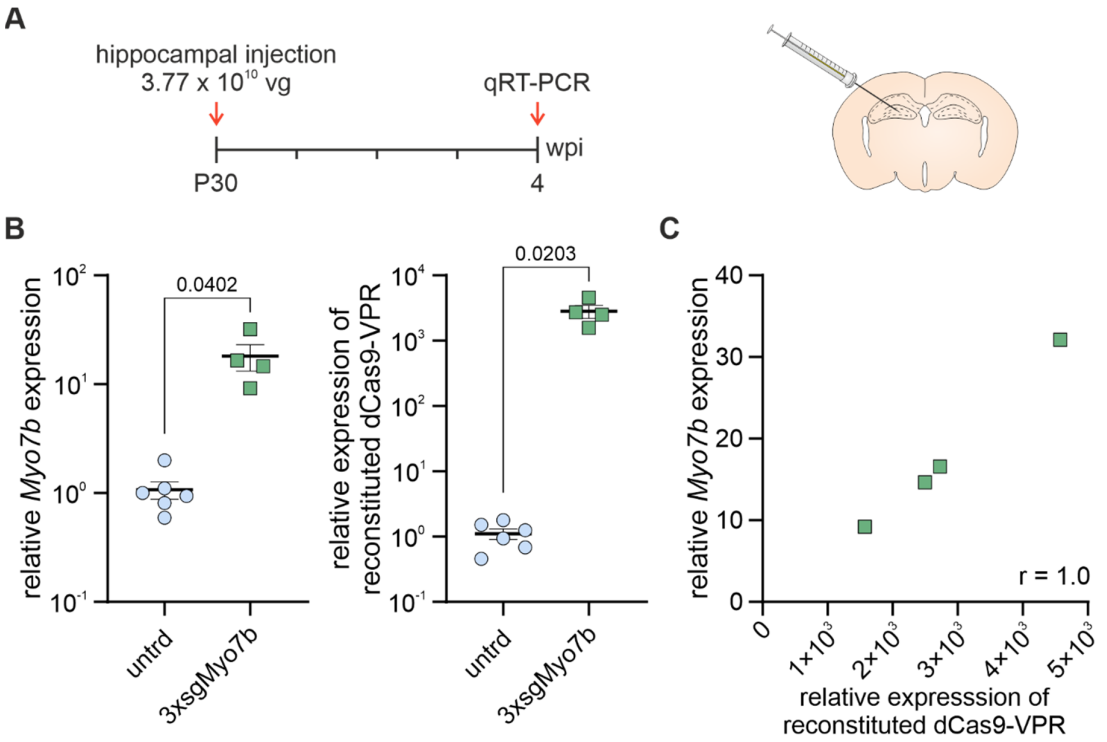

Figure 16: Transactivation of *Myo7b* in the hippocampus. A, Experimental design for evaluation of *Myo7b* transactivation after hippocampal injection. Hippocampal injections and isolation were performed by Verena Mehlfeld and Manuela Brümmer. **B**, *Myo7b* expression (left panel) and expression of reconstituted dCas9-VPR (right panel) in hippocampi of mice four weeks after injection with rAAV vectors for *Myo7b* transactivation (3xsgMyo7b, n = 4) compared to samples from untreated mice (untrd, n = 6). **C**, Correlation between *Myo7b* transactivation and dCas9-VPR reconstitution (n = 4). Spearman r is shown in the lower right corner. For statistical analysis in B, a two-tailed Welch's t-test was performed.

4.1.3 Transactivation of MYO7B in Human Retinal Organoids

Unlike the coding sequences, the promoter regions of certain genes are generally not as highly conserved across different mammalian species. The mouse-specific sgRNAs for transactivation of *Myo7b* can therefore not be used for transactivation of the human *MYO7B*. To develop an experimental framework which could be of direct therapeutic relevance for human patients, a new array of sgRNAs targeting the human *MYO7B* promoter region was tested in HEK293 cells, a widely used human cell line (Figure 17A, B). A significant increase in *MYO7B* transcript could be detected after cotransfection of HEK293 cells with plasmids encoding for split dCas9-VPR and the sgRNAs targeting the MYO7B promoter region (Figure 17B, C).

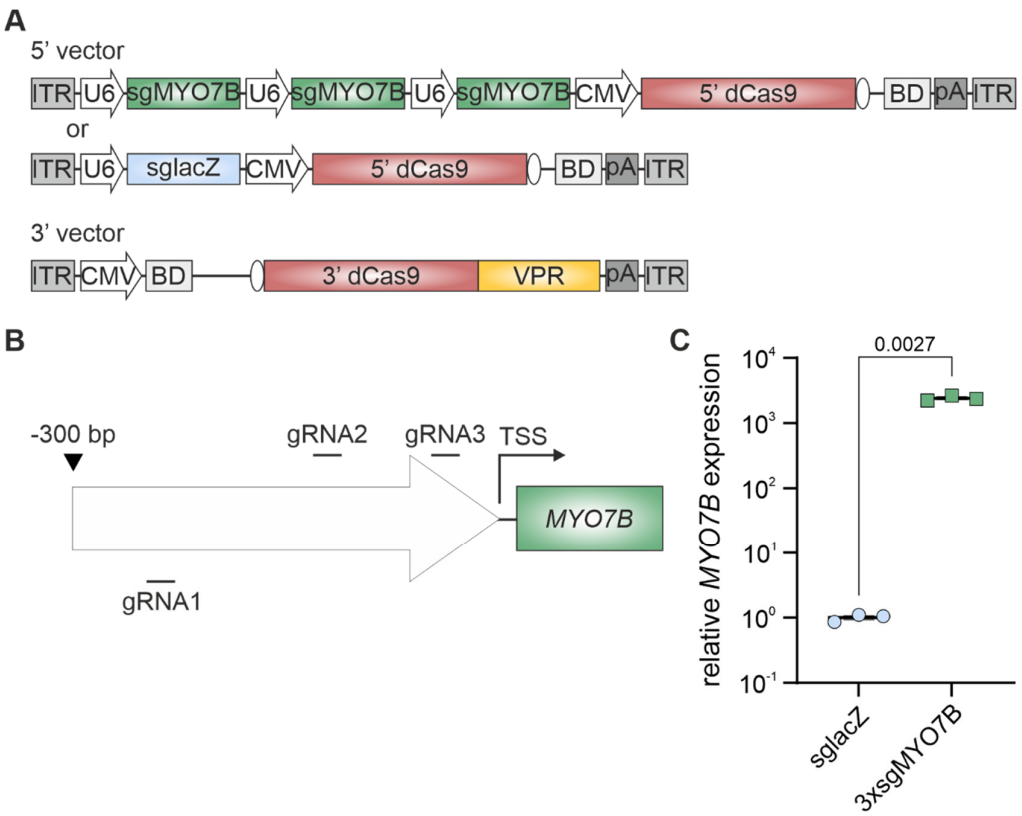

Figure 17: Transactivation of *MYO7B* in HEK293 cells. A, rAAV vector plasmids containing split dCas9-VPR and sgRNAs targeting the *MYO7B* promoter region (sgMYO7B). **B**, Binding positions of different sgRNAs targeting the *MYO7B* promoter region. **C**, Relative *MYO7B* expression in HEK293 cells after cotransfection with the plasmids shown in A. The 5' vector contained either sgRNAs for *MYO7B* transactivation (3xsgMYO7B, n = 3) or a control sgRNA targeting the bacterial *lacZ* gene (sglacZ, n = 3). For statistical analysis in C, a two-tailed Welch's t-test was performed.

Next, the dual REVeRT rAAV MYO7B transactivation approach was applied to transduce human retinal organoids. Human retinal organoids are currently the most suitable *in vitro* model for evaluating approaches designed to treat IRDs. For photoreceptor-specific expression, the dual rAAV vector cassettes were equipped with the human GRK promoter (Figure 18A) (Khani et al., 2007). Mature retinal organoids were transduced at DD 146 using the dual REVeRT rAAV system. This resulted in a significant increase in *MYO7B* mRNA three weeks post-transduction (Figure 18A-C).

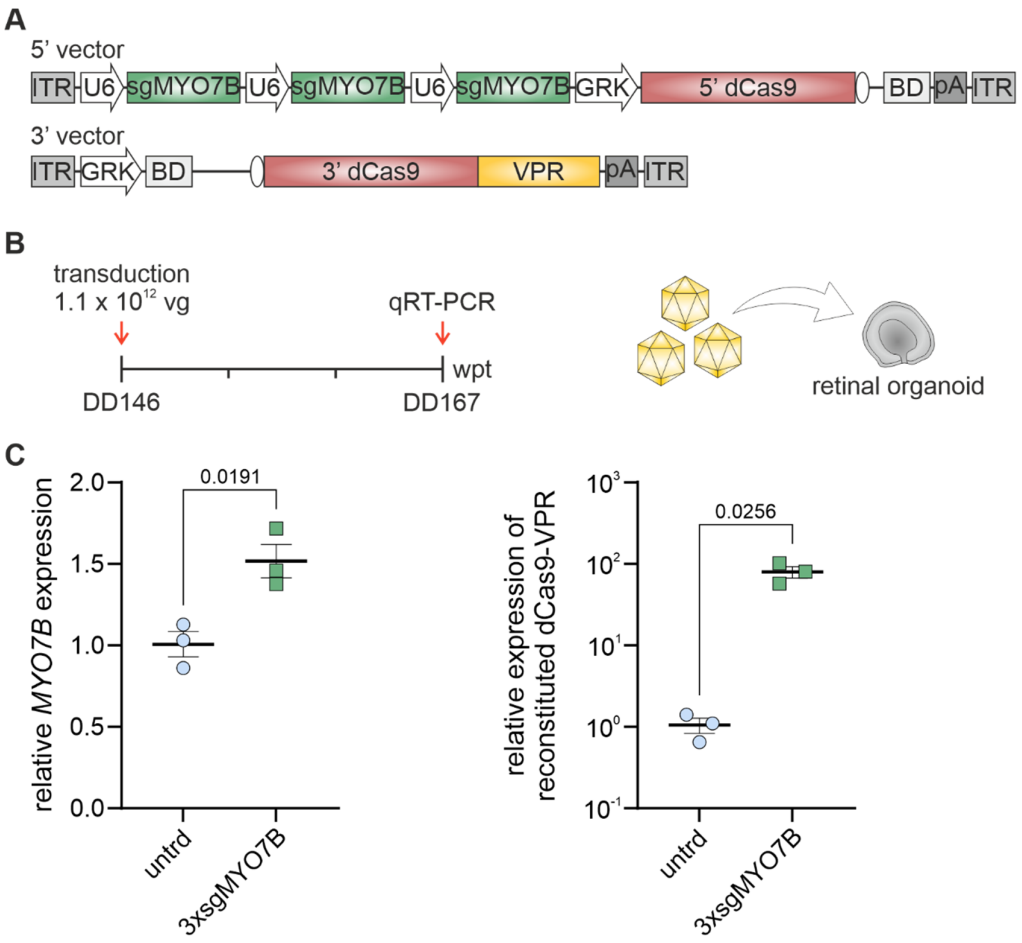

Figure 18: Transactivation of *MYO7B* in human retinal organoids. A, rAAV vector expression cassettes used for *MYO7B* transactivation in human retinal organoids. **B**, Experimental design for evaluation of *MYO7B* transactivation after transduction of human retinal organoids. Generation, cultivation, and transduction of human retinal organoids were performed by Nanda Boon. **C**, Relative *MYO7B* expression (left panel) and reconstitution of dCas9-VPR (right panel) after transduction of retinal organoids with the rAAV vectors shown in A (3xsgMYO7B, n = 3) compared to non-transduced retinal organoids (untrd, n = 3). GRK, G-protein-dependent rhodopsin kinase 1 promoter. DD, differentiation day. wpt, weeks post transduction. For statistical analysis in C, a two-tailed Welch's t-test was performed.

4.2 Simultaneous Gene Knockout and Transactivation for the Treatment of Gain-of-Function Mutations

4.2.1 Proof-of-Principle for Concurrent Gene Knockout and Activation

As mentioned in 2.2.4, the treatment of gain-of-function mutations remains a challenge for gene therapy. Gain-of-function mutations result in proteins with a new function that, even in small amounts, have negative effects on the affected cells. Therefore, current treatment strategies for these mutations either include the i) efficient suppression of the target gene

transcripts using RNAi or Cas9 along with the supplementation of the healthy copy (Cideciyan et al., 2018; Kiang et al., 2005; Tsai et al., 2018), ii) specific repression of the mutated transcript (Giannelli et al., 2018), or iii) correction of the mutated allele (Wang et al., 2020). Both strategies, however, come with some limitations. Mutation-specific strategies can only be used for the treatment of a single mutation and strategies that need the supplementation of a healthy gene copy are limited by target gene size and do not supply splice isoforms.

Some of these limitations can be elegantly overcome when combining the knockout of the disease-associated gene with a transcriptional activation of a functionally equivalent gene. This can be achieved by using a multiplexing approach that combines catalytically active Cas9-VPR with at least two separate sgRNAs equipped with spacer sequences of different lengths. In presence of sgRNA with a spacer length of less than 16 nt Cas9-VPR loses its nuclease activity and can thus be employed for transactivation of the functionally equivalent gene (Dahlman et al., 2015; Kiani et al., 2015). Another sgRNA containing a regular spacer sequence (20 nt) enables gene knockout. This concurrent knockout and activation (hereafter referred to as CONNACT) approach represents a new strategy for the treatment of gain-of-function mutations. I set out to evaluate CONNACT in the gain-of-function $Rho^{P23H/+}$ mouse model (Sakami et al., 2011). Treatment of this mouse model includes a knockout of the rod photoreceptor pigment rhodopsin and the activation of *Opn1mw*, the cone photoreceptor pigment M-opsin. The latter strategy has already been proven beneficial in a heterozygous rhodopsin-deficient mouse model (Bohm et al., 2020).

To assess the transactivation efficiency of sgRNAs with 15 nt spacer length, MEF cells were cotransfected with dCas9-VPR and different sgRNAs targeting the *Opn1mw* promoter region (Figure 19A). 661W cells could not be used for these experiments as they have a high endogenous expression of *Opn1mw* (Bohm et al., 2020). All sgRNAs tested showed transactivation of *Opn1mw* in MEF cells with variable efficiencies (Figure 19B).

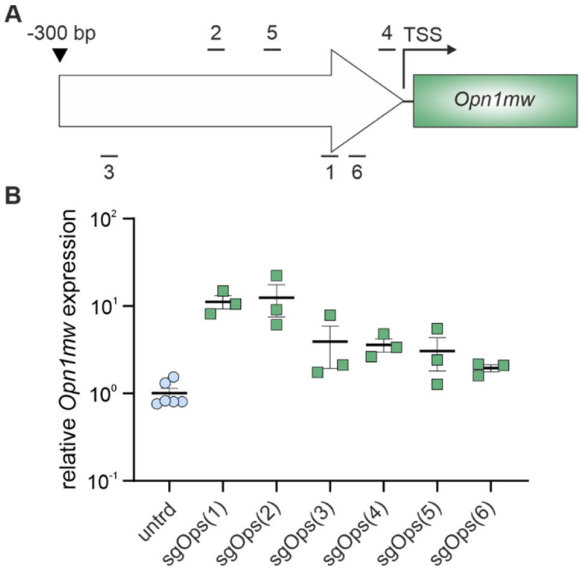

Figure 19: Evaluation of sgRNAs for the transactivation of *Opn1mw*. A, Binding position of different sgRNAs targeting the promoter region of *Opn1mw* (sgOps). **B**, Relative expression of *Opn1mw* after cotransfection of MEF cells with dCas9-VPR and different sgRNAs (n = 3). As a control, untreated MEF cells were used (untrd, n = 6).

For the following in vivo experiments, arrays of the two (sgOps1-2) or three (sgOps1-3) best performing sgRNAs were chosen. The different number of sgRNAs used for the *Opn1mw* transactivation is likely to affect the overall efficiency of *Opn1mw* transactivation allowing the assessment of dose dependency of the therapeutic outcome. For rod photoreceptor-specific expression the split Cas9-VPR dual rAAV vector cassettes were each equipped with a RHO promoter. The sgRNAs for *Opn1mw* transactivation were combined with a sgRNA targeting the first exon of rhodopsin for gene knockout (Figure 20A). Dual REVeRT rAAV vectors containing split Cas9-VPR and sgRNAs were subretinally injected at P21 to $Rho^{P23H/+}$ mice (Figure 20B, C). Four weeks after subretinal injection, a significant knockout of *Rho* could be observed. Furthermore, successful transactivation of *Opn1mw* was observed, which was further enhanced by the addition of a third *Opn1mw* promoter region targeting sgRNA (Figure 20D). *Rho* knockout and *Opn1mw* transactivation could also be confirmed by RNA-seq and revealed only a few differentially expressed transcripts compared to control injected retinas (Figure 20E, Supplementary Table 1). These results provided a proof-of-principle for the CONNACT strategy in the murine retina and could be confirmed by RNA-seq.

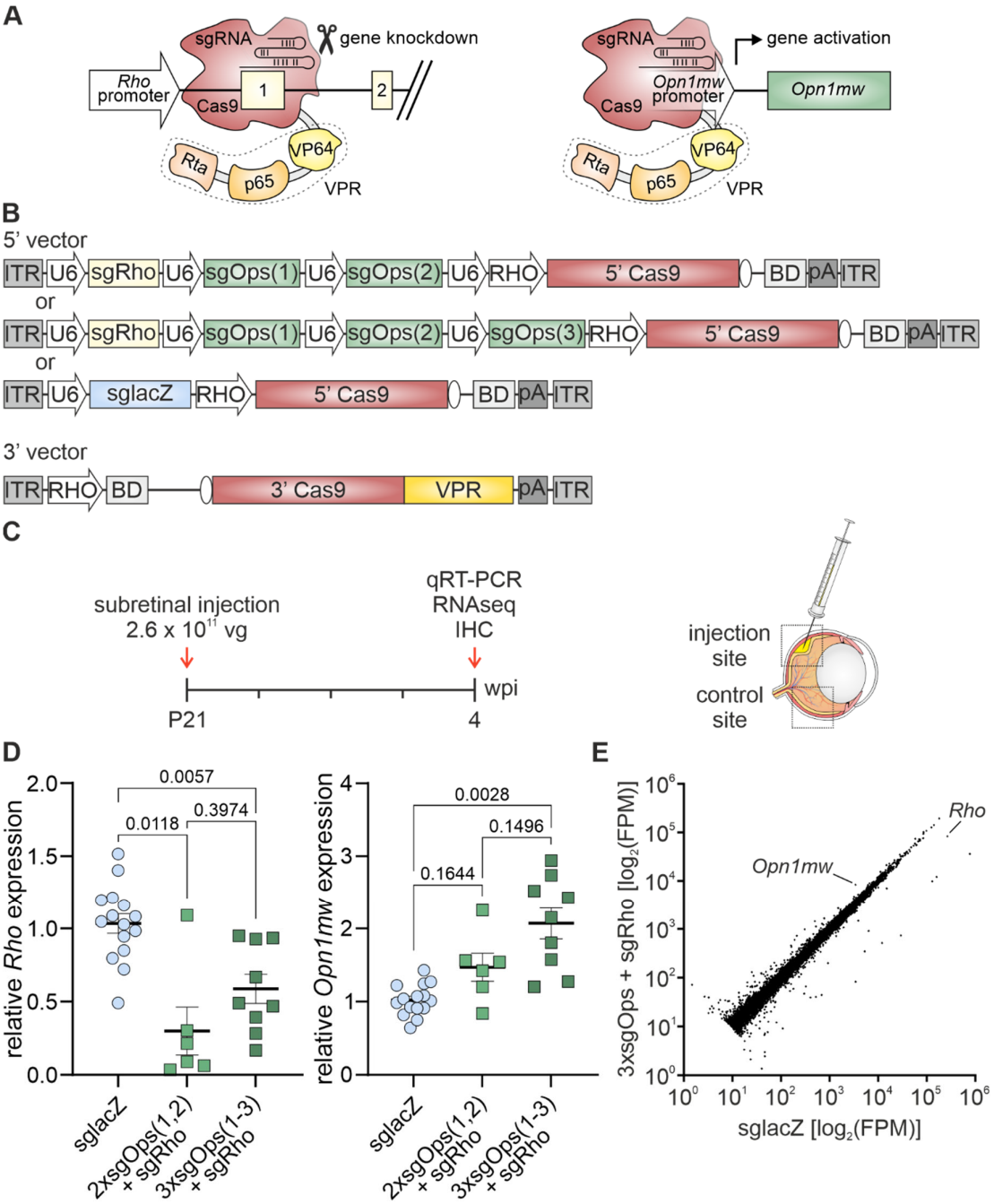

Figure 20: Simultaneous *Rho* knockout and *Opn1mw* transactivation in Rho$^{P23H/+}$ mice. **A**, In combination with different sgRNAs, nuclease active Cas9-VPR is used to target the first exon of rhodopsin for gene knockout (left) or to target the promoter region of *Opn1mw* for gene transactivation (right). **B**, Dual rAAV vector cassettes used for the expression of split Cas9-VPR. The 5' vector cassette included either a sgRNA for the knockout of *Rho* (sgRho, 20 nt spacer) and sgRNAs for the transactivation of *Opn1mw* (sgOps, 15 nt spacer) or a sgRNA targeting the bacterial lacZ gene (sglacZ) functioning as a control. **C**, Experimental design for CONNACT evaluation upon subretinal injection. **D**, Expression of *Rho* (left) and *Opn1mw* (right) in retinas upon injection with CONNACT (2xsgOps + sgRho, n = 6; 3xsgOps + sgRho, n = 9) relative to control injected retinas (sglacZ, n = 15). For statistical analysis, Welch's ANOVA with Dunnett's T3 multiple comparison test was performed. **E**, RNA-seq results from retinas injected with CONNACT (3xsgOps + sgRho, n

= 3) or control vectors (sglacZ, n = 4). Each dot represents a different transcript. sgRho, sgRNA targeting the first exon of *Rho*. sgOps, sgRNA targeting the promoter region of *Opn1mw*. sglacZ, sgRNA targeting *lacZ*. RHO, short human rhodopsin promoter. FPM, fragments per million.

To evaluate the simultaneous gene knockout and transactivation with the CONNACT system at the protein level, immunohistochemistry on retinal cryosctions of $Rho^{P23H/+}$ mice was performed four weeks after injection. At the injection site, a robust M-opsin staining could be observed outside of cone photoreceptor outer segments (Figure 21A). No M-opsin staining outside of the PNA-labelled cone photoreceptor outer segment was present at the contralateral control site of the same retina (Figure 21B). No gross changes in the intensity of the rhodopsin staining could be detected. Nevertheless, in some PNA negative outer segments, strong M-opsin staining was visible, but the rhodopsin signal was undetectable, indicating that these were rod outer segments with efficient *Opn1mw* transactivation and complete *Rho* knockout (Figure 21A).

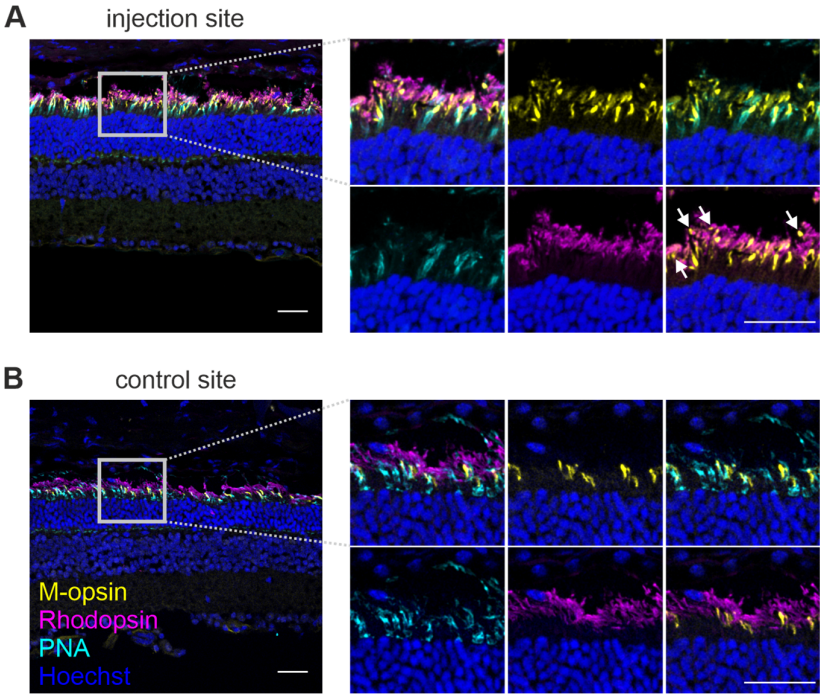

Figure 21: Immunostainings of $Rho^{P23H/+}$ mice. Immunohistochemistry was performed on retinal cryosections from mice injected with CONNACT (3xsgOps + sgRho). Depicted are representative staining from one mouse of the injection site (**A**) or control site (**B**) distal from the injection site (Fig, 21C). Magnifications of the areas marked with grey rectangles are shown on the right. PNA was used to label cone photoreceptors. White arrows indicate M-opsin staining inside rod photoreceptor outer segments that are lacking a Rhodopsin signal. Scale bar: 30 µm.

4.2.2 Functional Assessment of CONNACT in Rho$^{P23H/+}$ mice

Next, it was investigated whether CONNACT could improve retinal function and morphology in Rho$^{P23H/+}$ mice. ERG and OCT measurements were performed one and three months after subretinal injection. The contralateral eye of each mouse injected with dual rAAVs encoding for split Cas9-VPR and a sgRNA targeting the *lacZ* promoter served as a control.

One month after treatment, Rho$^{P23H/+}$ mice treated with the CONNACT system showed reduced amplitudes in ERG measurements obtained under scotopic conditions, suggesting a decrease in rod photoreceptor function most likely caused by the rhodopsin knockout (Figure 22A). In contrast, amplitudes of photopic and flicker ERG, which are mainly generated from cones, showed no significant difference (Figure 22B, C). This indicates that cone photoreceptors remain unaffected at this state. OCT measurements allow the assessment of the ONL thickness. The ONL thickness is determined by the number of photoreceptor nuclei and is therefore a direct parameter for assessing photoreceptor death. Upon treatment of Rho$^{P23H/+}$ mice with the CONNACT strategy the ONL thickness remained unchanged, suggesting no increase in photoreceptor survival (Figure 22D).

After 3 months, a pronounced reduction in scotopic ERG amplitudes was observed (Figure 23A). At this point, photopic amplitudes were also reduced, indicating a more rapid degeneration of cones after treatment (Figure 23B). Given that cone function remained unaffected one month after treatment (see above), the degeneration of cones 3 months post injection is presumably a secondary effect originating from the loss of rod photoreceptors. The effects on cones at this stage were also reflected in the reduction of the 10 Hz flicker ERGs and the ONL thickness (Figure 23C, D).

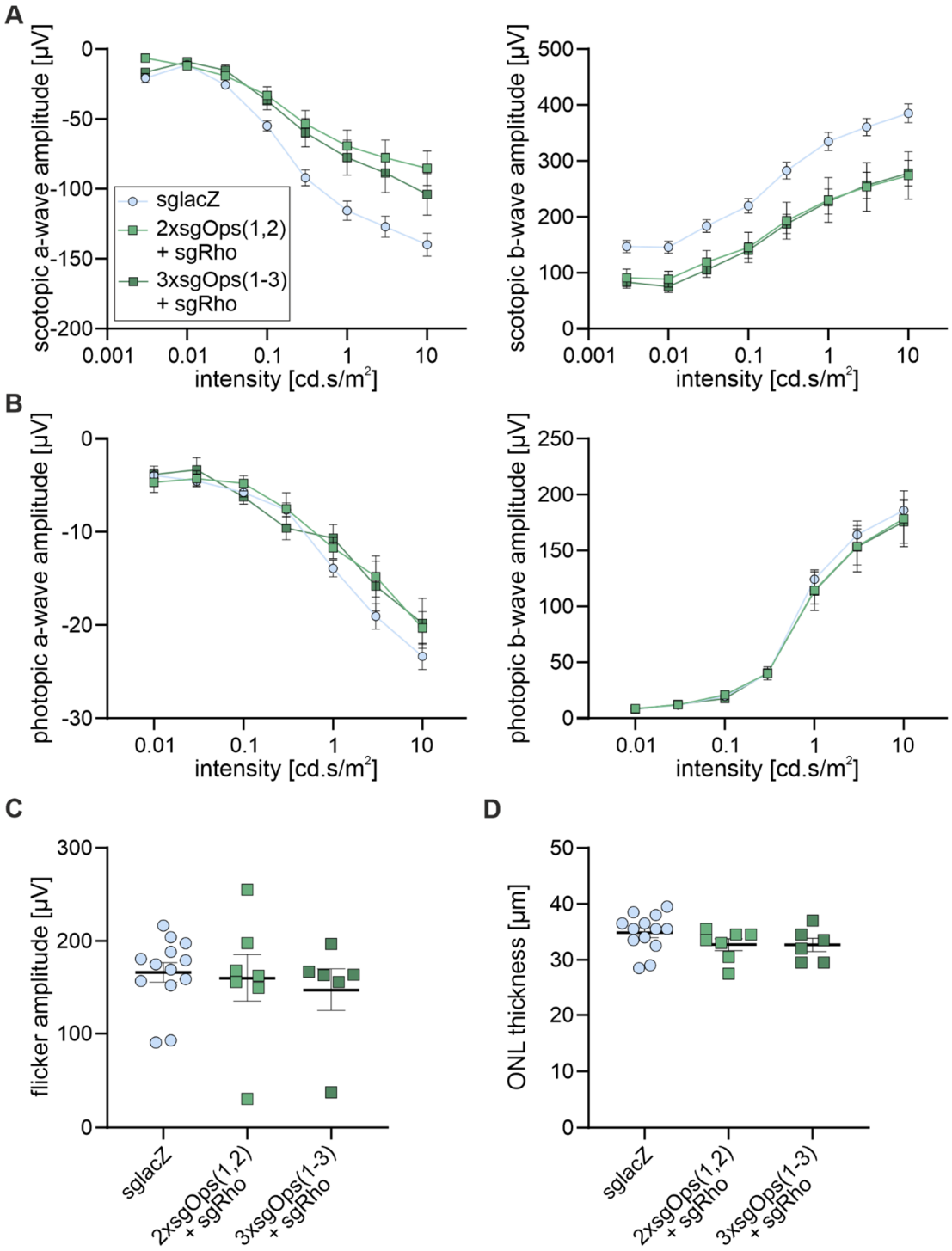

Figure 22: Evaluation of CONNACT on retinal function and morphology one month post injection. **A-B**, ERG measurements from Rho$^{P23H/+}$ mice injected with CONNACT (2xsgOps + sgRho, n = 7; 3xsgOps + sgRho, n = 6) or control (sglacZ, n = 13) vectors under scotopic (A) or photopic (B) conditions. **C**, Amplitudes generated by 10 Hz flicker ERG. **D**, Measurements of ONL thickness of treated and control eyes.

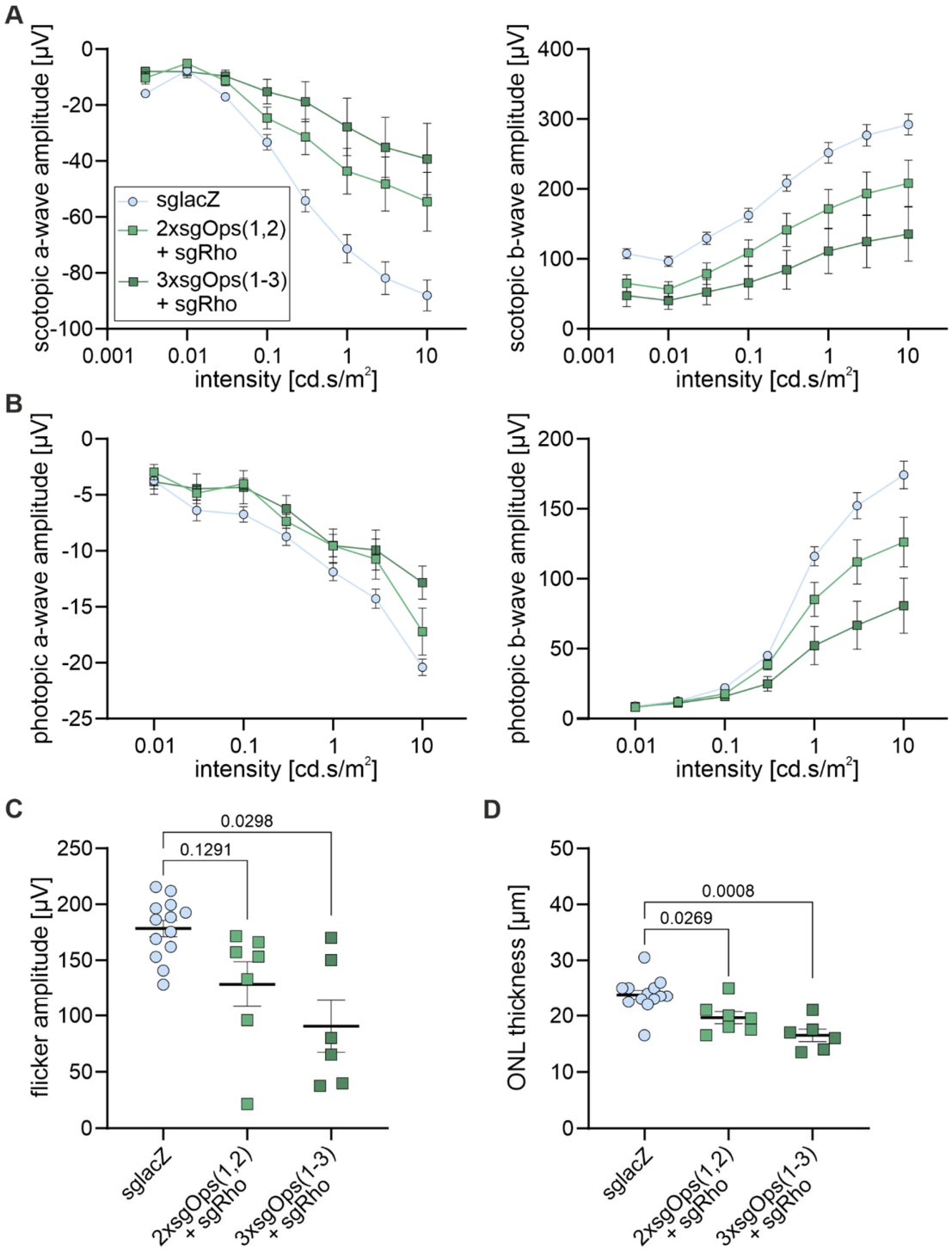

Figure 23: Evaluation of CONNACT three months post injection. A-B, ERG measurements from Rho$^{P23H/+}$ mice injected with CONNACT (2xsgOps + sgRho, n = 7; 3xsgOps + sgRho, n = 6) or control (sglacZ, n = 13) vectors under scotopic (A) or photopic (B) conditions. **C**, Amplitudes generated by 10 Hz flicker ERG. **D**, Measurements of ONL thickness of treated and control eyes. For statistical analysis, Welch's ANOVA with Dunnett's T3 multiple comparison test was performed.

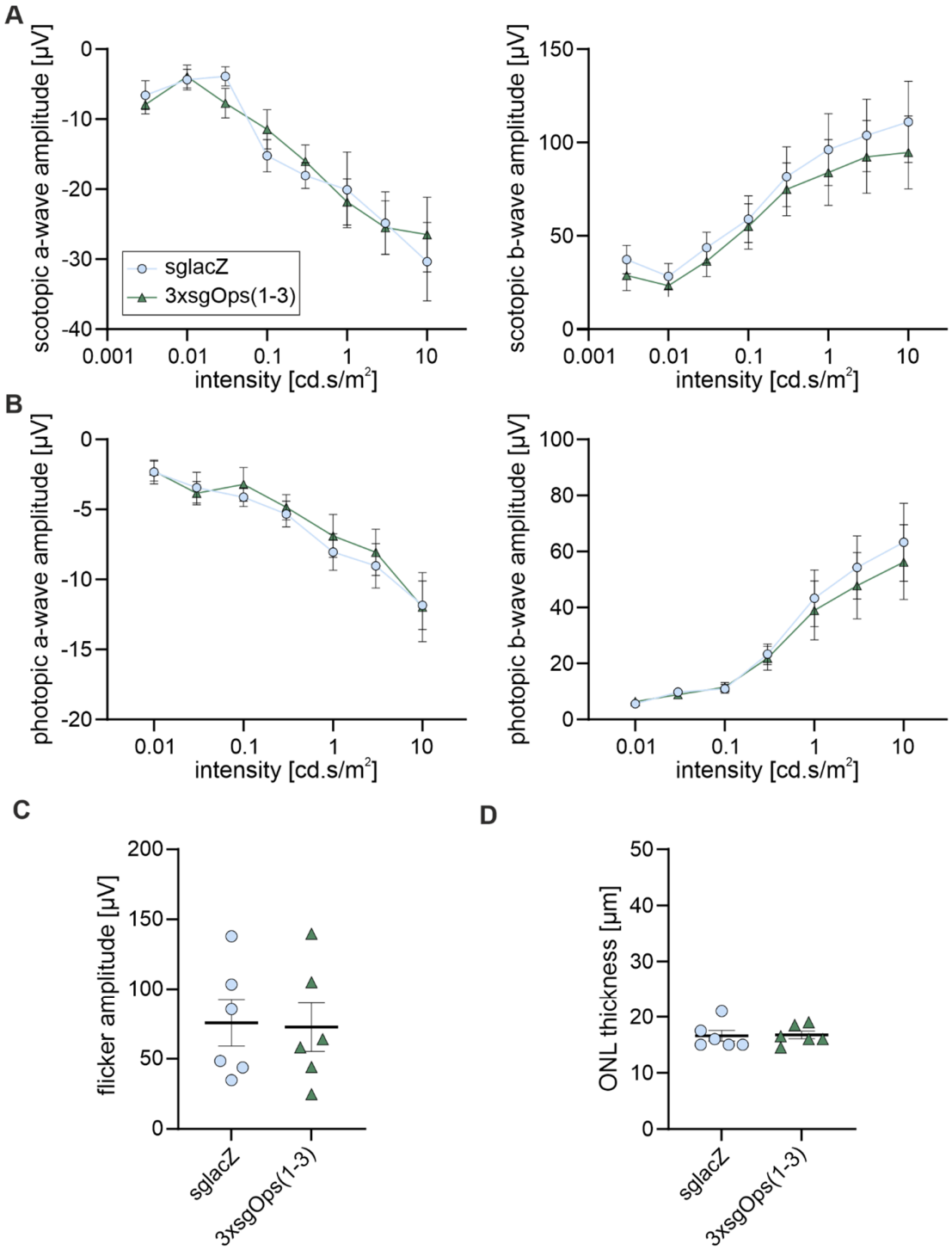

Figure 24: Evaluation of effects from *Opn1mw* transactivation on retinal function and morphology. A-B, ERG measurements from Rho$^{P23H/+}$ mice six months after subretinal injection with dual rAAV vectors including split Cas9-VPR and three sgRNAs (15 nt spacer) for the transactivation of *Opn1mw* (3xsgOps(1-3), n =6) or a control sgRNA (sglacZ, n = 6) under scotopic (A) or photopic (B) conditions. **C**, Amplitudes generated by 10 Hz flicker ERG. **D**, Measurements of ONL thickness of treated and control eyes.

Under these conditions, the CONNACT strategy accelerated the retinal degeneration accompanied by a decreased retinal function. To investigate whether the increased degeneration was caused by off-target effects due to the *Opn1mw* transactivation in combination with the catalytically active Cas9-VPR, $Rho^{P23H/+}$ mice were subretinally injected with dual REVeRT rAAV vectors expressing split Cas9-VPR and the sgRNAs for Opn1mw transactivation. However, no significant changes were observed between the transactivation group and the control group even six months after injection (Figure 24A-D). Another plausible explanation for the accelerated retinal degeneration upon treatment with the CONNACT strategy is that the moderate transactivation of *Opn1mw* was not sufficient to compensate for the pronounced knockout of *Rho*. This is in line with the previous studies on rhodopsin-deficient mice showing that the disease progression depends on the amount of the rhodopsin protein (Humphries et al., 1997).

4.2.3 Evaluation of sgRNAs for Enhanced *Opn1mw* Transactivation

To optimise the *Opn1mw* transactivation efficiency, nine new sgRNAs targeting the *Opn1mw* promoter region were designed and compared to the evaluated (Figure 25A). Transactivation efficiency was assessed after cotransfection of MEF cells with dCas9-VPR and sgRNAs. While sgOps(1) and sgOps(2) remained the best performing sgRNAs in their region, the new sgOps(3a) outperformed sgOps(3) (Figure 25B). Next, it was evaluated whether the higher transactivation efficiency could also be observed when sgOps(3) is replaced by sgOps(3a) in the sgRNA array. Indeed, a 2.8-fold increase in transactivation efficiency could be detected for the 3xsgOps(1,2,3a) combination compared to the original 3xsgOps(1-3) array (Figure 25C).

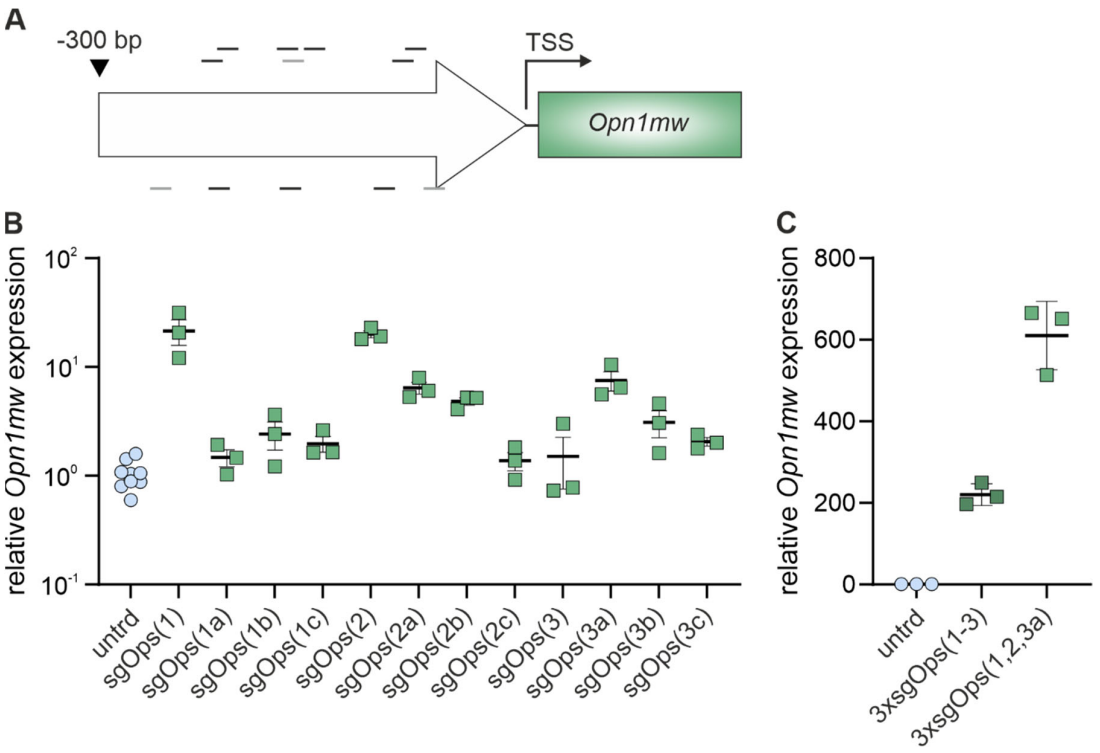

Figure 25: Evaluation of additional sgRNAs for the transactivation of *Opn1mw*. A, Binding positions of sgRNAs targeting the *Opn1mw* promoter region. The previously used sgRNAs are depicted in grey (sgOps1-3) and newly designed sgRNAs are depicted in black. **B**, Relative *Opn1mw* expression in MEF cells transfected with dCas9-VPR and sgRNAs targeting the *Opn1mw* promoter region. **C**, Comparison of *Opn1mw* transactivation efficiency of the previously used sgRNA array (3xsgOps(1-3)) and the optimised sgRNA array (3xsgOps(1,2,3a)). n = 3 for all conditions. bp, base pairs. TSS, transcriptional start site. untrd, untreated. nt, nucleotides.

Subsequently, it was investigated whether this increased transactivation efficiency using the 3xsgOps1,2,3a also persisted *in vivo*. Rho$^{P23H/+}$ mice were subretinally injected at P21 with dual rAAV vectors expressing Cas9-VPR and the optimised sgRNA array. The optimised sgRNA array could still reach the same reduction in *Rho* transcript compared to the previously used sgRNA array *in vivo* (Figure 26A). But surprisingly, no significant difference could be observed for transactivation of *Opn1mw* compared to the previous sgRNA array (Figure 26B).

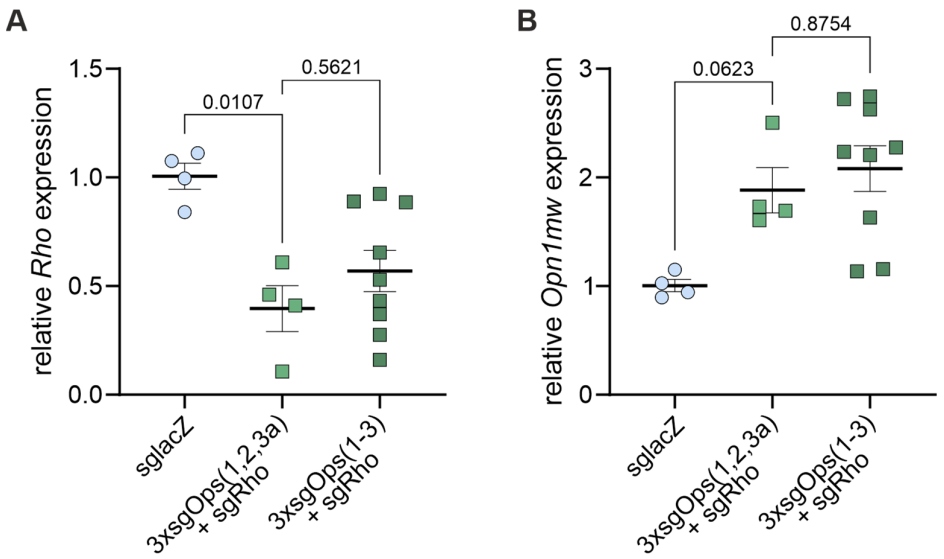

Figure 26: *Opn1mw* transactivation and *Rho* knockout in Rho$^{P23H/+}$ mice with optimised CONNACT vectors. Relative *Rho* (**A**) and *Opn1mw* (**B**) expression in the retina of Rho$^{P23H/+}$ mice four weeks after subretinal injection with the optimised CONNACT (3xsgOps(1,2,3a) + sgRho, n = 4) or control (sglacZ, n = 4) vectors. For comparison, activation and knockout efficiency reached with the previous system were included (3xsgOps(1-3) + sgRho, n = 9). Welch's ANOVA with Dunnett's T3 comparison test was used for statistical analysis.

Assessment of retinal function by ERG one month post injection showed a reduction in scotopic a- and b-wave amplitudes comparable to the previous treatment (Figure 27A). In addition, no improvement was observed in photopic ERG or OCT measurements (Figure 27B-D). Overall, these results were in accordance with the missing increase of *Opn1mw* transactivation with the optimised sgRNA array observed by qRT-PCR (Figure 26B).

In conclusion, a proof-of-principle for the CONNACT system was provided *in vivo*, but it needs further improvement before it can be used for the treatment of gain-of-function mutations in rhodopsin.

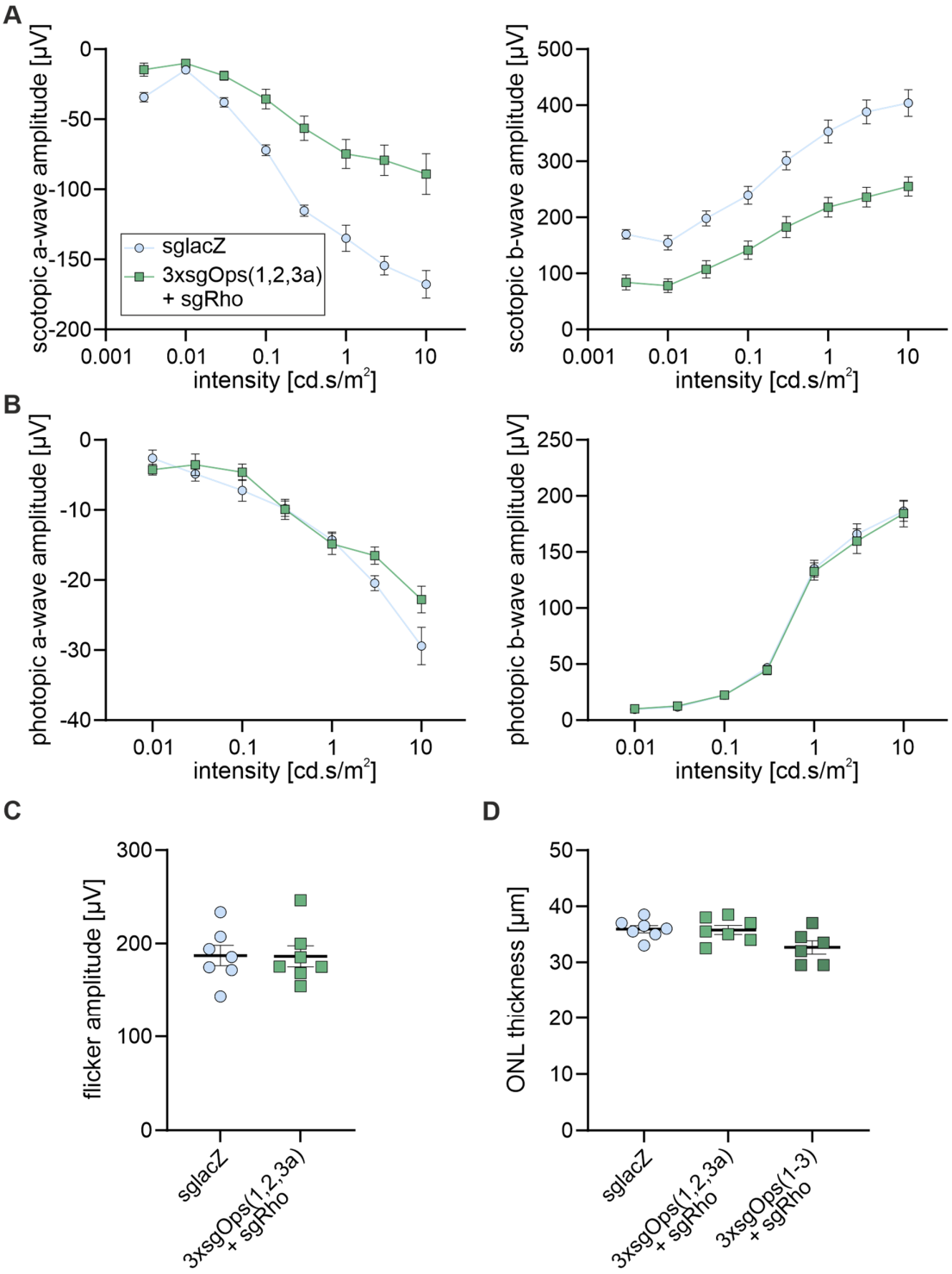

Figure 28: Treatment effects on retinal function and morphology with optimised CONNACT vectors. A-B, ERG measurements from Rho$^{P23H/+}$ mice one month after subretinal injection with optimised CONNACT (3xsgOps(1,2,3a) + sgRho, n = 7) or control (sglacZ, n = 7) vectors under scotopic (A) or photopic (B) conditions. **C**, Amplitudes generate by 10 Hz flicker ERG. **D**, Measurements of ONL thickness of treated and control eyes. Values obtained with the previous system (3xsgOps(1-3) + sgRho, n =6) are included for comparison.

4.3 Development of a Gene-Independent Therapy Approach for Inherited Retinal Diseases

4.3.1 Evaluation of CONNACT for Neuroprotection and Cellular Reprogramming

The CONNACT strategy per se is not limited to the treatment of gain-of-function mutations. In fact, it can be modified to develop a gene-independent approach for the treatment of IRDs by transactivating neuroprotective genes combined with a simultaneous knockdown of genes known to impact photoreceptor fate. Because of the central role of cones in visual perception in humans, long-term preservation of their survival, structure, and function represents the most attractive goal for patients suffering from IRDs. One way to achieve this goal is to reprogram rods into cone-like photoreceptors by the knockout of the transcription factor *Nrl* (Figure 5). The reprogrammed photoreceptors lack the expression of most rod-specific genes (Montana et al., 2013). Taking advantage of the CONNACT strategy established herein cone photoreceptor survival could be further enhanced by the transactivation of neuroprotective factors such as RdCVF encoded by *Nxnl1*. This strategy based on reprogramming and activation of trophic factors (hereafter referred to as REACT) was evaluated in vitro in 661W cells (Figure 28).

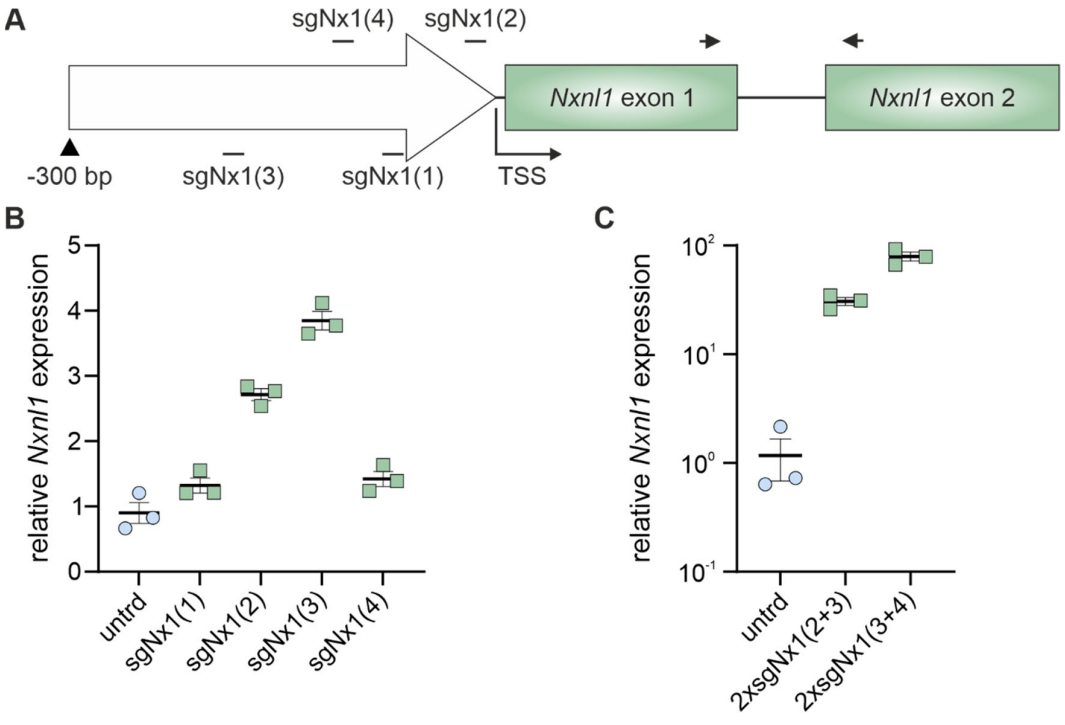

Figure 28: Transactivation of *Nxnl1* in 661W cells. A, Binding positions of sgRNAs targeting the *Nxnl1* promoter region. Black arrows indicate the position of primers used for qRT-PCR in B and C. **B**, *Nxnl1* expression in 661W cells cotransfected with plasmids

encoding for split Cas9-VPR and sgRNAs targeting the *Nxnl1* promoter region (sgNx1-4) relative to untreated 661W cells (untrd). **C**, Relative *Nxnl1* expression for 661W cells cotransfected with plasmids encoding for split Cas9-VPR and a sgRNA array of two sgRNAs. n = 3 for all conditions.

First, new sgRNAs targeting the *Nxnl1* promoter region (sgNx1) were designed and tested for their *Nxnl1* transactivation efficiency in 661W cells (Figure 28A, B). The three best performing sgRNAs were tested combined in arrays of two sgRNAs each. The array of sgNx1(3) and sgNx1(4) resulted in the highest transactivation and was used for all further experiments (Figure 28C).

Nxnl2 is a functionally equivalent counterpart of *Nxnl1,* and it also encodes two splice isoforms (Jaillard et al., 2012). Similar to the *Nxnl1* isoforms, the short *Nxnl2* isoform is a tropic factor (RdCVF2) and the long isoform functions as a thioredoxin enzyme (Figure 10). Due to the AAV packaging capacity, the uppermost number of sgRNAs that can be included in the 5' vector is four. As efficient *Nrl* knockout can be achieved with one and the *Nxnl1* transactivation with two sgRNAs, the remaining place can be used to include one sgRNA for *Nxnl2* transactivation.

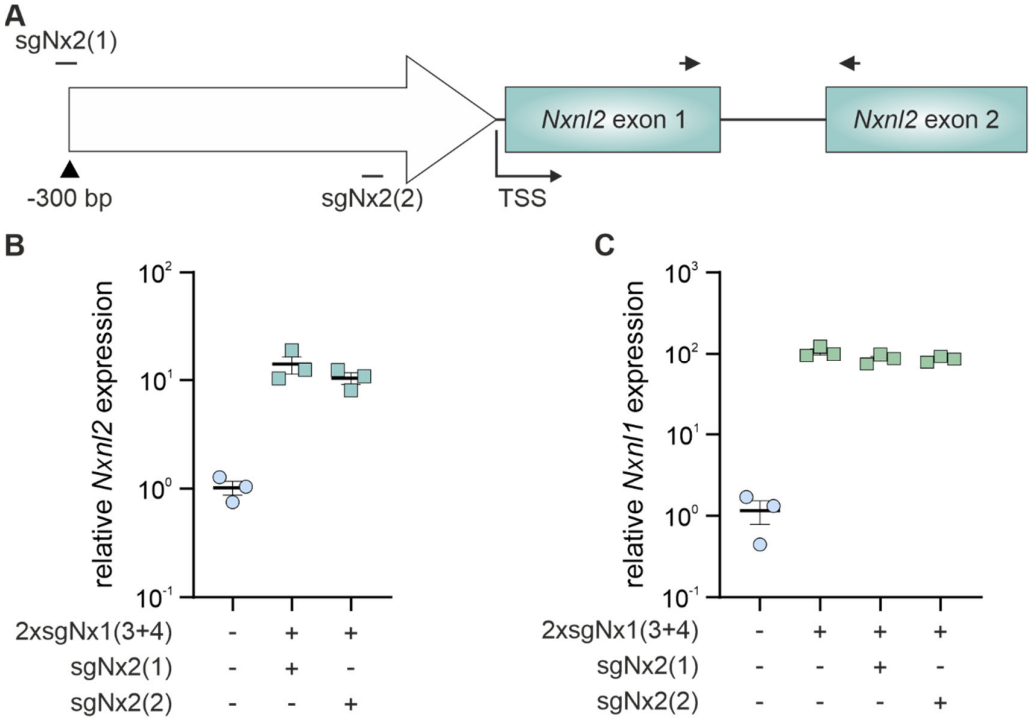

Figure 29: Transactivation of *Nxnl2* in 661W. A, Binding positions of sgRNAs targeting the *Nxnl2* promoter region. Black arrows indicate the position of primers used for qRT-PCR in B. **B**, Relative *Nxnl2* expression in 661W cells cotransfected with plasmids encoding for split Cas9-VPR and a sgRNA array containing sgRNAs targeting the *Nxnl2* promoter region

(sgNx2) and the *Nxnl1* promoter region (2xsgNx1(3+4). **C**, Relative *Nxnl1* expression for 661W cells cotransfected with plasmids encoding for split Cas9-VPR and a sgRNA array for the transactivation of *Nxnl1* and *Nxnl2*. n = 3 for all conditions.

Two sgRNAs targeting the *Nxnl2* promoter region (sgNx2) were designed and compared by cotransfection of 661W cells (Figure 29A). A slightly higher transfection efficiency could be observed for the first sgRNA (Figure 29B).

The experiments described above were designed to detect the transactivation efficiency of the long isoform of *Nxnl1* and *Nxnl2*. To assess transactivation of the short isoforms, each encoding a thioredoxin enzyme, specific reverse primers were used for qRT-PCR (Figure 30A). Using this approach, increased expression of the short *Nxnl1* isoform (RdCVF) was observed. This increase was not affected in the presence of one *Nxnl2* promoter region-targeting sgRNA (sgNx2(1)). However, almost no increase in RdCVF mRNA was observed when sgNx2(1) was replaced by sgNx2(2), another sgRNA targeting the *Nxnl1* promoter region (Figure 30B). Based on these results, sgNx2(1) was used for further REACT experiments.

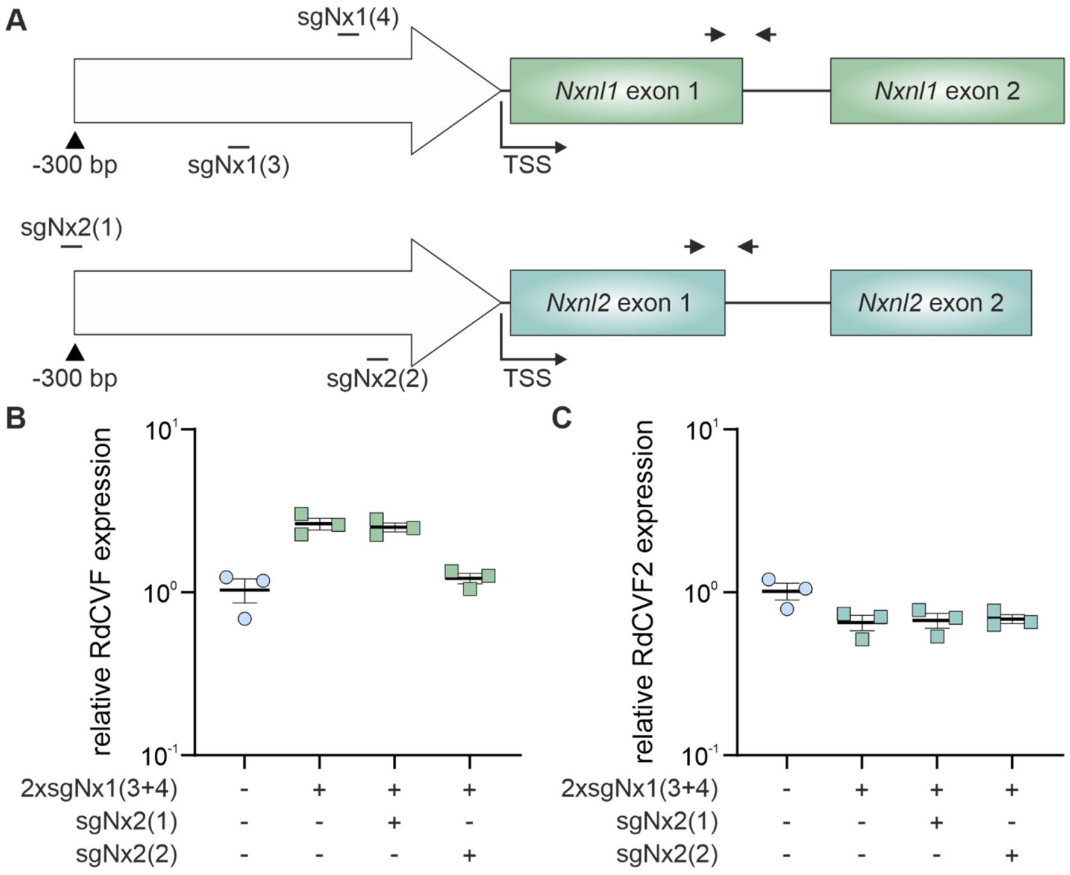

Figure 30: Transactivation of short splice isoforms with Cas9-VPR. A, Binding positions of sgRNAs targeting the *Nxnl1 or Nxnl2* promoter region. Black arrows indicate the position

of primers used for qRT-PCR in B or C. **B-C**, Relative expression of RdCVF (B) and RdCVF2 (C) in 661W cells cotransfected with plasmids encoding for split Cas9-VPR and a sgRNA targeted to the promoter region of *Nxnl1* (sgNx1(3+4)) or *Nxnl2* (sgNx2). n = 3 for all conditions.

No transactivation of the short isoform of *Nxnl2* could be detected (Figure 30C). Compared to the long isoform of *Nxnl1,* the transactivation of the short isoform was less efficient. For *Nxnl2* the increase in transcript of the long isoform was already very low, which might be the reason for the missing transactivation of the RdCVF2 transcript.

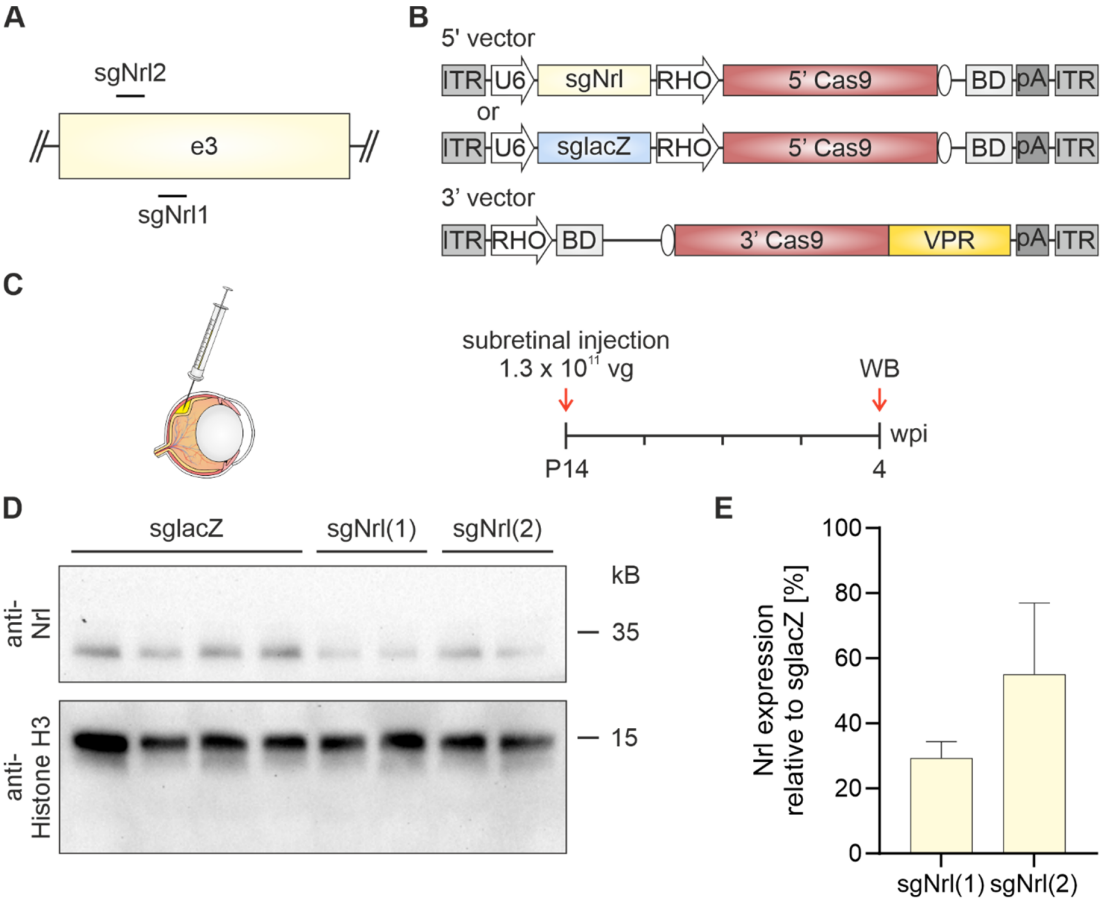

Figure 31: Evaluation of sgRNAs for the knockout of *Nrl* in WT mice. A, Binding positions of sgRNAs on the third exon of Nrl. **B**, Dual rAAV vector cassettes containing Cas9-VPR and a sgRNA targeting *Nrl* (sgNrl) or *lacZ* (sglacZ). **C**, Experimental design for evaluation of *Nrl* knockout efficiency after subretinal injection of WT mice. **D**, Western blot of lysates obtained from retinas four weeks after subretinal injection. **E**, Semi-quantitative analysis from western blot signals obtained in D (n = 2) relative to signals obtained from control injected eyes (sglacZ).

Next, a previously published (sgNrl(1)) and a new designed (sgNrl(2)) sgRNA targeting the third exon of *Nrl* (Figure 31A) were tested (W. Yu et al., 2017). The knockout efficiency was evaluated at the protein level after subretinal injection. Dual rAAVs containing split Cas9-VPR and a sgRNA were injected subretinally into WT mice at P14. The early timepoint

of injection was chosen because photoreceptors of younger mice are expected to be more responsive to reprogramming (Figure 31B, C). In line with the published results, both sgRNAs showed an efficient knockout of Nrl in the murine retina. The reduction rate of the first sgRNA targeting *Nrl* was higher and resulted in an overall reduction of the Nrl western blot band intensity by 71.55 % compared to retinas of WT mice control injected with dual rAAV vectors expressing Cas9-VPR and a lacZ targeting sgRNA (Figure 31D, E).

4.3.2 Evaluation of REACT in the Murine Retina

Next, the REACT strategy using the best performing sgRNAs was tested *in vivo*. Since the rod photoreceptor-specific RHO promoter might not be functional in reprogrammed rods after successful *Nrl* knockout, it was replaced by a GRK1 promoter that drives expression in both rod and cone photoreceptors (Figure 32A). Subretinal injection of WT mice was performed at P14 (Figure 32B). Successful knockout of *Nrl* was confirmed by western blot using retinal lysates from two mice (Figure 32C). Transactivation of both *Nxnl1* isoforms and the long isoform of *Nxnl2* could be detected (Figure 32D-F). In agreement with the *in vitro* results, no significant transactivation of RdCVF2 could be observed (Figure 32G).

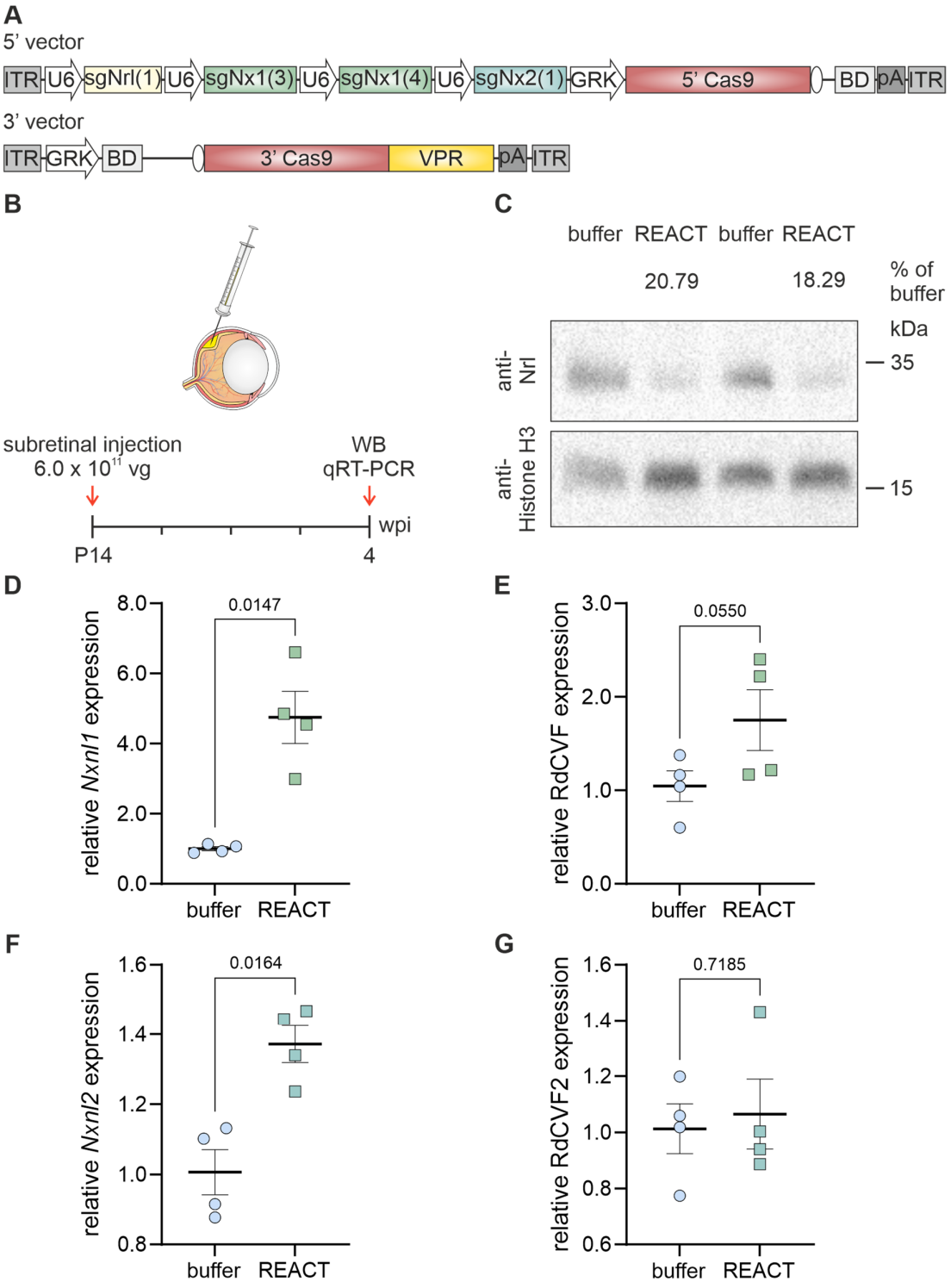

Figure 32: Evaluation of REACT in WT mice. A, REACT rAAV vector cassettes used for the knockout of *Nrl* and simultaneous activation of *Nxnl1* and *Nxnl2*. **B**, Experimental design for *in vivo* experiments using REACT. **C**, Western blot of lysates obtained from retinas four weeks after subretinal injection with REACT vectors (REACT, n = 2). The band intensity relative to bands obtained from retinas injected with the rAAV formulation buffer (buffer, n =2) is depicted above the western blot. **D-G**, Relative expression of *Nxnl1* (D),

RdCVF (E), *Nxnl2* (F) and RdCVF2 (G) (n = 4). For statistical analysis in D-G, a two-tailed paired t-test was performed.

It was further investigated whether the knockout of *Nrl* led to successful reprogramming of rods by evaluating the expression of the rod-specific genes *Rho* and *Nr2e3*, a downstream transcription factor of the *Nrl* pathway (Cheng et al., 2004). A reduction in transcript levels was observed for both *Rho* and *Nr2e3* compared to control injected eyes (Figure 33A, B). However, transactivation of the cone opsins *Opn1mw* and *Opn1sw* could not be detected (Figure 33C, D). This suggests that reprogramming of adult rod photoreceptors into cones by suppression of *Nrl* is incomplete, which is consistent with other studies (Montana et al., 2013).

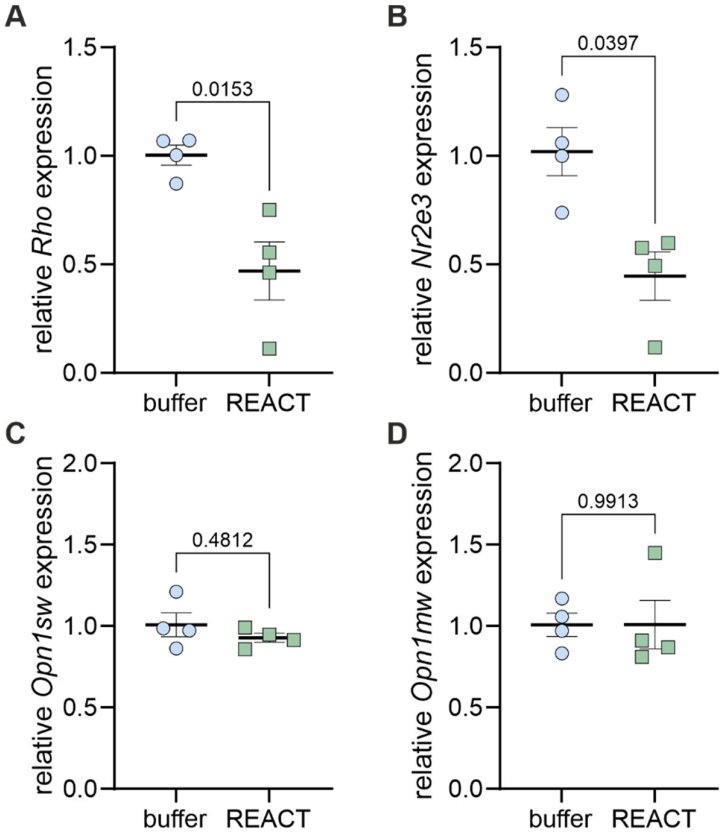

Figure 33: Effect of the *Nrl* knockout on the expression of photoreceptor-specific genes. **A-D,** Relative expression of *Rho* (A), *Nr2e3* (B), *Opn1sw* (C) and *Opn1mw* (D) in murine retinas four weeks after subretinal injection of REACT (n = 4). For statistical analysis, a two-tailed paired t-test was performed.

4.3.3 Evaluation of REACT in the Rho$^{P23H/+}$ Mouse Model

Finally, the efficiency of REACT in the RhoP23H/+ mouse model was evaluated. Mice were subretinally injected at P14 with dual rAAVs expressing the REACT components. The control contralateral eye of each mouse was injected with the rAAV formulation buffer.

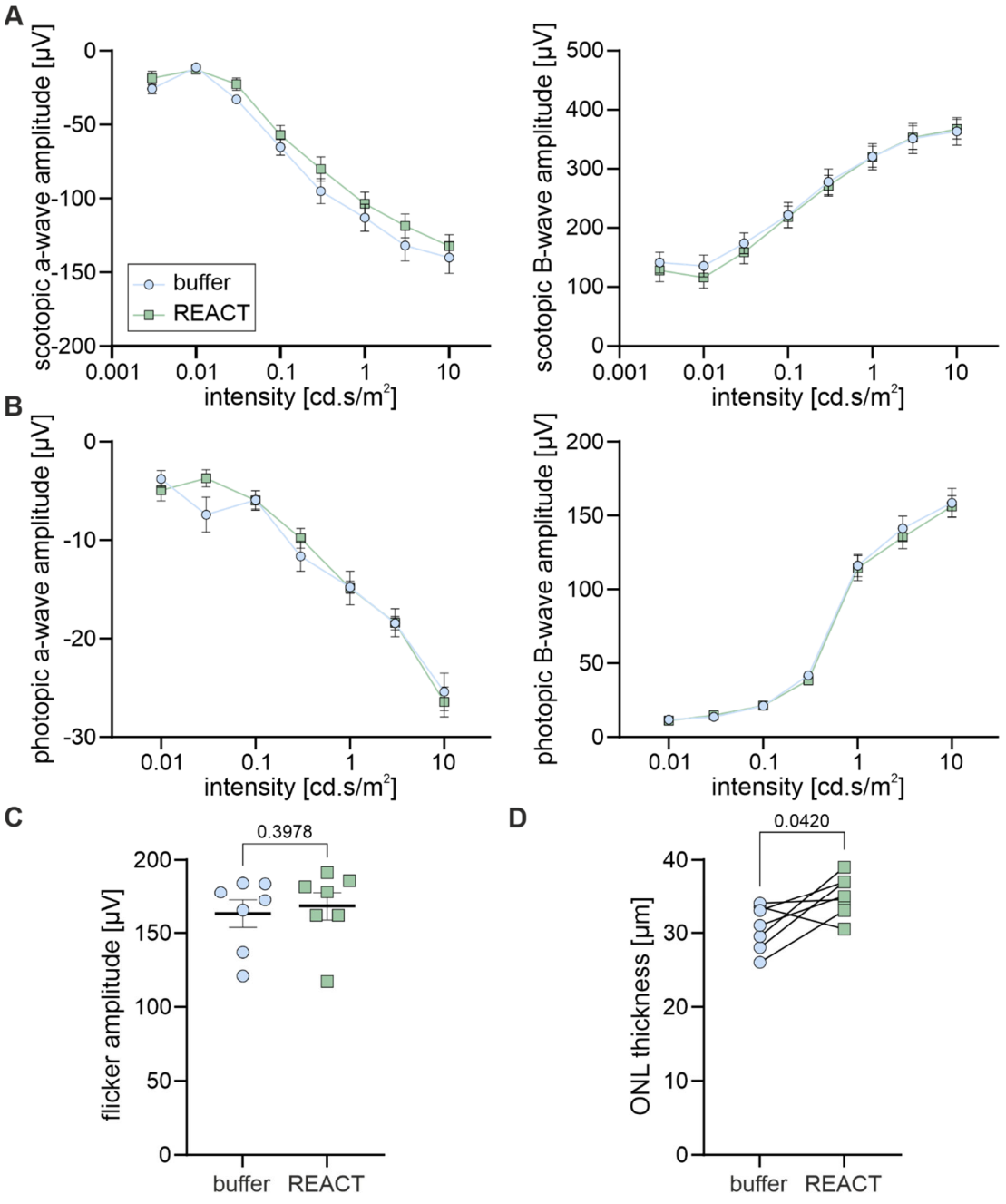

Figure 34: Effects of REACT on the retinal function and morphology in Rho$^{P23H/+}$ mice. **A-B**, ERG measurements from Rho$^{P23H/+}$ mice one month after subretinal injection with REACT (n = 7) or control (sglacZ, n = 7) vectors under photopic (A) or scotopic (B) conditions. **C**, Amplitudes generate by 10 Hz flicker ERG. **D**, Pairwise comparison of ONL

thickness of treated and contralateral control eyes. For statistical analysis in C and D, a two-tailed paired t-test was performed.

One month after subretinal injection, treatment effects were evaluated by ERG and OCT measurements. No changes in ERG amplitudes could be observed (Figure 34A-C). This is expected at that stage, given that REACT will most likely enhance only the survival of cones and the degeneration of cone photoreceptors becomes detectable at approximately three months of age in $Rho^{P23H/+}$mice. Nevertheless, a significant increase in ONL thickness could already be observed in OCT measurement of treated mice (Figure 34D). These results provide preliminary evidence that the REACT strategy may be an attractive new tool to prevent cone photoreceptor degeneration.

5 Discussion

5.1 Transcriptional Activation for Gene Therapy

5.1.1 MYO7B Transactivation for the Treatment of Usher Syndrome Type Ib

In the first part of the study, the transactivation of *Myo7b* for therapy of loss-of-function mutation in *Myo7a* was evaluated. It was shown that the gut-specific MYO7B can be transactivated with high efficiency in the murine retina. The main limitation of this study is the lack of evidence for the functionality of transactivated MYO7B in the murine retina. In contrast to humans, mouse models harbouring mutations in *Myo7a* do not show a severe retinal phenotype (Calabro et al., 2019; Lillo et al., 2003). This makes the mouse an unsuitable model organism for the evaluation of a therapy for Usher syndrome type Ib on retinal function (Calabro et al., 2019). Other large animal models (e.g., pigs), which are likely to have a more comparable phenotype to human patients, are currently being developed. MYO7A-deficient pigs could be used as a more appropriate model for assessing the effects on retinal function and morphology.

The successful transactivation of *MYO7B* in human retinal organoids (Figure 18) suggests that the transactivation system is functional in the human retina. sgRNAs for gene transactivation need to be designed specifically to every organism, therefore human retinal organoids are an important tool for the development of retinal transactivation therapies. In addition, retinal organoids can be used as disease models (Zhang et al., 2021). Such organoids are created from human pluripotent stem cells that have been altered by genome editing or derived from patient cells and can be used to evaluate treatment effects. For example, retinal organoids derived from an *RP2* retinitis pigmentosa patient showed an increase in ONL thickness after transduction with rAAVs containing a healthy copy of the mutated gene (Lane et al., 2020). No retinal organoid models have yet been developed for mutations in MYO7A. MYO7A-deficient retinal organoids would be a valuable model to evaluate the potential of the dual rAAV *MYO7B* transactivation system. Transduction and expression efficiency in retinal organoids could be further increased by using AAV serotypes with higher transduction rates and the strong ubiquitous CMV promoter (McClements et al., 2022).

In Usher syndrome type Ib, retinal degeneration is accompanied by congenital hearing loss and variable vestibular dysfunction (Delmaghani & El-Amraoui, 2022). The early onset of

hearing loss allows for diagnosis and retinal treatment before severe degeneration of photoreceptors. In principle, transactivation of *MYO7B* could also be used for the treatment of hearing loss and vestibular dysfunction by local administration to the inner ear (Maguire & Corey, 2020; Pan et al., 2017). Currently, hearing loss is treated with cochlear implants (Delmaghani & El-Amraoui, 2022). Although cochlear implants are a tremendous benefit to deaf patients, the enabled sound recognition is not comparable to regular auditory function (Geleoc & Holt, 2014). The inner ear is already fully developed in the second trimester of pregnancy (Hepper & Shahidullah, 1994). There may be a small treatment window after birth, but postnatal gene replacement or transactivation therapy would likely be too late to restore hearing (Toms et al., 2020).

Another important question is whether *MYO7B* transactivation offers advantages over classical gene replacement of *MYO7A* by dual rAAV vectors. Dual rAAV strategies for the delivery of split *MYO7A* have already been developed (Lopes et al., 2013; Trapani et al., 2014). However, depending on the dual rAAV strategies used, the use of split *MYO7A* could cause side effects resulting from the expression of the protein halves alone (Trapani et al., 2015). In contrast to gene replacement, transactivation by dCas9-VPR drives expression from a natural genomic locus, allowing the expression of different splice isoforms and long non-coding RNAs.

It remains to be determined whether the advantages of dCas9-VPR can counterbalance the most obvious disadvantage of this system, the long-term expression of a bacterial protein in retinal cells.

5.1.2 CRISPRa for the Treatment of other Diseases

An important advantage of CRISPRa is that systems for the transactivation of other genes can be easily developed by simply exchanging the sgRNAs. By contrast, dual rAAV gene replacement strategies require new design and validation of split constructs for every new gene. The number of diseases which possess potential functional counterparts is quite high. For instance, about 45 % of IRD-causing genes have counterparts that meet these criteria (Riedmayr et al., 2022). In addition to functionally equivalent genes, transactivation of cell-protective or disease-modifying genes also represent an attractive approach for inherited or acquired diseases (Becirovic, 2022). Another advantage of CRISPRa-based strategies is that transactivation is completely independent of target gene size. This strategy can therefore be

used preferably to target very large genes which cannot be packaged into dual rAAVs. One example is the laminin-α1 gene (*LAMA1*), which is associated with cerebellar dysplasia and retinal dystrophy (Aldinger et al., 2014). *LAMA1* possess a functional equivalent, the *LAMA2* gene, which is a highly attractive target for transactivation. Mutations in *LAMA2* cause muscular dystrophy and it has already been shown that transactivation of *Lama1* improves the disease phenotype in mice carrying a splice site mutation in *Lama2* (Kemaladewi et al., 2019).

In this study, the high versatility of the dCas9-VPR system to facilitate transactivation in brain, heart, skeletal muscle, lung, liver, and retina has been demonstrated. The combination of systemic application with specific promoters enables the treatment of multisystemic or difficult to reach tissues and could reduce the injury caused by local injections. With the AAV9 serotype, it should even be possible to facilitate treatment of the central nervous system after systemic administration, as AAV9 vectors can cross the blood-brain barrier (Zincarelli et al., 2008).

Furthermore, the transactivation approach allows for the supplementation of multiple genes (Cong et al., 2013; Mali et al., 2013). Multiplexed transactivation could be used for the treatment of polygenic diseases or the additional transactivation of cell-protective genes, which could act synergistically to increase treatment success. In contrast to gene replacement, transactivation leads to expression from a natural gene locus and should include the expression of splice isoforms and non-coding RNAs. The supplementation of multiple splice isoforms is of particular importance if the isoforms perform different functions in the cell, such as the *Nxnl1* isoforms (Leveillard & Sahel, 2017). In contrast to gene correction with other CRISPR-based approaches, treatment strategies based on transcriptional activation are mutation-independent (van der Bent et al., 2018; Wang et al., 2020).

The dCas9-VPR system itself does not induce permanent changes to the genome, and CRISPR-mediated transactivation has been shown to cause no off-target effects after long-term expression *in vivo* (Kemaladewi et al., 2019; Liao et al., 2017; Matharu et al., 2019). As a protein of bacterial origin, Cas9 carries the risk of causing immune responses. After intramuscular injection of AAVs containing *Sp*Cas9 in mice, elevated levels of monocytes and T-cells have been observed, but no cytotoxicity (Chew et al., 2016)**.** While the risk of immunogenicity is lower after local injection to immune-privileged tissues such as the retina, it presents a problem for systemic treatment. Additionally, activation of the immune system by pre-existing antibodies or T-cells specific to *Sp*Cas9 could cause a reduction in treatment

efficiency (Charlesworth et al., 2019; Simhadri et al., 2018; Wagner et al., 2019). Since *Sp*Cas9 delivered by rAAV vectors is only expressed inside the target cells, it should not be exposed to neutralizing antibodies, but treated cells could be the target of cytotoxic T-cells. *Sp*Cas9-reactive regulatory T-cells also already exist in humans and have been shown to reduce immune reactions caused by *Sp*Cas9 (Wagner et al., 2019). They could be useful in preventing severe immune reactions along with the administration of immunosuppressive treatment. Another way to circumvent immunogenicity would be the use of Cas9 variants derived from bacteria that are non-pathogenic to humans or artificially modified variants with immunosilenced T-cell epitopes (Ferdosi et al., 2019). Neutralisation by an immune reaction displays a specific risk for gene transactivation therapies, as they rely on permanent expression in the target cells. This is in contrast to CRISPR-Cas gene-editing tools, which are causing permanent modifications in the genome and are no longer needed after successful editing. dCas9-VPR needs to be delivered in vectors that support long-term expression, such as AAVs. Although this issue remains to be further investigated, long-term therapeutic effects utilizing CRISPRa might thus require the co-medication of immunosuppressive drugs.

5.2 Potential of the CONNACT Strategy for the Treatment of Retinal Diseases and Beyond

5.2.1 CONNACT for the Treatment of Gain-of-Function Mutations

In addition to simple gene transactivation, this study evaluated the use of the CONNACT strategy, which combines transactivation and gene knockout in a single CRISPR-Cas9 module. The CONNACT system is built on the discovery that sgRNAs with shortened spacer lengths can be used for the transactivation of genes with a catalytically active Cas9-VPR (Dahlman et al., 2015; Kiani et al., 2015). In the first experiments, the CONNACT system was evaluated for the treatment of gain-of-function mutations in rhodopsin by knockout of *Rho* and transactivation of the functionally equivalent *Opn1mw*. After subretinal injection of $Rho^{P23H/+}$ mice a proof-of-concept of the CONNACT strategy could be provided for *in vivo* application (Figure 20). Unfortunately, no benefit in $Rho^{P23H/+}$ mice was observed after one and three months of treatment (Figures 22, 23). The lack of therapeutic benefit might be explained by the strong *Rho* knockout and rather weak Opn1mw transactivation. The average reduction of *Rho* transcript in the retina of subretinally injected $Rho^{P23H/+}$ mice was between 43 and 70 % (Figure 20). As a single subretinal injection covers only one third of the retina,

it can be concluded that the knockout of *Rho* alleles was highly efficient in transduced cells. Mice lacking any rhodopsin expression display a more severe phenotype compared to the $Rho^{P23H/+}$ mice (Humphries et al., 1997; Sakami et al., 2011). Sufficient amounts of M-opsin as a rhodopsin substitute are therefore likely to be crucial for treatment success. In the murine retina, the ratio between rods and cones is 33:1, and a reduction of 50 % in rhodopsin already results in a mild phenotype (Carter-Dawson & LaVail, 1979; Humphries et al., 1997). For this reason, the total knockout of rhodopsin by CRISPR-Cas9 most likely needs to be compensated by an *Opn1mw* gene activation of at least 15-fold to enable successful treatment. Such values could not be reached even after optimisation of the sgRNA array. At this point, the *Opn1mw* expression could only be further evaluated by increasing the number of sgRNAs targeting its promoter region or further evaluation and optimisation of new sgRNAs.

The difficulties of complete *Rho* knockout could be overcome by using a CONNACT system with a Cas9 variant that can distinguish between the mutated and healthy alleles. Since most Cas9 variants are unable to confidently distinguish between single mismatches in their spacer sequence, the P23H causing point mutation should be part of the PAM sequence to ensure a specific knockout of the defective allele (Chen et al., 2017; Hsu et al., 2013). The SpCas9-VQR variant recognises an NGA PAM sequence and has been used to specifically disrupt the mutated allele harbouring a C>A transversion mutation in the $Rho^{P23H/+}$ mouse model where a reduced disease progression could be observed upon treatment (Giannelli et al., 2018). The key limitation of such a system is that it is tailored to the treatment of one specific mutation. While the P23H mutation in rhodopsin is the most frequent gain-of-function mutation in North America, the high frequency is based on a founder effect (Farrar et al., 1990). In Europe and Asia, the P23H mutation is almost non-existent and other mutations such as P347L are more frequent (Fernandez-San Jose et al., 2015; Kim et al., 2011). As there are over 150 different mutations known in rhodopsin, mutation-specific approaches might not be appropriate (Athanasiou et al., 2018).

Other treatment options for gain-of-function mutations in rhodopsin are based on the degradation of *RHO* mRNA (Meng et al., 2020). Antisense oligonucleotides (AONs) are small single-stranded DNA molecules that target complementary mRNA. The resulting double-stranded fragments are then cleaved by RNase H1 (Crooke, 2017). AONs can be used to specifically target the P23H mutant mRNA and thus remove the mutated rhodopsin without harming the correct version (Murray et al., 2015). An obstacle with AONs is that

they cannot be delivered by vectors for long-term expression as they are DNA molecules. Therefore, long term therapy would require multiple applications, which entails a higher risk of side effects. Short hairpin RNAs (shRNAs), on the other hand, can be delivered via rAAV vectors for permanent expression in post-mitotic cells. They assemble in a silencing complex and induce target mRNA degradation (Hutvagner & Zamore, 2002). The disruption of *RHO* transcript off both alleles by shRNAs, with the codelivery of a healthy *RHO* coding sequence, that is altered in such a way to be unaffected by the shRNA, within the same rAAV, enables the treatment of gain-of-function mutations in rhodopsin (Cideciyan et al., 2018; Kiang et al., 2005). The main difficulty of strategies based on RNA degradation is that they only achieve an incomplete knockdown of *RHO* transcript in the target cells in contrast to methods altering the genomic sequence. For a complete knockout of *Rho*, CRISPR-Cas9 has been used. By delivery of two rAAV vectors, one expressing Cas9 and the other two sgRNAs targeting *Rho* and a modified healthy gene copy, the treatment of gain-of-function mutations is possible (Tsai et al., 2018). The packaging of the sgRNAs together with the replacement coding sequence ensures that the knockout only takes place if the new healthy copy is also delivered. However, this strategy is only feasible for genes with a coding sequence small enough to be packaged together with the two sgRNAs into one rAAV. As the CONNACT system is independent of target gene size it could also be used for the treatment of diseases that require the supplementation of larger genes.

Other diseases caused by gain-of-function mutations that could potentially be treated with the CONNACT system are, for example, catecholaminergic polymorphic ventricular tachycardia or osteogenesis imperfecta. Mutations in the ryanodine receptor type 2 (RyR2), an intracellular calcium release channel in the sarcoplasmic reticulum, cause arrhythmogenic disorders and can lead to sudden death (Sleiman et al., 2021). Dominant mutations in RyR2 are the main reason for catecholaminergic polymorphic ventricular tachycardia (Priori et al., 2001). The cardiac RyR2 is induced by Ca^{2+} influx and is responsible for the release of Ca^{2+} from the sarcoplasmic reticulum into the cytosol of the cardiac myocytes (Bers, 2002). In the skeletal muscle, the highly similar RyR1 facilitates a rapid release of Ca^{2+} from the endoplasmic reticulum (Witherspoon & Meilleur, 2016). Due to the large coding sequence of RyR2, 16.6 kB, a knockout combined with the supplementation of a healthy RyR2 copy is not possible in two rAAV vectors. Knockout of RyR2 and the transactivation of RyR1 with the CONNACT system could be delivered in dual rAAVs and used for the treatment of dominant catecholaminergic polymorphic ventricular tachycardia. To ensure efficient treatment of cardiac myocytes, systemic injections with the dual rAAVs REVeRT

transactivation system could be performed. The use of a cardiac-specific promoter would increase the safety of the system, but the possible higher risk of immunogenicity due to systemic application needs to be investigated. Furthermore, CONNACT could be used for the treatment of gain-of-function mutations in the collagen α1(I) chain (COL1A1), which cause bone dysplasia (Etich et al., 2020). COL1A1 is present in the bone extracellular matrix but is also necessary to ensure structure and stability in other tissues (Marini et al., 2017). A specific knockout of the affected COL1A1 allele could reduce the severity of the disease, but mild symptoms would remain due to haploinsufficiency (Rousseau et al., 2014). The combined knockout of COL1A1 with simultaneous transactivation of COL2A1, a highly similar homologue, with the CONNACT system could be used for the treatment of osteogenesis imperfecta.

To enable lifelong treatment, the CONNACT system relies on constant expression. While CRISPR-Cas transactivation has proven safe in long-term expression and shortened sgRNAs can even be used to protect off-target sites from disruption by Cas9 (Rose et al., 2020), long-term expression of 20 nt spacer length sgRNAs with catalytically active Cas9 could be a risk. The treatment success depends on constant supplementation of the functionally equivalent protein and thus Cas9-VPR expression, whereas the knockout of both target alleles should be completed shortly after the treatment application. The risk of off-target effects by nuclease active Cas9 could be reduced by limiting the expression of the knockout sgRNA. One way would be the codelivery of the knockout sgRNA as RNA molecules or part of a DNA plasmid packaged into non-viral vectors (Behr et al., 2021). This system would allow a transient expression of the sgRNA. However, delivery of an additional component comes with complications in the production and quality control of a future therapeutic. Another way would be the use of inducible sgRNAs, which are activated by administration of small molecules (Tang et al., 2017). The limitation of inducible systems is that they do not allow full control and often show off-state activity. Flanking a sequence with CRISPR-Cas recognition sites facilitates simultaneous cutting on both ends and the excision of the respective sequence (Cong et al., 2013). This technique could be used to remove the knockout sgRNA from the AAV episome after transduction. If the knockout sgRNA expression cassette is flanked by its recognition site, the knockout sgRNA would not only recognise the target site but also the sequences next to its coding sequence and could excise itself from the episome. The advantage of such a self-cutting system is that no additional component is needed and the knockout sgRNA can be completely removed. However, the target gene knockout efficiency could be reduced and production of rAAVs

would only be possible if the split Cas9-VPR is not expressed in the rAAV production cell line, otherwise, truncation of the transgene at this stage could not be excluded.

5.2.2 REACT as a Gene-Independent Treatment Strategy

In the third part of the study, a system for gene-independent treatment for retinal gene therapy was developed. IRDs are a group of different rare diseases and patient groups that share the same mutation are usually quite small, moreover, there are still patients with no clear genetic diagnosis (Perea-Romero et al., 2021). A gene-independent strategy based on reprogramming and neuroprotection could be used to benefit a large heterogeneous group of patients. A proof-of-principle for the combination of reprogramming of rod photoreceptors based on *Nrl* knockout and neuroprotection by transactivation of the trophic factors *Nxnl1* and *Nxnl2* was provided (Figure 32). Additionally, first results of the treatment evaluation of the REACT system show a promising effect on retinal morphology (Figure 34D). Further evaluation of the system in long-term studies and different disease models needs to be provided to assess the full therapeutic potential of REACT. A comparison of the REACT system with its individual components, cellular reprogramming, and supplementation of neuroprotective factors, should be performed to evaluate the higher benefit of the combination.

To further optimise the REACT system, a strong ubiquitous promoter such as CMV could be used to drive split Cas9-VPR expression. Since Cas9-VPR expression levels have been linked to the transactivation efficiency (Figure 14E), a higher expression of the split Cas9-VPR fragments should further increase expression levels of the neuroprotective components of the REACT system. Furthermore, the use of a ubiquitous promoter would allow *Nxnl1* and *Nxnl2* transactivation in additional retinal cell types such as Müller glia or RPE cells, which could enhance the neuroprotective effect. The knockout of *Nrl* should not affect other cell types, as it is mainly expressed in rod photoreceptor cells in the mature retina (Swain et al., 2001). While this study provided a proof-of-principle that Cas9-VPR mediated transactivation can be used to increase the expression of multiple genes and splice isoforms simultaneously (Figure 32D-G), it should be considered to focus only on *Nxnl1* transactivation for future therapeutic use. This way, a third sgRNA targeting the *Nxnl1* promoter region could be included to further enhance transactivation efficiency. In addition, it should be noted that a less complex system would simplify the approval by authorities and quality control of a future therapeutic, so the combination of gene transactivation should

only be considered if a synergistic effect is expected. Since *Nxnl1* and *Nxnl2* are functionally related, transactivation of both genes probably has an additive but not necessarily synergistic effect. Whereas additional transactivation of downstream genes of the RdCVF pathway, such as the RdCVF receptor basigin, could further improve treatment success and should be evaluated.

The reprogramming of rods into cone-like photoreceptors enables the suppression of rod-specific gene expression. An increase in the expression of cone-specific genes on the other hand is impeded by epigenetic modifications in mature photoreceptors (Montana et al., 2013). For this reason, treatment strategies based on reprogramming by *NRL* knockout can be used to abolish the expression of mutated rod-specific genes and thus prevent disease progression and cone photoreceptor degeneration but lead to a loss in rod photoreceptor function (Montana et al., 2013; W. Yu et al., 2017). Therefore, dim-light and peripheral vision could decrease upon treatment. This loss might be acceptable for patients to maintain cone photoreceptor function and daylight vision. It should be noted that retinitis pigmentosa patients might have already lost many rods before the onset of first symptoms, subsequential diagnosis and a potential treatment application (Leinonen et al., 2020). Reprogramming with the REACT system did not result in an increased expression of cone opsins (Figure 33C, D). In contrast, by targeting Cas9-VPR to the *Opn1mw* promoter region, an increase in *Opn1mw* expression could be achieved despite its methylation status in the mature retina (Figure 20D, E) (Bohm et al., 2020). It would be interesting to investigate if a combination of *Nrl* knockout with the transactivation of cone opsins would lead to full reprogramming of rods into functional cone-like photoreceptors and could improve the therapeutic effect of REACT.

5.2.3 Additional Applications for CONNACT

CRISPR-Cas technology plays an important role in the development of innovative treatments for different diseases (Karimian et al., 2020; Katti et al., 2022; Martinez-Escobar et al., 2020). The CONNACT system allows the combination of different strategies that could have synergistic effects. In cancer therapy, for example, the knockout of oncogenes or multidrug resistance genes combined with the transactivation of tumour suppressor genes. The knockout of different genes has already been proven to be beneficial in cancer therapy. For example, the knockout of the protein kinase PLK1, which is required for mitosis, decreased tumour growth and increased survival in mouse models of glioblastoma and metastatic ovarian adenocarcinoma (Rosenblum et al., 2020). A problem of PLK1 knockout

is that other dividing cells could also be affected, leading to serious side effects. The targeting of cancer-specific mutations such as fusion oncogenes would be less harmful. The disruption of fusion oncogenes, which are a product of chromosomal rearrangements and often lead to constant expression of tyrosine kinases or transcription factors, has been shown to result in the specific elimination of cancer cells (Martinez-Lage et al., 2020). Other targets for gene knockout are multidrug resistance genes such as *MDR1* (Ha et al., 2016). Their knockout would restore the sensitivity of cancer cells to chemotherapeutic treatments. To increase treatment efficiency the CONNACT system could be used to combine the knockout of these genes with the transactivation of silenced tumour suppressor genes such as *MASPIN*, *REPRIMO*, or *PTEN* that have been shown to decrease cancer proliferation (Garcia-Bloj et al., 2016; Moses et al., 2019). Transactivation of the mutant tumour product themselves could also improve treatment efficiency, as increased expression leads to higher antigen presentation and subsequent T-cell response (G. Wang et al., 2019). The treatment of neurodegenerative diseases could be facilitated by the transactivation of neuroprotective genes and the simultaneous knockout of cell-damaging genes. For example, the accumulation of amyloid-β protein is linked to Alzheimer's disease (Zhang et al., 2011). Amyloid-β is produced from amyloid precursor protein (APP) following β-cleavage. In contrast, α-cleavage initiates a non-amylogenic pathway and results in the generation of neuroprotective sAPPα. Specific editing of the C-terminus of amyloid precursor protein by CRISPR-Cas has been shown to inhibit β-cleavage (Sun et al., 2019), to further increase sAPPα concentration the CONNACT system could be used to combine gene editing with the transactivation of Adam10 that induces the α-cleavage pathway (Park et al., 2021). Such a combination could increase the therapeutic benefit for patients suffering from Alzheimer's disease.

In conclusion, the CONNACT system shows great therapeutic potential for the treatment of IRDs and offers new treatment options for a wide range of inherited and acquired diseases.

6 References

Ait-Ali, N., Fridlich, R., Millet-Puel, G., Clerin, E., Delalande, F., Jaillard, C., Blond, F., Perrocheau, L., Reichman, S., Byrne, L. C., Olivier-Bandini, A., Bellalou, J., Moyse, E., Bouillaud, F., Nicol, X., Dalkara, D., van Dorsselaer, A., Sahel, J. A., & Leveillard, T. (2015). Rod-derived cone viability factor promotes cone survival by stimulating aerobic glycolysis. *Cell*, *161*(4), 817-832. https://doi.org/10.1016/j.cell.2015.03.023

Aldinger, K. A., Mosca, S. J., Tetreault, M., Dempsey, J. C., Ishak, G. E., Hartley, T., Phelps, I. G., Lamont, R. E., O'Day, D. R., Basel, D., Gripp, K. W., Baker, L., Stephan, M. J., Bernier, F. P., Boycott, K. M., Majewski, J., University of Washington Center for Mendelian, G., Care4Rare, C., Parboosingh, J. S., . . . Doherty, D. (2014). Mutations in LAMA1 cause cerebellar dysplasia and cysts with and without retinal dystrophy. *Am J Hum Genet*, *95*(2), 227-234. https://doi.org/10.1016/j.ajhg.2014.07.007

Amoasii, L., Long, C., Li, H., Mireault, A. A., Shelton, J. M., Sanchez-Ortiz, E., McAnally, J. R., Bhattacharyya, S., Schmidt, F., Grimm, D., Hauschka, S. D., Bassel-Duby, R., & Olson, E. N. (2017). Single-cut genome editing restores dystrophin expression in a new mouse model of muscular dystrophy. *Sci Transl Med*, *9*(418). https://doi.org/10.1126/scitranslmed.aan8081

Athanasiou, D., Aguila, M., Bellingham, J., Li, W., McCulley, C., Reeves, P. J., & Cheetham, M. E. (2018). The molecular and cellular basis of rhodopsin retinitis pigmentosa reveals potential strategies for therapy. *Prog Retin Eye Res*, *62*, 1-23. https://doi.org/10.1016/j.preteyeres.2017.10.002

Bailey, S. R., & Maus, M. V. (2019). Gene editing for immune cell therapies. *Nat Biotechnol*, *37*(12), 1425-1434. https://doi.org/10.1038/s41587-019-0137-8

Bakondi, B., Lv, W., Lu, B., Jones, M. K., Tsai, Y., Kim, K. J., Levy, R., Akhtar, A. A., Breunig, J. J., Svendsen, C. N., & Wang, S. (2016). In Vivo CRISPR/Cas9 Gene Editing Corrects Retinal Dystrophy in the S334ter-3 Rat Model of Autosomal Dominant Retinitis Pigmentosa. *Mol Ther*, *24*(3), 556-563. https://doi.org/10.1038/mt.2015.220

Barrangou, R., Fremaux, C., Deveau, H., Richards, M., Boyaval, P., Moineau, S., Romero, D. A., & Horvath, P. (2007). CRISPR provides acquired resistance against viruses in prokaryotes. *Science*, *315*(5819), 1709-1712. https://doi.org/10.1126/science.1138140

Baylor, D. A. (1987). Photoreceptor signals and vision. Proctor lecture. *Invest Ophthalmol Vis Sci*, *28*(1), 34-49. https://www.ncbi.nlm.nih.gov/pubmed/3026986

Becirovic, E. (2022). Maybe you can turn me on: CRISPRa-based strategies for therapeutic applications. *Cell Mol Life Sci*, *79*(2), 130. https://doi.org/10.1007/s00018-022-04175-8

Beerli, R. R., Segal, D. J., Dreier, B., & Barbas, C. F., 3rd. (1998). Toward controlling gene expression at will: specific regulation of the erbB-2/HER-2 promoter by using polydactyl zinc finger proteins constructed from modular building blocks. *Proc Natl Acad Sci U S A*, *95*(25), 14628-14633. https://doi.org/10.1073/pnas.95.25.14628

Behr, M., Zhou, J., Xu, B., & Zhang, H. (2021). In vivo delivery of CRISPR-Cas9 therapeutics: Progress and challenges. *Acta Pharm Sin B*, *11*(8), 2150-2171. https://doi.org/10.1016/j.apsb.2021.05.020

Bers, D. M. (2002). Cardiac excitation-contraction coupling. *Nature*, *415*(6868), 198-205. https://doi.org/10.1038/415198a

Bibikova, M., Beumer, K., Trautman, J. K., & Carroll, D. (2003). Enhancing gene targeting with designed zinc finger nucleases. *Science*, *300*(5620), 764. https://doi.org/10.1126/science.1079512

Bibikova, M., Golic, M., Golic, K. G., & Carroll, D. (2002). Targeted chromosomal cleavage and mutagenesis in Drosophila using zinc-finger nucleases. *Genetics*, *161*(3), 1169-1175. https://doi.org/10.1093/genetics/161.3.1169

Bikard, D., Jiang, W., Samai, P., Hochschild, A., Zhang, F., & Marraffini, L. A. (2013). Programmable repression and activation of bacterial gene expression using an engineered CRISPR-Cas system. *Nucleic Acids Res*, *41*(15), 7429-7437. https://doi.org/10.1093/nar/gkt520

Boch, J., Scholze, H., Schornack, S., Landgraf, A., Hahn, S., Kay, S., Lahaye, T., Nickstadt, A., & Bonas, U. (2009). Breaking the code of DNA binding specificity of TAL-type III effectors. *Science*, *326*(5959), 1509-1512. https://doi.org/10.1126/science.1178811

Bohm, S., Splith, V., Riedmayr, L. M., Rotzer, R. D., Gasparoni, G., Nordstrom, K. J. V., Wagner, J. E., Hinrichsmeyer, K. S., Walter, J., Wahl-Schott, C., Fenske, S., Biel, M., Michalakis, S., & Becirovic, E. (2020). A gene therapy for inherited blindness using dCas9-VPR-mediated transcriptional activation. *Sci Adv*, *6*(34), eaba5614. https://doi.org/10.1126/sciadv.aba5614

Bolger, A. M., Lohse, M., & Usadel, B. (2014). Trimmomatic: a flexible trimmer for Illumina sequence data. *Bioinformatics*, *30*(15), 2114-2120. https://doi.org/10.1093/bioinformatics/btu170

Bolotin, A., Quinquis, B., Sorokin, A., & Ehrlich, S. D. (2005). Clustered regularly interspaced short palindrome repeats (CRISPRs) have spacers of extrachromosomal origin. *Microbiology (Reading)*, *151*(Pt 8), 2551-2561. https://doi.org/10.1099/mic.0.28048-0

Brouns, S. J., Jore, M. M., Lundgren, M., Westra, E. R., Slijkhuis, R. J., Snijders, A. P., Dickman, M. J., Makarova, K. S., Koonin, E. V., & van der Oost, J. (2008). Small CRISPR RNAs guide antiviral defense in prokaryotes. *Science*, *321*(5891), 960-964. https://doi.org/10.1126/science.1159689

Bulcha, J. T., Wang, Y., Ma, H., Tai, P. W. L., & Gao, G. (2021). Viral vector platforms within the gene therapy landscape. *Signal Transduct Target Ther*, *6*(1), 53. https://doi.org/10.1038/s41392-021-00487-6

Byrne, L. C., Dalkara, D., Luna, G., Fisher, S. K., Clerin, E., Sahel, J. A., Leveillard, T., & Flannery, J. G. (2015). Viral-mediated RdCVF and RdCVFL expression protects cone and rod photoreceptors in retinal degeneration. *J Clin Invest*, *125*(1), 105-116. https://doi.org/10.1172/JCI65654

Calabro, K. R., Boye, S. L., Choudhury, S., Fajardo, D., Peterson, J. J., Li, W., Crosson, S. M., Kim, M. J., Ding, D., Salvi, R., Someya, S., & Boye, S. E. (2019). A Novel Mouse Model of MYO7A USH1B Reveals Auditory and Visual System Haploinsufficiencies. *Front Neurosci*, *13*, 1255. https://doi.org/10.3389/fnins.2019.01255

Carter-Dawson, L. D., & LaVail, M. M. (1979). Rods and cones in the mouse retina. I. Structural analysis using light and electron microscopy. *J Comp Neurol*, *188*(2), 245-262. https://doi.org/10.1002/cne.901880204

Carvalho, L. S., Turunen, H. T., Wassmer, S. J., Luna-Velez, M. V., Xiao, R., Bennett, J., & Vandenberghe, L. H. (2017). Evaluating Efficiencies of Dual AAV Approaches for Retinal Targeting. *Front Neurosci*, *11*, 503. https://doi.org/10.3389/fnins.2017.00503

Casson, R. J., Chidlow, G., Han, G., & Wood, J. P. (2013). An explanation for the Warburg effect in the adult mammalian retina. *Clin Exp Ophthalmol*, *41*(5), 517. https://doi.org/10.1111/ceo.12050

Chang, H. H. Y., Pannunzio, N. R., Adachi, N., & Lieber, M. R. (2017). Non-homologous DNA end joining and alternative pathways to double-strand break repair. *Nat Rev Mol Cell Biol*, *18*(8), 495-506. https://doi.org/10.1038/nrm.2017.48

Charlesworth, C. T., Deshpande, P. S., Dever, D. P., Camarena, J., Lemgart, V. T., Cromer, M. K., Vakulskas, C. A., Collingwood, M. A., Zhang, L., Bode, N. M., Behlke, M. A., Dejene, B., Cieniewicz, B., Romano, R., Lesch, B. J., Gomez-Ospina, N., Mantri, S., Pavel-Dinu, M., Weinberg, K. I., & Porteus, M. H. (2019). Identification of preexisting adaptive immunity to Cas9 proteins in humans. *Nat Med*, *25*(2), 249-254. https://doi.org/10.1038/s41591-018-0326-x

Chavez, A., Scheiman, J., Vora, S., Pruitt, B. W., Tuttle, M., E, P. R. I., Lin, S., Kiani, S., Guzman, C. D., Wiegand, D. J., Ter-Ovanesyan, D., Braff, J. L., Davidsohn, N., Housden, B. E., Perrimon, N., Weiss, R., Aach, J., Collins, J. J., & Church, G. M. (2015). Highly efficient Cas9-mediated transcriptional programming. *Nat Methods*, *12*(4), 326-328. https://doi.org/10.1038/nmeth.3312

Chavez, A., Tuttle, M., Pruitt, B. W., Ewen-Campen, B., Chari, R., Ter-Ovanesyan, D., Haque, S. J., Cecchi, R. J., Kowal, E. J. K., Buchthal, J., Housden, B. E., Perrimon, N., Collins, J. J., & Church, G. (2016). Comparison of Cas9 activators in multiple species. *Nat Methods*, *13*(7), 563-567. https://doi.org/10.1038/nmeth.3871

Chen, F., Alphonse, M., & Liu, Q. (2020). Strategies for nonviral nanoparticle-based delivery of CRISPR/Cas9 therapeutics. *Wiley Interdiscip Rev Nanomed Nanobiotechnol*, *12*(3), e1609. https://doi.org/10.1002/wnan.1609

Chen, J. S., Dagdas, Y. S., Kleinstiver, B. P., Welch, M. M., Sousa, A. A., Harrington, L. B., Sternberg, S. H., Joung, J. K., Yildiz, A., & Doudna, J. A. (2017). Enhanced proofreading governs CRISPR-Cas9 targeting accuracy. *Nature*, *550*(7676), 407-410. https://doi.org/10.1038/nature24268

Cheng, A. W., Jillette, N., Lee, P., Plaskon, D., Fujiwara, Y., Wang, W., Taghbalout, A., & Wang, H. (2016). Casilio: a versatile CRISPR-Cas9-Pumilio hybrid for gene regulation and genomic labeling. *Cell Res*, *26*(2), 254-257. https://doi.org/10.1038/cr.2016.3

Cheng, H., Khanna, H., Oh, E. C., Hicks, D., Mitton, K. P., & Swaroop, A. (2004). Photoreceptor-specific nuclear receptor NR2E3 functions as a transcriptional activator in rod photoreceptors. *Hum Mol Genet*, *13*(15), 1563-1575. https://doi.org/10.1093/hmg/ddh173

Chew, W. L., Tabebordbar, M., Cheng, J. K., Mali, P., Wu, E. Y., Ng, A. H., Zhu, K., Wagers, A. J., & Church, G. M. (2016). A multifunctional AAV-CRISPR-Cas9 and its host response. *Nat Methods*, *13*(10), 868-874. https://doi.org/10.1038/nmeth.3993

Christian, M., Cermak, T., Doyle, E. L., Schmidt, C., Zhang, F., Hummel, A., Bogdanove, A. J., & Voytas, D. F. (2010). Targeting DNA double-strand breaks with TAL effector nucleases. *Genetics*, *186*(2), 757-761. https://doi.org/10.1534/genetics.110.120717

Cideciyan, A. V., Sudharsan, R., Dufour, V. L., Massengill, M. T., Iwabe, S., Swider, M., Lisi, B., Sumaroka, A., Marinho, L. F., Appelbaum, T., Rossmiller, B., Hauswirth, W. W., Jacobson, S. G., Lewin, A. S., Aguirre, G. D., & Beltran, W. A. (2018). Mutation-independent rhodopsin gene therapy by knockdown and replacement with a single AAV vector. *Proc Natl Acad Sci U S A*, *115*(36), E8547-E8556. https://doi.org/10.1073/pnas.1805055115

Colasante, G., Lignani, G., Brusco, S., Di Berardino, C., Carpenter, J., Giannelli, S., Valassina, N., Bido, S., Ricci, R., Castoldi, V., Marenna, S., Church, T., Massimino, L., Morabito, G., Benfenati, F., Schorge, S., Leocani, L., Kullmann, D. M., & Broccoli, V. (2020). dCas9-Based Scn1a Gene Activation Restores Inhibitory

Interneuron Excitability and Attenuates Seizures in Dravet Syndrome Mice. *Mol Ther*, *28*(1), 235-253. https://doi.org/10.1016/j.ymthe.2019.08.018

Colasante, G., Qiu, Y., Massimino, L., Di Berardino, C., Cornford, J. H., Snowball, A., Weston, M., Jones, S. P., Giannelli, S., Lieb, A., Schorge, S., Kullmann, D. M., Broccoli, V., & Lignani, G. (2020). In vivo CRISPRa decreases seizures and rescues cognitive deficits in a rodent model of epilepsy. *Brain*, *143*(3), 891-905. https://doi.org/10.1093/brain/awaa045

Cong, L., Ran, F. A., Cox, D., Lin, S., Barretto, R., Habib, N., Hsu, P. D., Wu, X., Jiang, W., Marraffini, L. A., & Zhang, F. (2013). Multiplex genome engineering using CRISPR/Cas systems. *Science*, *339*(6121), 819-823. https://doi.org/10.1126/science.1231143

Cronin, T., Raffelsberger, W., Lee-Rivera, I., Jaillard, C., Niepon, M. L., Kinzel, B., Clerin, E., Petrosian, A., Picaud, S., Poch, O., Sahel, J. A., & Leveillard, T. (2010). The disruption of the rod-derived cone viability gene leads to photoreceptor dysfunction and susceptibility to oxidative stress. *Cell Death Differ*, *17*(7), 1199-1210. https://doi.org/10.1038/cdd.2010.2

Crooke, S. T. (2017). Molecular Mechanisms of Antisense Oligonucleotides. *Nucleic Acid Ther*, *27*(2), 70-77. https://doi.org/10.1089/nat.2016.0656

Dahlman, J. E., Abudayyeh, O. O., Joung, J., Gootenberg, J. S., Zhang, F., & Konermann, S. (2015). Orthogonal gene knockout and activation with a catalytically active Cas9 nuclease. *Nat Biotechnol*, *33*(11), 1159-1161. https://doi.org/10.1038/nbt.3390

Delmaghani, S., & El-Amraoui, A. (2022). The genetic and phenotypic landscapes of Usher syndrome: from disease mechanisms to a new classification. *Hum Genet*. https://doi.org/10.1007/s00439-022-02448-7

Deltcheva, E., Chylinski, K., Sharma, C. M., Gonzales, K., Chao, Y., Pirzada, Z. A., Eckert, M. R., Vogel, J., & Charpentier, E. (2011). CRISPR RNA maturation by trans-encoded small RNA and host factor RNase III. *Nature*, *471*(7340), 602-607. https://doi.org/10.1038/nature09886

Deng, W. T., Sakurai, K., Kolandaivelu, S., Kolesnikov, A. V., Dinculescu, A., Li, J., Zhu, P., Liu, X., Pang, J., Chiodo, V. A., Boye, S. L., Chang, B., Ramamurthy, V., Kefalov, V. J., & Hauswirth, W. W. (2013). Cone phosphodiesterase-6alpha' restores rod function and confers distinct physiological properties in the rod phosphodiesterase-6beta-deficient rd10 mouse. *J Neurosci*, *33*(29), 11745-11753. https://doi.org/10.1523/JNEUROSCI.1536-13.2013

Deng, W. T., Sakurai, K., Liu, J., Dinculescu, A., Li, J., Pang, J., Min, S. H., Chiodo, V. A., Boye, S. L., Chang, B., Kefalov, V. J., & Hauswirth, W. W. (2009). Functional interchangeability of rod and cone transducin alpha-subunits. *Proc Natl Acad Sci U S A*, *106*(42), 17681-17686. https://doi.org/10.1073/pnas.0901382106

Ding, Q., Strong, A., Patel, K. M., Ng, S. L., Gosis, B. S., Regan, S. N., Cowan, C. A., Rader, D. J., & Musunuru, K. (2014). Permanent alteration of PCSK9 with in vivo CRISPR-Cas9 genome editing. *Circ Res*, *115*(5), 488-492. https://doi.org/10.1161/CIRCRESAHA.115.304351

Dobin, A., Davis, C. A., Schlesinger, F., Drenkow, J., Zaleski, C., Jha, S., Batut, P., Chaisson, M., & Gingeras, T. R. (2013). STAR: ultrafast universal RNA-seq aligner. *Bioinformatics*, *29*(1), 15-21. https://doi.org/10.1093/bioinformatics/bts635

Doudna, J. A., & Charpentier, E. (2014). Genome editing. The new frontier of genome engineering with CRISPR-Cas9. *Science*, *346*(6213), 1258096. https://doi.org/10.1126/science.1258096

Duan, D., Yue, Y., Yan, Z., & Engelhardt, J. F. (2000). A new dual-vector approach to enhance recombinant adeno-associated virus-mediated gene expression through intermolecular cis activation. *Nat Med*, *6*(5), 595-598. https://doi.org/10.1038/75080

Durai, S., Mani, M., Kandavelou, K., Wu, J., Porteus, M. H., & Chandrasegaran, S. (2005). Zinc finger nucleases: custom-designed molecular scissors for genome engineering of plant and mammalian cells. *Nucleic Acids Res*, *33*(18), 5978-5990. https://doi.org/10.1093/nar/gki912

Etich, J., Lessmeier, L., Rehberg, M., Sill, H., Zaucke, F., Netzer, C., & Semler, O. (2020). Osteogenesis imperfecta-pathophysiology and therapeutic options. *Mol Cell Pediatr*, *7*(1), 9. https://doi.org/10.1186/s40348-020-00101-9

Euler, T., Haverkamp, S., Schubert, T., & Baden, T. (2014). Retinal bipolar cells: elementary building blocks of vision. *Nat Rev Neurosci*, *15*(8), 507-519. https://doi.org/10.1038/nrn3783

Farrar, G. J., Kenna, P., Redmond, R., McWilliam, P., Bradley, D. G., Humphries, M. M., Sharp, E. M., Inglehearn, C. F., Bashir, R., Jay, M., & et al. (1990). Autosomal dominant retinitis pigmentosa: absence of the rhodopsin proline----histidine substitution (codon 23) in pedigrees from Europe. *Am J Hum Genet*, *47*(6), 941-945. https://www.ncbi.nlm.nih.gov/pubmed/2239971

Fenner, B. J., Tan, T. E., Barathi, A. V., Tun, S. B. B., Yeo, S. W., Tsai, A. S. H., Lee, S. Y., Cheung, C. M. G., Chan, C. M., Mehta, J. S., & Teo, K. Y. C. (2021). Gene-Based Therapeutics for Inherited Retinal Diseases. *Front Genet*, *12*, 794805. https://doi.org/10.3389/fgene.2021.794805

Ferdosi, S. R., Ewaisha, R., Moghadam, F., Krishna, S., Park, J. G., Ebrahimkhani, M. R., Kiani, S., & Anderson, K. S. (2019). Multifunctional CRISPR-Cas9 with engineered immunosilenced human T cell epitopes. *Nat Commun*, *10*(1), 1842. https://doi.org/10.1038/s41467-019-09693-x

Fernandez-San Jose, P., Blanco-Kelly, F., Corton, M., Trujillo-Tiebas, M. J., Gimenez, A., Avila-Fernandez, A., Garcia-Sandoval, B., Lopez-Molina, M. I., Hernan, I., Carballo, M., Riveiro-Alvarez, R., & Ayuso, C. (2015). Prevalence of Rhodopsin mutations in autosomal dominant Retinitis Pigmentosa in Spain: clinical and analytical review in 200 families. *Acta Ophthalmol*, *93*(1), e38-44. https://doi.org/10.1111/aos.12486

Friedmann, T., & Roblin, R. (1972). Gene therapy for human genetic disease? *Science*, *175*(4025), 949-955. https://doi.org/10.1126/science.175.4025.949

Garcia-Bloj, B., Moses, C., Sgro, A., Plani-Lam, J., Arooj, M., Duffy, C., Thiruvengadam, S., Sorolla, A., Rashwan, R., Mancera, R. L., Leisewitz, A., Swift-Scanlan, T., Corvalan, A. H., & Blancafort, P. (2016). Waking up dormant tumor suppressor genes with zinc fingers, TALEs and the CRISPR/dCas9 system. *Oncotarget*, *7*(37), 60535-60554. https://doi.org/10.18632/oncotarget.11142

Garneau, J. E., Dupuis, M. E., Villion, M., Romero, D. A., Barrangou, R., Boyaval, P., Fremaux, C., Horvath, P., Magadan, A. H., & Moineau, S. (2010). The CRISPR/Cas bacterial immune system cleaves bacteriophage and plasmid DNA. *Nature*, *468*(7320), 67-71. https://doi.org/10.1038/nature09523

Gaudelli, N. M., Komor, A. C., Rees, H. A., Packer, M. S., Badran, A. H., Bryson, D. I., & Liu, D. R. (2017). Programmable base editing of A*T to G*C in genomic DNA without DNA cleavage. *Nature*, *551*(7681), 464-471. https://doi.org/10.1038/nature24644

Geleoc, G. S., & Holt, J. R. (2014). Sound strategies for hearing restoration. *Science*, *344*(6184), 1241062. https://doi.org/10.1126/science.1241062

Ghosh, A., Yue, Y., Lai, Y., & Duan, D. (2008). A hybrid vector system expands adeno-associated viral vector packaging capacity in a transgene-independent manner. *Mol Ther*, *16*(1), 124-130. https://doi.org/10.1038/sj.mt.6300322

Giannelli, S. G., Luoni, M., Castoldi, V., Massimino, L., Cabassi, T., Angeloni, D., Demontis, G. C., Leocani, L., Andreazzoli, M., & Broccoli, V. (2018). Cas9/sgRNA

selective targeting of the P23H Rhodopsin mutant allele for treating retinitis pigmentosa by intravitreal AAV9.PHP.B-based delivery. *Hum Mol Genet*, *27*(5), 761-779. https://doi.org/10.1093/hmg/ddx438

Gibson, D. G., Young, L., Chuang, R. Y., Venter, J. C., Hutchison, C. A., 3rd, & Smith, H. O. (2009). Enzymatic assembly of DNA molecules up to several hundred kilobases. *Nat Methods*, *6*(5), 343-345. https://doi.org/10.1038/nmeth.1318

Gilbert, L. A., Larson, M. H., Morsut, L., Liu, Z., Brar, G. A., Torres, S. E., Stern-Ginossar, N., Brandman, O., Whitehead, E. H., Doudna, J. A., Lim, W. A., Weissman, J. S., & Qi, L. S. (2013). CRISPR-mediated modular RNA-guided regulation of transcription in eukaryotes. *Cell*, *154*(2), 442-451. https://doi.org/10.1016/j.cell.2013.06.044

Gwack, Y., Baek, H. J., Nakamura, H., Lee, S. H., Meisterernst, M., Roeder, R. G., & Jung, J. U. (2003). Principal role of TRAP/mediator and SWI/SNF complexes in Kaposi's sarcoma-associated herpesvirus RTA-mediated lytic reactivation. *Mol Cell Biol*, *23*(6), 2055-2067. https://doi.org/10.1128/MCB.23.6.2055-2067.2003

Ha, J. S., Byun, J., & Ahn, D. R. (2016). Overcoming doxorubicin resistance of cancer cells by Cas9-mediated gene disruption. *Sci Rep*, *6*, 22847. https://doi.org/10.1038/srep22847

Haapaniemi, E., Botla, S., Persson, J., Schmierer, B., & Taipale, J. (2018). CRISPR-Cas9 genome editing induces a p53-mediated DNA damage response. *Nat Med*, *24*(7), 927-930. https://doi.org/10.1038/s41591-018-0049-z

Haft, D. H., Selengut, J., Mongodin, E. F., & Nelson, K. E. (2005). A guild of 45 CRISPR-associated (Cas) protein families and multiple CRISPR/Cas subtypes exist in prokaryotic genomes. *PLoS Comput Biol*, *1*(6), e60. https://doi.org/10.1371/journal.pcbi.0010060

Hepper, P. G., & Shahidullah, B. S. (1994). Development of fetal hearing. *Arch Dis Child Fetal Neonatal Ed*, *71*(2), F81-87. https://doi.org/10.1136/fn.71.2.f81

High, K. A., & Roncarolo, M. G. (2019). Gene Therapy. *N Engl J Med*, *381*(5), 455-464. https://doi.org/10.1056/NEJMra1706910

Hilton, I. B., D'Ippolito, A. M., Vockley, C. M., Thakore, P. I., Crawford, G. E., Reddy, T. E., & Gersbach, C. A. (2015). Epigenome editing by a CRISPR-Cas9-based acetyltransferase activates genes from promoters and enhancers. *Nat Biotechnol*, *33*(5), 510-517. https://doi.org/10.1038/nbt.3199

Hoon, M., Okawa, H., Della Santina, L., & Wong, R. O. (2014). Functional architecture of the retina: development and disease. *Prog Retin Eye Res*, *42*, 44-84. https://doi.org/10.1016/j.preteyeres.2014.06.003

Hsu, P. D., Scott, D. A., Weinstein, J. A., Ran, F. A., Konermann, S., Agarwala, V., Li, Y., Fine, E. J., Wu, X., Shalem, O., Cradick, T. J., Marraffini, L. A., Bao, G., & Zhang, F. (2013). DNA targeting specificity of RNA-guided Cas9 nucleases. *Nat Biotechnol*, *31*(9), 827-832. https://doi.org/10.1038/nbt.2647

Humphries, M. M., Rancourt, D., Farrar, G. J., Kenna, P., Hazel, M., Bush, R. A., Sieving, P. A., Sheils, D. M., McNally, N., Creighton, P., Erven, A., Boros, A., Gulya, K., Capecchi, M. R., & Humphries, P. (1997). Retinopathy induced in mice by targeted disruption of the rhodopsin gene. *Nat Genet*, *15*(2), 216-219. https://doi.org/10.1038/ng0297-216

Hutvagner, G., & Zamore, P. D. (2002). A microRNA in a multiple-turnover RNAi enzyme complex. *Science*, *297*(5589), 2056-2060. https://doi.org/10.1126/science.1073827

Ishino, Y., Shinagawa, H., Makino, K., Amemura, M., & Nakata, A. (1987). Nucleotide sequence of the iap gene, responsible for alkaline phosphatase isozyme conversion in Escherichia coli, and identification of the gene product. *J Bacteriol*, *169*(12), 5429-5433. https://doi.org/10.1128/jb.169.12.5429-5433.1987

Jaillard, C., Mouret, A., Niepon, M. L., Clerin, E., Yang, Y., Lee-Rivera, I., Ait-Ali, N., Millet-Puel, G., Cronin, T., Sedmak, T., Raffelsberger, W., Kinzel, B., Trembleau, A., Poch, O., Bennett, J., Wolfrum, U., Lledo, P. M., Sahel, J. A., & Leveillard, T. (2012). Nxnl2 splicing results in dual functions in neuronal cell survival and maintenance of cell integrity. *Hum Mol Genet*, *21*(10), 2298-2311. https://doi.org/10.1093/hmg/dds050

Jansen, R., Embden, J. D., Gaastra, W., & Schouls, L. M. (2002). Identification of genes that are associated with DNA repeats in prokaryotes. *Mol Microbiol*, *43*(6), 1565-1575. https://doi.org/10.1046/j.1365-2958.2002.02839.x

Jat, P. S., Cepko, C. L., Mulligan, R. C., & Sharp, P. A. (1986). Recombinant retroviruses encoding simian virus 40 large T antigen and polyomavirus large and middle T antigens. *Mol Cell Biol*, *6*(4), 1204-1217. https://doi.org/10.1128/mcb.6.4.1204-1217.1986

Jinek, M., Chylinski, K., Fonfara, I., Hauer, M., Doudna, J. A., & Charpentier, E. (2012). A programmable dual-RNA-guided DNA endonuclease in adaptive bacterial immunity. *Science*, *337*(6096), 816-821. https://doi.org/10.1126/science.1225829

Jinek, M., East, A., Cheng, A., Lin, S., Ma, E., & Doudna, J. (2013). RNA-programmed genome editing in human cells. *Elife*, *2*, e00471. https://doi.org/10.7554/eLife.00471

Kang, S. H., Lee, W. J., An, J. H., Lee, J. H., Kim, Y. H., Kim, H., Oh, Y., Park, Y. H., Jin, Y. B., Jun, B. H., Hur, J. K., Kim, S. U., & Lee, S. H. (2020). Prediction-based highly sensitive CRISPR off-target validation using target-specific DNA enrichment. *Nat Commun*, *11*(1), 3596. https://doi.org/10.1038/s41467-020-17418-8

Karimian, A., Gorjizadeh, N., Alemi, F., Asemi, Z., Azizian, K., Soleimanpour, J., Malakouti, F., Targhazeh, N., Majidinia, M., & Yousefi, B. (2020). CRISPR/Cas9 novel therapeutic road for the treatment of neurodegenerative diseases. *Life Sci*, *259*, 118165. https://doi.org/10.1016/j.lfs.2020.118165

Katti, A., Diaz, B. J., Caragine, C. M., Sanjana, N. E., & Dow, L. E. (2022). CRISPR in cancer biology and therapy. *Nat Rev Cancer*, *22*(5), 259-279. https://doi.org/10.1038/s41568-022-00441-w

Kearns, N. A., Pham, H., Tabak, B., Genga, R. M., Silverstein, N. J., Garber, M., & Maehr, R. (2015). Functional annotation of native enhancers with a Cas9-histone demethylase fusion. *Nat Methods*, *12*(5), 401-403. https://doi.org/10.1038/nmeth.3325

Kemaladewi, D. U., Bassi, P. S., Erwood, S., Al-Basha, D., Gawlik, K. I., Lindsay, K., Hyatt, E., Kember, R., Place, K. M., Marks, R. M., Durbeej, M., Prescott, S. A., Ivakine, E. A., & Cohn, R. D. (2019). A mutation-independent approach for muscular dystrophy via upregulation of a modifier gene. *Nature*, *572*(7767), 125-130. https://doi.org/10.1038/s41586-019-1430-x

Khani, S. C., Pawlyk, B. S., Bulgakov, O. V., Kasperek, E., Young, J. E., Adamian, M., Sun, X., Smith, A. J., Ali, R. R., & Li, T. (2007). AAV-mediated expression targeting of rod and cone photoreceptors with a human rhodopsin kinase promoter. *Invest Ophthalmol Vis Sci*, *48*(9), 3954-3961. https://doi.org/10.1167/iovs.07-0257

Kiang, A. S., Palfi, A., Ader, M., Kenna, P. F., Millington-Ward, S., Clark, G., Kennan, A., O'Reilly, M., Tam, L. C., Aherne, A., McNally, N., Humphries, P., & Farrar, G. J. (2005). Toward a gene therapy for dominant disease: validation of an RNA interference-based mutation-independent approach. *Mol Ther*, *12*(3), 555-561. https://doi.org/10.1016/j.ymthe.2005.03.028

Kiani, S., Chavez, A., Tuttle, M., Hall, R. N., Chari, R., Ter-Ovanesyan, D., Qian, J., Pruitt, B. W., Beal, J., Vora, S., Buchthal, J., Kowal, E. J., Ebrahimkhani, M. R., Collins, J. J., Weiss, R., & Church, G. (2015). Cas9 gRNA engineering for genome editing,

activation and repression. *Nat Methods*, *12*(11), 1051-1054. https://doi.org/10.1038/nmeth.3580

Kim, K. J., Kim, C., Bok, J., Kim, K. S., Lee, E. J., Park, S. P., Chung, H., Han, B. G., Kim, H. L., Kimm, K., Yu, H. G., & Lee, J. Y. (2011). Spectrum of rhodopsin mutations in Korean patients with retinitis pigmentosa. *Mol Vis*, *17*, 844-853. https://www.ncbi.nlm.nih.gov/pubmed/21677794

Kim, Y. G., Cha, J., & Chandrasegaran, S. (1996). Hybrid restriction enzymes: zinc finger fusions to Fok I cleavage domain. *Proc Natl Acad Sci U S A*, *93*(3), 1156-1160. https://doi.org/10.1073/pnas.93.3.1156

Kingston, R. E., Chen, C. A., & Okayama, H. (2003). Calcium phosphate transfection. *Curr Protoc Cell Biol*, *Chapter 20*, Unit 20 23. https://doi.org/10.1002/0471143030.cb2003s19

Komor, A. C., Kim, Y. B., Packer, M. S., Zuris, J. A., & Liu, D. R. (2016). Programmable editing of a target base in genomic DNA without double-stranded DNA cleavage. *Nature*, *533*(7603), 420-424. https://doi.org/10.1038/nature17946

Konermann, S., Brigham, M. D., Trevino, A. E., Joung, J., Abudayyeh, O. O., Barcena, C., Hsu, P. D., Habib, N., Gootenberg, J. S., Nishimasu, H., Nureki, O., & Zhang, F. (2015). Genome-scale transcriptional activation by an engineered CRISPR-Cas9 complex. *Nature*, *517*(7536), 583-588. https://doi.org/10.1038/nature14136

Lane, A., Jovanovic, K., Shortall, C., Ottaviani, D., Panes, A. B., Schwarz, N., Guarascio, R., Hayes, M. J., Palfi, A., Chadderton, N., Farrar, G. J., Hardcastle, A. J., & Cheetham, M. E. (2020). Modeling and Rescue of RP2 Retinitis Pigmentosa Using iPSC-Derived Retinal Organoids. *Stem Cell Reports*, *15*(1), 67-79. https://doi.org/10.1016/j.stemcr.2020.05.007

Lawhorn, I. E., Ferreira, J. P., & Wang, C. L. (2014). Evaluation of sgRNA target sites for CRISPR-mediated repression of TP53. *PLoS One*, *9*(11), e113232. https://doi.org/10.1371/journal.pone.0113232

Leinonen, H., Pham, N. C., Boyd, T., Santoso, J., Palczewski, K., & Vinberg, F. (2020). Homeostatic plasticity in the retina is associated with maintenance of night vision during retinal degenerative disease. *Elife*, *9*. https://doi.org/10.7554/eLife.59422

Leveillard, T., Mohand-Said, S., Lorentz, O., Hicks, D., Fintz, A. C., Clerin, E., Simonutti, M., Forster, V., Cavusoglu, N., Chalmel, F., Dolle, P., Poch, O., Lambrou, G., & Sahel, J. A. (2004). Identification and characterization of rod-derived cone viability factor. *Nat Genet*, *36*(7), 755-759. https://doi.org/10.1038/ng1386

Leveillard, T., & Sahel, J. A. (2017). Metabolic and redox signaling in the retina. *Cell Mol Life Sci*, *74*(20), 3649-3665. https://doi.org/10.1007/s00018-016-2318-7

Levy, J. M., Yeh, W. H., Pendse, N., Davis, J. R., Hennessey, E., Butcher, R., Koblan, L. W., Comander, J., Liu, Q., & Liu, D. R. (2020). Cytosine and adenine base editing of the brain, liver, retina, heart and skeletal muscle of mice via adeno-associated viruses. *Nat Biomed Eng*, *4*(1), 97-110. https://doi.org/10.1038/s41551-019-0501-5

Liao, H. K., Hatanaka, F., Araoka, T., Reddy, P., Wu, M. Z., Sui, Y., Yamauchi, T., Sakurai, M., O'Keefe, D. D., Nunez-Delicado, E., Guillen, P., Campistol, J. M., Wu, C. J., Lu, L. F., Esteban, C. R., & Izpisua Belmonte, J. C. (2017). In Vivo Target Gene Activation via CRISPR/Cas9-Mediated Trans-epigenetic Modulation. *Cell*, *171*(7), 1495-1507 e1415. https://doi.org/10.1016/j.cell.2017.10.025

Liao, Y., Smyth, G. K., & Shi, W. (2014). featureCounts: an efficient general purpose program for assigning sequence reads to genomic features. *Bioinformatics*, *30*(7), 923-930. https://doi.org/10.1093/bioinformatics/btt656

Lillo, C., Kitamoto, J., Liu, X., Quint, E., Steel, K. P., & Williams, D. S. (2003). Mouse models for Usher syndrome 1B. *Adv Exp Med Biol*, *533*, 143-150. https://doi.org/10.1007/978-1-4615-0067-4_18

Lim, C. K. W., Gapinske, M., Brooks, A. K., Woods, W. S., Powell, J. E., Zeballos, C. M., Winter, J., Perez-Pinera, P., & Gaj, T. (2020). Treatment of a Mouse Model of ALS by In Vivo Base Editing. *Mol Ther*, *28*(4), 1177-1189. https://doi.org/10.1016/j.ymthe.2020.01.005

Lopes, V. S., Boye, S. E., Louie, C. M., Boye, S., Dyka, F., Chiodo, V., Fofo, H., Hauswirth, W. W., & Williams, D. S. (2013). Retinal gene therapy with a large MYO7A cDNA using adeno-associated virus. *Gene Ther*, *20*(8), 824-833. https://doi.org/10.1038/gt.2013.3

Love, M. I., Huber, W., & Anders, S. (2014). Moderated estimation of fold change and dispersion for RNA-seq data with DESeq2. *Genome Biol*, *15*(12), 550. https://doi.org/10.1186/s13059-014-0550-8

Maeder, M. L., Linder, S. J., Cascio, V. M., Fu, Y., Ho, Q. H., & Joung, J. K. (2013). CRISPR RNA-guided activation of endogenous human genes. *Nat Methods*, *10*(10), 977-979. https://doi.org/10.1038/nmeth.2598

Maeder, M. L., Stefanidakis, M., Wilson, C. J., Baral, R., Barrera, L. A., Bounoutas, G. S., Bumcrot, D., Chao, H., Ciulla, D. M., DaSilva, J. A., Dass, A., Dhanapal, V., Fennell, T. J., Friedland, A. E., Giannoukos, G., Gloskowski, S. W., Glucksmann, A., Gotta, G. M., Jayaram, H., . . . Jiang, H. (2019). Development of a gene-editing approach to restore vision loss in Leber congenital amaurosis type 10. *Nat Med*, *25*(2), 229-233. https://doi.org/10.1038/s41591-018-0327-9

Maguire, C. A., & Corey, D. P. (2020). Viral vectors for gene delivery to the inner ear. *Hear Res*, *394*, 107927. https://doi.org/10.1016/j.heares.2020.107927

Makarova, K. S., Grishin, N. V., Shabalina, S. A., Wolf, Y. I., & Koonin, E. V. (2006). A putative RNA-interference-based immune system in prokaryotes: computational analysis of the predicted enzymatic machinery, functional analogies with eukaryotic RNAi, and hypothetical mechanisms of action. *Biol Direct*, *1*, 7. https://doi.org/10.1186/1745-6150-1-7

Makarova, K. S., Haft, D. H., Barrangou, R., Brouns, S. J., Charpentier, E., Horvath, P., Moineau, S., Mojica, F. J., Wolf, Y. I., Yakunin, A. F., van der Oost, J., & Koonin, E. V. (2011). Evolution and classification of the CRISPR-Cas systems. *Nat Rev Microbiol*, *9*(6), 467-477. https://doi.org/10.1038/nrmicro2577

Mali, P., Yang, L., Esvelt, K. M., Aach, J., Guell, M., DiCarlo, J. E., Norville, J. E., & Church, G. M. (2013). RNA-guided human genome engineering via Cas9. *Science*, *339*(6121), 823-826. https://doi.org/10.1126/science.1232033

Marinho, H. S., Real, C., Cyrne, L., Soares, H., & Antunes, F. (2014). Hydrogen peroxide sensing, signaling and regulation of transcription factors. *Redox Biol*, *2*, 535-562. https://doi.org/10.1016/j.redox.2014.02.006

Marini, J. C., Forlino, A., Bachinger, H. P., Bishop, N. J., Byers, P. H., Paepe, A., Fassier, F., Fratzl-Zelman, N., Kozloff, K. M., Krakow, D., Montpetit, K., & Semler, O. (2017). Osteogenesis imperfecta. *Nat Rev Dis Primers*, *3*, 17052. https://doi.org/10.1038/nrdp.2017.52

Martinez-Escobar, A., Luna-Callejas, B., & Ramon-Gallegos, E. (2020). CRISPR-dCas9-Based Artificial Transcription Factors to Improve Efficacy of Cancer Treatment With Drug Repurposing: Proposal for Future Research. *Front Oncol*, *10*, 604948. https://doi.org/10.3389/fonc.2020.604948

Martinez-Lage, M., Torres-Ruiz, R., Puig-Serra, P., Moreno-Gaona, P., Martin, M. C., Moya, F. J., Quintana-Bustamante, O., Garcia-Silva, S., Carcaboso, A. M., Petazzi, P., Bueno, C., Mora, J., Peinado, H., Segovia, J. C., Menendez, P., & Rodriguez-Perales, S. (2020). In vivo CRISPR/Cas9 targeting of fusion oncogenes for selective elimination of cancer cells. *Nat Commun*, *11*(1), 5060. https://doi.org/10.1038/s41467-020-18875-x

Masland, R. H. (2012). The neuronal organization of the retina. *Neuron*, *76*(2), 266-280. https://doi.org/10.1016/j.neuron.2012.10.002

Matharu, N., Rattanasopha, S., Tamura, S., Maliskova, L., Wang, Y., Bernard, A., Hardin, A., Eckalbar, W. L., Vaisse, C., & Ahituv, N. (2019). CRISPR-mediated activation of a promoter or enhancer rescues obesity caused by haploinsufficiency. *Science*, *363*(6424). https://doi.org/10.1126/science.aau0629

McClements, M. E., Steward, H., Atkin, W., Goode, E. A., Gandara, C., Chichagova, V., & MacLaren, R. E. (2022). Tropism of AAV Vectors in Photoreceptor-Like Cells of Human iPSC-Derived Retinal Organoids. *Transl Vis Sci Technol*, *11*(4), 3. https://doi.org/10.1167/tvst.11.4.3

McDonald, J. I., Celik, H., Rois, L. E., Fishberger, G., Fowler, T., Rees, R., Kramer, A., Martens, A., Edwards, J. R., & Challen, G. A. (2016). Reprogrammable CRISPR/Cas9-based system for inducing site-specific DNA methylation. *Biol Open*, *5*(6), 866-874. https://doi.org/10.1242/bio.019067

Mears, A. J., Kondo, M., Swain, P. K., Takada, Y., Bush, R. A., Saunders, T. L., Sieving, P. A., & Swaroop, A. (2001). Nrl is required for rod photoreceptor development. *Nat Genet*, *29*(4), 447-452. https://doi.org/10.1038/ng774

Meng, D., Ragi, S. D., & Tsang, S. H. (2020). Therapy in Rhodopsin-Mediated Autosomal Dominant Retinitis Pigmentosa. *Mol Ther*, *28*(10), 2139-2149. https://doi.org/10.1016/j.ymthe.2020.08.012

Michalakis, S., Muhlfriedel, R., Tanimoto, N., Krishnamoorthy, V., Koch, S., Fischer, M. D., Becirovic, E., Bai, L., Huber, G., Beck, S. C., Fahl, E., Buning, H., Paquet-Durand, F., Zong, X., Gollisch, T., Biel, M., & Seeliger, M. W. (2010). Restoration of cone vision in the CNGA3-/- mouse model of congenital complete lack of cone photoreceptor function. *Mol Ther*, *18*(12), 2057-2063. https://doi.org/10.1038/mt.2010.149

Miller, J., McLachlan, A. D., & Klug, A. (1985). Repetitive zinc-binding domains in the protein transcription factor IIIA from Xenopus oocytes. *EMBO J*, *4*(6), 1609-1614. https://www.ncbi.nlm.nih.gov/pubmed/4040853

Mojica, F. J., Diez-Villasenor, C., Garcia-Martinez, J., & Soria, E. (2005). Intervening sequences of regularly spaced prokaryotic repeats derive from foreign genetic elements. *J Mol Evol*, *60*(2), 174-182. https://doi.org/10.1007/s00239-004-0046-3

Mojica, F. J. M., Diez-Villasenor, C., Garcia-Martinez, J., & Almendros, C. (2009). Short motif sequences determine the targets of the prokaryotic CRISPR defence system. *Microbiology (Reading)*, *155*(Pt 3), 733-740. https://doi.org/10.1099/mic.0.023960-0

Montana, C. L., Kolesnikov, A. V., Shen, S. Q., Myers, C. A., Kefalov, V. J., & Corbo, J. C. (2013). Reprogramming of adult rod photoreceptors prevents retinal degeneration. *Proc Natl Acad Sci U S A*, *110*(5), 1732-1737. https://doi.org/10.1073/pnas.1214387110

Moscou, M. J., & Bogdanove, A. J. (2009). A simple cipher governs DNA recognition by TAL effectors. *Science*, *326*(5959), 1501. https://doi.org/10.1126/science.1178817

Moses, C., Nugent, F., Waryah, C. B., Garcia-Bloj, B., Harvey, A. R., & Blancafort, P. (2019). Activating PTEN Tumor Suppressor Expression with the CRISPR/dCas9 System. *Mol Ther Nucleic Acids*, *14*, 287-300. https://doi.org/10.1016/j.omtn.2018.12.003

Muralidharan, V., & Muir, T. W. (2006). Protein ligation: an enabling technology for the biophysical analysis of proteins. *Nat Methods*, *3*(6), 429-438. https://doi.org/10.1038/nmeth886

Murray, S. F., Jazayeri, A., Matthes, M. T., Yasumura, D., Yang, H., Peralta, R., Watt, A., Freier, S., Hung, G., Adamson, P. S., Guo, S., Monia, B. P., LaVail, M. M., &

McCaleb, M. L. (2015). Allele-Specific Inhibition of Rhodopsin With an Antisense Oligonucleotide Slows Photoreceptor Cell Degeneration. *Invest Ophthalmol Vis Sci*, *56*(11), 6362-6375. https://doi.org/10.1167/iovs.15-16400

Nakai, H., Storm, T. A., & Kay, M. A. (2000). Increasing the size of rAAV-mediated expression cassettes in vivo by intermolecular joining of two complementary vectors. *Nat Biotechnol*, *18*(5), 527-532. https://doi.org/10.1038/75390

Nathans, J., Thomas, D., & Hogness, D. S. (1986). Molecular genetics of human color vision: the genes encoding blue, green, and red pigments. *Science*, *232*(4747), 193-202. https://doi.org/10.1126/science.2937147

Nishida, K., Arazoe, T., Yachie, N., Banno, S., Kakimoto, M., Tabata, M., Mochizuki, M., Miyabe, A., Araki, M., Hara, K. Y., Shimatani, Z., & Kondo, A. (2016). Targeted nucleotide editing using hybrid prokaryotic and vertebrate adaptive immune systems. *Science*, *353*(6305). https://doi.org/10.1126/science.aaf8729

Nonnenmacher, M., & Weber, T. (2012). Intracellular transport of recombinant adeno-associated virus vectors. *Gene Ther*, *19*(6), 649-658. https://doi.org/10.1038/gt.2012.6

Pan, B., Askew, C., Galvin, A., Heman-Ackah, S., Asai, Y., Indzhykulian, A. A., Jodelka, F. M., Hastings, M. L., Lentz, J. J., Vandenberghe, L. H., Holt, J. R., & Geleoc, G. S. (2017). Gene therapy restores auditory and vestibular function in a mouse model of Usher syndrome type 1c. *Nat Biotechnol*, *35*(3), 264-272. https://doi.org/10.1038/nbt.3801

Park, H., Hwang, Y., & Kim, J. (2021). Transcriptional activation with Cas9 activator nanocomplexes rescues Alzheimer's disease pathology. *Biomaterials*, *279*, 121229. https://doi.org/10.1016/j.biomaterials.2021.121229

Patel, A., Zhao, J., Duan, D., & Lai, Y. (2019). Design of AAV Vectors for Delivery of Large or Multiple Transgenes. *Methods Mol Biol*, *1950*, 19-33. https://doi.org/10.1007/978-1-4939-9139-6_2

Pavletich, N. P., & Pabo, C. O. (1991). Zinc finger-DNA recognition: crystal structure of a Zif268-DNA complex at 2.1 A. *Science*, *252*(5007), 809-817. https://doi.org/10.1126/science.2028256

Perea-Romero, I., Gordo, G., Iancu, I. F., Del Pozo-Valero, M., Almoguera, B., Blanco-Kelly, F., Carreno, E., Jimenez-Rolando, B., Lopez-Rodriguez, R., Lorda-Sanchez, I., Martin-Merida, I., Perez de Ayala, L., Riveiro-Alvarez, R., Rodriguez-Pinilla, E., Tahsin-Swafiri, S., Trujillo-Tiebas, M. J., Group, E. S., Group, E. S., Associated Clinical Study, G., . . . Ayuso, C. (2021). Genetic landscape of 6089 inherited retinal dystrophies affected cases in Spain and their therapeutic and extended epidemiological implications. *Sci Rep*, *11*(1), 1526. https://doi.org/10.1038/s41598-021-81093-y

Perez-Pinera, P., Kocak, D. D., Vockley, C. M., Adler, A. F., Kabadi, A. M., Polstein, L. R., Thakore, P. I., Glass, K. A., Ousterout, D. G., Leong, K. W., Guilak, F., Crawford, G. E., Reddy, T. E., & Gersbach, C. A. (2013). RNA-guided gene activation by CRISPR-Cas9-based transcription factors. *Nat Methods*, *10*(10), 973-976. https://doi.org/10.1038/nmeth.2600

Pergolizzi, R. G., Ropper, A. E., Dragos, R., Reid, A. C., Nakayama, K., Tan, Y., Ehteshami, J. R., Coleman, S. H., Silver, R. B., Hackett, N. R., Menez, A., & Crystal, R. G. (2003). In vivo trans-splicing of 5' and 3' segments of pre-mRNA directed by corresponding DNA sequences delivered by gene transfer. *Mol Ther*, *8*(6), 999-1008. https://doi.org/10.1016/j.ymthe.2003.08.022

Petrs-Silva, H., Dinculescu, A., Li, Q., Min, S. H., Chiodo, V., Pang, J. J., Zhong, L., Zolotukhin, S., Srivastava, A., Lewin, A. S., & Hauswirth, W. W. (2009). High-

efficiency transduction of the mouse retina by tyrosine-mutant AAV serotype vectors. *Mol Ther*, *17*(3), 463-471. https://doi.org/10.1038/mt.2008.269

Pourcel, C., Salvignol, G., & Vergnaud, G. (2005). CRISPR elements in Yersinia pestis acquire new repeats by preferential uptake of bacteriophage DNA, and provide additional tools for evolutionary studies. *Microbiology (Reading)*, *151*(Pt 3), 653-663. https://doi.org/10.1099/mic.0.27437-0

Priori, S. G., Napolitano, C., Tiso, N., Memmi, M., Vignati, G., Bloise, R., Sorrentino, V., & Danieli, G. A. (2001). Mutations in the cardiac ryanodine receptor gene (hRyR2) underlie catecholaminergic polymorphic ventricular tachycardia. *Circulation*, *103*(2), 196-200. https://doi.org/10.1161/01.cir.103.2.196

Qi, L. S., Larson, M. H., Gilbert, L. A., Doudna, J. A., Weissman, J. S., Arkin, A. P., & Lim, W. A. (2013). Repurposing CRISPR as an RNA-guided platform for sequence-specific control of gene expression. *Cell*, *152*(5), 1173-1183. https://doi.org/10.1016/j.cell.2013.02.022

Quinn, P. M., Buck, T. M., Ohonin, C., Mikkers, H. M. M., & Wijnholds, J. (2018). Production of iPS-Derived Human Retinal Organoids for Use in Transgene Expression Assays. *Methods Mol Biol*, *1715*, 261-273. https://doi.org/10.1007/978-1-4939-7522-8_19

RetNet. https://sph.uth.edu/RetNet/.

Riedmayr, L. M., Hinrichsmeyer, K. S., Karguth, N., Bohm, S., Splith, V., Michalakis, S., & Becirovic, E. (2022). dCas9-VPR-mediated transcriptional activation of functionally equivalent genes for gene therapy. *Nat Protoc*, *17*(3), 781-818. https://doi.org/10.1038/s41596-021-00666-3

Rose, J. C., Popp, N. A., Richardson, C. D., Stephany, J. J., Mathieu, J., Wei, C. T., Corn, J. E., Maly, D. J., & Fowler, D. M. (2020). Suppression of unwanted CRISPR-Cas9 editing by co-administration of catalytically inactivating truncated guide RNAs. *Nat Commun*, *11*(1), 2697. https://doi.org/10.1038/s41467-020-16542-9

Rosenblum, D., Gutkin, A., Kedmi, R., Ramishetti, S., Veiga, N., Jacobi, A. M., Schubert, M. S., Friedmann-Morvinski, D., Cohen, Z. R., Behlke, M. A., Lieberman, J., & Peer, D. (2020). CRISPR-Cas9 genome editing using targeted lipid nanoparticles for cancer therapy. *Sci Adv*, *6*(47). https://doi.org/10.1126/sciadv.abc9450

Rouet, P., Smih, F., & Jasin, M. (1994). Introduction of double-strand breaks into the genome of mouse cells by expression of a rare-cutting endonuclease. *Mol Cell Biol*, *14*(12), 8096-8106. https://doi.org/10.1128/mcb.14.12.8096-8106.1994

Rousseau, J., Gioia, R., Layrolle, P., Lieubeau, B., Heymann, D., Rossi, A., Marini, J. C., Trichet, V., & Forlino, A. (2014). Allele-specific Col1a1 silencing reduces mutant collagen in fibroblasts from Brtl mouse, a model for classical osteogenesis imperfecta. *Eur J Hum Genet*, *22*(5), 667-674. https://doi.org/10.1038/ejhg.2013.198

Sakami, S., Maeda, T., Bereta, G., Okano, K., Golczak, M., Sumaroka, A., Roman, A. J., Cideciyan, A. V., Jacobson, S. G., & Palczewski, K. (2011). Probing mechanisms of photoreceptor degeneration in a new mouse model of the common form of autosomal dominant retinitis pigmentosa due to P23H opsin mutations. *J Biol Chem*, *286*(12), 10551-10567. https://doi.org/10.1074/jbc.M110.209759

Sapranauskas, R., Gasiunas, G., Fremaux, C., Barrangou, R., Horvath, P., & Siksnys, V. (2011). The Streptococcus thermophilus CRISPR/Cas system provides immunity in Escherichia coli. *Nucleic Acids Res*, *39*(21), 9275-9282. https://doi.org/10.1093/nar/gkr606

Schaefer, K. A., Wu, W. H., Colgan, D. F., Tsang, S. H., Bassuk, A. G., & Mahajan, V. B. (2017). Unexpected mutations after CRISPR-Cas9 editing in vivo. *Nat Methods*, *14*(6), 547-548. https://doi.org/10.1038/nmeth.4293

Schmittgen, T. D., & Livak, K. J. (2008). Analyzing real-time PCR data by the comparative C(T) method. *Nat Protoc*, *3*(6), 1101-1108. https://doi.org/10.1038/nprot.2008.73

Schmitz, M. L., & Baeuerle, P. A. (1991). The p65 subunit is responsible for the strong transcription activating potential of NF-kappa B. *EMBO J*, *10*(12), 3805-3817. https://www.ncbi.nlm.nih.gov/pubmed/1935902

Shah, N. H., & Muir, T. W. (2014). Inteins: Nature's Gift to Protein Chemists. *Chem Sci*, *5*(1), 446-461. https://doi.org/10.1039/C3SC52951G

Shi, G., Yau, K. W., Chen, J., & Kefalov, V. J. (2007). Signaling properties of a short-wave cone visual pigment and its role in phototransduction. *J Neurosci*, *27*(38), 10084-10093. https://doi.org/10.1523/JNEUROSCI.2211-07.2007

Simhadri, V. L., McGill, J., McMahon, S., Wang, J., Jiang, H., & Sauna, Z. E. (2018). Prevalence of Pre-existing Antibodies to CRISPR-Associated Nuclease Cas9 in the USA Population. *Mol Ther Methods Clin Dev*, *10*, 105-112. https://doi.org/10.1016/j.omtm.2018.06.006

Sleiman, Y., Lacampagne, A., & Meli, A. C. (2021). "Ryanopathies" and RyR2 dysfunctions: can we further decipher them using in vitro human disease models? *Cell Death Dis*, *12*(11), 1041. https://doi.org/10.1038/s41419-021-04337-9

Smithies, O., Gregg, R. G., Boggs, S. S., Koralewski, M. A., & Kucherlapati, R. S. (1985). Insertion of DNA sequences into the human chromosomal beta-globin locus by homologous recombination. *Nature*, *317*(6034), 230-234. https://doi.org/10.1038/317230a0

Song, Y., Lou, H. H., Boyer, J. L., Limberis, M. P., Vandenberghe, L. H., Hackett, N. R., Leopold, P. L., Wilson, J. M., & Crystal, R. G. (2009). Functional cystic fibrosis transmembrane conductance regulator expression in cystic fibrosis airway epithelial cells by AAV6.2-mediated segmental trans-splicing. *Hum Gene Ther*, *20*(3), 267-281. https://doi.org/10.1089/hum.2008.173

Sternberg, S. H., Redding, S., Jinek, M., Greene, E. C., & Doudna, J. A. (2014). DNA interrogation by the CRISPR RNA-guided endonuclease Cas9. *Nature*, *507*(7490), 62-67. https://doi.org/10.1038/nature13011

Sun, J., Carlson-Stevermer, J., Das, U., Shen, M., Delenclos, M., Snead, A. M., Koo, S. Y., Wang, L., Qiao, D., Loi, J., Petersen, A. J., Stockton, M., Bhattacharyya, A., Jones, M. V., Zhao, X., McLean, P. J., Sproul, A. A., Saha, K., & Roy, S. (2019). CRISPR/Cas9 editing of APP C-terminus attenuates beta-cleavage and promotes alpha-cleavage. *Nat Commun*, *10*(1), 53. https://doi.org/10.1038/s41467-018-07971-8

Sun, L., Li, J., & Xiao, X. (2000). Overcoming adeno-associated virus vector size limitation through viral DNA heterodimerization. *Nat Med*, *6*(5), 599-602. https://doi.org/10.1038/75087

Swain, P. K., Hicks, D., Mears, A. J., Apel, I. J., Smith, J. E., John, S. K., Hendrickson, A., Milam, A. H., & Swaroop, A. (2001). Multiple phosphorylated isoforms of NRL are expressed in rod photoreceptors. *J Biol Chem*, *276*(39), 36824-36830. https://doi.org/10.1074/jbc.M105855200

Swaroop, A., Kim, D., & Forrest, D. (2010). Transcriptional regulation of photoreceptor development and homeostasis in the mammalian retina. *Nat Rev Neurosci*, *11*(8), 563-576. https://doi.org/10.1038/nrn2880

Tanenbaum, M. E., Gilbert, L. A., Qi, L. S., Weissman, J. S., & Vale, R. D. (2014). A protein-tagging system for signal amplification in gene expression and fluorescence imaging. *Cell*, *159*(3), 635-646. https://doi.org/10.1016/j.cell.2014.09.039

Tang, W., Hu, J. H., & Liu, D. R. (2017). Aptazyme-embedded guide RNAs enable ligand-responsive genome editing and transcriptional activation. *Nat Commun*, *8*, 15939. https://doi.org/10.1038/ncomms15939

Thomas, K. R., Folger, K. R., & Capecchi, M. R. (1986). High frequency targeting of genes to specific sites in the mammalian genome. *Cell*, *44*(3), 419-428. https://doi.org/10.1016/0092-8674(86)90463-0

Toms, M., Pagarkar, W., & Moosajee, M. (2020). Usher syndrome: clinical features, molecular genetics and advancing therapeutics. *Ther Adv Ophthalmol*, *12*, 2515841420952194. https://doi.org/10.1177/2515841420952194

Tornabene, P., & Trapani, I. (2020). Can Adeno-Associated Viral Vectors Deliver Effectively Large Genes? *Hum Gene Ther*, *31*(1-2), 47-56. https://doi.org/10.1089/hum.2019.220

Tornabene, P., Trapani, I., Minopoli, R., Centrulo, M., Lupo, M., de Simone, S., Tiberi, P., Dell'Aquila, F., Marrocco, E., Iodice, C., Iuliano, A., Gesualdo, C., Rossi, S., Giaquinto, L., Albert, S., Hoyng, C. B., Polishchuk, E., Cremers, F. P. M., Surace, E. M., . . . Auricchio, A. (2019). Intein-mediated protein trans-splicing expands adeno-associated virus transfer capacity in the retina. *Sci Transl Med*, *11*(492). https://doi.org/10.1126/scitranslmed.aav4523

Trapani, I., Colella, P., Sommella, A., Iodice, C., Cesi, G., de Simone, S., Marrocco, E., Rossi, S., Giunti, M., Palfi, A., Farrar, G. J., Polishchuk, R., & Auricchio, A. (2014). Effective delivery of large genes to the retina by dual AAV vectors. *EMBO Mol Med*, *6*(2), 194-211. https://doi.org/10.1002/emmm.201302948

Trapani, I., Toriello, E., de Simone, S., Colella, P., Iodice, C., Polishchuk, E. V., Sommella, A., Colecchi, L., Rossi, S., Simonelli, F., Giunti, M., Bacci, M. L., Polishchuk, R. S., & Auricchio, A. (2015). Improved dual AAV vectors with reduced expression of truncated proteins are safe and effective in the retina of a mouse model of Stargardt disease. *Hum Mol Genet*, *24*(23), 6811-6825. https://doi.org/10.1093/hmg/ddv386

Trapani, I., Tornabene, P., & Auricchio, A. (2021). Large gene delivery to the retina with AAV vectors: are we there yet? *Gene Ther*, *28*(5), 220-222. https://doi.org/10.1038/s41434-020-0174-4

Truong, D. J., Kuhner, K., Kuhn, R., Werfel, S., Engelhardt, S., Wurst, W., & Ortiz, O. (2015). Development of an intein-mediated split-Cas9 system for gene therapy. *Nucleic Acids Res*, *43*(13), 6450-6458. https://doi.org/10.1093/nar/gkv601

Tsai, Y. T., Wu, W. H., Lee, T. T., Wu, W. P., Xu, C. L., Park, K. S., Cui, X., Justus, S., Lin, C. S., Jauregui, R., Su, P. Y., & Tsang, S. H. (2018). Clustered Regularly Interspaced Short Palindromic Repeats-Based Genome Surgery for the Treatment of Autosomal Dominant Retinitis Pigmentosa. *Ophthalmology*, *125*(9), 1421-1430. https://doi.org/10.1016/j.ophtha.2018.04.001

Turner, D. L., & Cepko, C. L. (1987). A common progenitor for neurons and glia persists in rat retina late in development. *Nature*, *328*(6126), 131-136. https://doi.org/10.1038/328131a0

Urnov, F. D. (2018). Genome Editing B.C. (Before CRISPR): Lasting Lessons from the "Old Testament". *CRISPR J*, *1*(1), 34-46. https://doi.org/10.1089/crispr.2018.29007.fyu

van der Bent, M. L., Paulino da Silva Filho, O., van Luijk, J., Brock, R., & Wansink, D. G. (2018). Assisted delivery of antisense therapeutics in animal models of heritable neurodegenerative and neuromuscular disorders: a systematic review and meta-analysis. *Sci Rep*, *8*(1), 4181. https://doi.org/10.1038/s41598-018-22316-7

Verbakel, S. K., van Huet, R. A. C., Boon, C. J. F., den Hollander, A. I., Collin, R. W. J., Klaver, C. C. W., Hoyng, C. B., Roepman, R., & Klevering, B. J. (2018). Non-syndromic retinitis pigmentosa. *Prog Retin Eye Res*, *66*, 157-186. https://doi.org/10.1016/j.preteyeres.2018.03.005

Villiger, L., Grisch-Chan, H. M., Lindsay, H., Ringnalda, F., Pogliano, C. B., Allegri, G., Fingerhut, R., Haberle, J., Matos, J., Robinson, M. D., Thony, B., & Schwank, G. (2018). Treatment of a metabolic liver disease by in vivo genome base editing in

adult mice. *Nat Med*, *24*(10), 1519-1525. https://doi.org/10.1038/s41591-018-0209-1

Vojta, A., Dobrinic, P., Tadic, V., Bockor, L., Korac, P., Julg, B., Klasic, M., & Zoldos, V. (2016). Repurposing the CRISPR-Cas9 system for targeted DNA methylation. *Nucleic Acids Res*, *44*(12), 5615-5628. https://doi.org/10.1093/nar/gkw159

Wagner, D. L., Amini, L., Wendering, D. J., Burkhardt, L. M., Akyuz, L., Reinke, P., Volk, H. D., & Schmueck-Henneresse, M. (2019). High prevalence of Streptococcus pyogenes Cas9-reactive T cells within the adult human population. *Nat Med*, *25*(2), 242-248. https://doi.org/10.1038/s41591-018-0204-6

Wagner, J. E., Zobel, L., Gerhardt, M. J., O'Riordan, C. R., Frederick, A., Petersen-Jones, S. M., Biel, M., & Michalakis, S. (2021). In Vivo Potency Testing of Subretinal rAAV5.hCNGB1 Gene Therapy in the Cngb1 Knockout Mouse Model of Retinitis Pigmentosa. *Hum Gene Ther*, *32*(19-20), 1158-1170. https://doi.org/10.1089/hum.2021.121

Wang, D., Tai, P. W. L., & Gao, G. (2019). Adeno-associated virus vector as a platform for gene therapy delivery. *Nat Rev Drug Discov*, *18*(5), 358-378. https://doi.org/10.1038/s41573-019-0012-9

Wang, D., Zhang, F., & Gao, G. (2020). CRISPR-Based Therapeutic Genome Editing: Strategies and In Vivo Delivery by AAV Vectors. *Cell*, *181*(1), 136-150. https://doi.org/10.1016/j.cell.2020.03.023

Wang, G., Chow, R. D., Bai, Z., Zhu, L., Errami, Y., Dai, X., Dong, M. B., Ye, L., Zhang, X., Renauer, P. A., Park, J. J., Shen, L., Ye, H., Fuchs, C. S., & Chen, S. (2019). Multiplexed activation of endogenous genes by CRISPRa elicits potent antitumor immunity. *Nat Immunol*, *20*(11), 1494-1505. https://doi.org/10.1038/s41590-019-0500-4

Whatley, M., Francis, A., Ng, Z. Y., Khoh, X. E., Atlas, M. D., Dilley, R. J., & Wong, E. Y. M. (2020). Usher Syndrome: Genetics and Molecular Links of Hearing Loss and Directions for Therapy. *Front Genet*, *11*, 565216. https://doi.org/10.3389/fgene.2020.565216

Willett, K., & Bennett, J. (2013). Immunology of AAV-Mediated Gene Transfer in the Eye. *Front Immunol*, *4*, 261. https://doi.org/10.3389/fimmu.2013.00261

Witherspoon, J. W., & Meilleur, K. G. (2016). Review of RyR1 pathway and associated pathomechanisms. *Acta Neuropathol Commun*, *4*(1), 121. https://doi.org/10.1186/s40478-016-0392-6

Wright, W. D., Shah, S. S., & Heyer, W. D. (2018). Homologous recombination and the repair of DNA double-strand breaks. *J Biol Chem*, *293*(27), 10524-10535. https://doi.org/10.1074/jbc.TM118.000372

Wu, H., Hu, Z., & Liu, X. Q. (1998). Protein trans-splicing by a split intein encoded in a split DnaE gene of Synechocystis sp. PCC6803. *Proc Natl Acad Sci U S A*, *95*(16), 9226-9231. https://doi.org/10.1073/pnas.95.16.9226

Wu, Y., Zeng, J., Roscoe, B. P., Liu, P., Yao, Q., Lazzarotto, C. R., Clement, K., Cole, M. A., Luk, K., Baricordi, C., Shen, A. H., Ren, C., Esrick, E. B., Manis, J. P., Dorfman, D. M., Williams, D. A., Biffi, A., Brugnara, C., Biasco, L., . . . Bauer, D. E. (2019). Highly efficient therapeutic gene editing of human hematopoietic stem cells. *Nat Med*, *25*(5), 776-783. https://doi.org/10.1038/s41591-019-0401-y

Wu, Z., Yang, H., & Colosi, P. (2010). Effect of genome size on AAV vector packaging. *Mol Ther*, *18*(1), 80-86. https://doi.org/10.1038/mt.2009.255

Xu, J. (2005). Preparation, culture, and immortalization of mouse embryonic fibroblasts. *Curr Protoc Mol Biol*, *Chapter 28*, Unit 28 21. https://doi.org/10.1002/0471142727.mb2801s70

Xu, X., Tao, Y., Gao, X., Zhang, L., Li, X., Zou, W., Ruan, K., Wang, F., Xu, G. L., & Hu, R. (2016). A CRISPR-based approach for targeted DNA demethylation. *Cell Discov*, *2*, 16009. https://doi.org/10.1038/celldisc.2016.9

Yamagata, T., Raveau, M., Kobayashi, K., Miyamoto, H., Tatsukawa, T., Ogiwara, I., Itohara, S., Hensch, T. K., & Yamakawa, K. (2020). CRISPR/dCas9-based Scn1a gene activation in inhibitory neurons ameliorates epileptic and behavioral phenotypes of Dravet syndrome model mice. *Neurobiol Dis*, *141*, 104954. https://doi.org/10.1016/j.nbd.2020.104954

Yan, Z., Zhang, Y., Duan, D., & Engelhardt, J. F. (2000). Trans-splicing vectors expand the utility of adeno-associated virus for gene therapy. *Proc Natl Acad Sci U S A*, *97*(12), 6716-6721. https://doi.org/10.1073/pnas.97.12.6716

Yang, Y., Mohand-Said, S., Danan, A., Simonutti, M., Fontaine, V., Clerin, E., Picaud, S., Leveillard, T., & Sahel, J. A. (2009). Functional cone rescue by RdCVF protein in a dominant model of retinitis pigmentosa. *Mol Ther*, *17*(5), 787-795. https://doi.org/10.1038/mt.2009.28

Yau, K. W., & Hardie, R. C. (2009). Phototransduction motifs and variations. *Cell*, *139*(2), 246-264. https://doi.org/10.1016/j.cell.2009.09.029

Ye, J., Coulouris, G., Zaretskaya, I., Cutcutache, I., Rozen, S., & Madden, T. L. (2012). Primer-BLAST: a tool to design target-specific primers for polymerase chain reaction. *BMC Bioinformatics*, *13*, 134. https://doi.org/10.1186/1471-2105-13-134

Yin, H., Xue, W., Chen, S., Bogorad, R. L., Benedetti, E., Grompe, M., Koteliansky, V., Sharp, P. A., Jacks, T., & Anderson, D. G. (2014). Genome editing with Cas9 in adult mice corrects a disease mutation and phenotype. *Nat Biotechnol*, *32*(6), 551-553. https://doi.org/10.1038/nbt.2884

Yu, I. M., Planelles-Herrero, V. J., Sourigues, Y., Moussaoui, D., Sirkia, H., Kikuti, C., Stroebel, D., Titus, M. A., & Houdusse, A. (2017). Myosin 7 and its adaptors link cadherins to actin. *Nat Commun*, *8*, 15864. https://doi.org/10.1038/ncomms15864

Yu, W., Mookherjee, S., Chaitankar, V., Hiriyanna, S., Kim, J. W., Brooks, M., Ataeijannati, Y., Sun, X., Dong, L., Li, T., Swaroop, A., & Wu, Z. (2017). Nrl knockdown by AAV-delivered CRISPR/Cas9 prevents retinal degeneration in mice. *Nat Commun*, *8*, 14716. https://doi.org/10.1038/ncomms14716

Zhang, X., Wang, W., & Jin, Z. B. (2021). Retinal organoids as models for development and diseases. *Cell Regen*, *10*(1), 33. https://doi.org/10.1186/s13619-021-00097-1

Zhang, Y. W., Thompson, R., Zhang, H., & Xu, H. (2011). APP processing in Alzheimer's disease. *Mol Brain*, *4*, 3. https://doi.org/10.1186/1756-6606-4-3

Zincarelli, C., Soltys, S., Rengo, G., & Rabinowitz, J. E. (2008). Analysis of AAV serotypes 1-9 mediated gene expression and tropism in mice after systemic injection. *Mol Ther*, *16*(6), 1073-1080. https://doi.org/10.1038/mt.2008.76

7 Appendix

Supplementary Table 1: Differentially expressed genes

Gene	ID	log2FoldChange	pvalue	padj
Rad54b	ENSMUSG00000078773	2.36	1.72E-16	3.79E-13
Manba	ENSMUSG00000028164	1.77	8.14E-38	1.08E-33
Slc6a2	ENSMUSG00000055368	1.65	1.88E-29	1.24E-25
Gm19410	ENSMUSG00000109372	1.59	4.31E-10	5.18E-07
Frrs1	ENSMUSG00000033386	1.46	5.76E-13	1.09E-09
Podn	ENSMUSG00000028600	1.39	6.49E-12	1.07E-08
Opn1mw	**ENSMUSG00000031394**	**1.29**	**1.87E-25**	**8.22E-22**
Ifi47	ENSMUSG00000078920	1.20	1.09E-06	5.61E-04
Gm16062	ENSMUSG00000087249	1.18	6.95E-07	4.48E-04
Iigp1	ENSMUSG00000054072	1.13	1.91E-06	7.88E-04
BC065403	ENSMUSG00000097211	1.13	1.40E-04	1.01E-02
Cutal	ENSMUSG00000026870	1.09	6.47E-06	1.68E-03
1500026H17Rik	ENSMUSG00000097383	1.09	9.25E-05	7.69E-03
Fam204a	ENSMUSG00000057858	1.09	6.62E-17	1.75E-13
Shisa2	ENSMUSG00000044461	1.07	4.18E-18	1.38E-14
Gucy1a2	ENSMUSG00000041624	-1.07	1.00E-03	2.95E-02
Malat1	ENSMUSG00000092341	-1.10	1.77E-03	3.98E-02
Klf12	ENSMUSG00000072294	-1.17	2.02E-06	7.97E-04
Kcnh5	ENSMUSG00000034402	-1.18	3.85E-04	1.72E-02
Dok6	ENSMUSG00000073514	-1.28	5.92E-05	5.79E-03
Gm11808	ENSMUSG00000068240	-1.28	7.70E-04	2.51E-02
Gm340	ENSMUSG00000090673	-1.55	6.85E-06	1.68E-03
Rho	**ENSMUSG00000030324**	**-1.69**	**6.85E-06**	**1.68E-03**
Cdr1	ENSMUSG00000090546	-2.22	4.37E-04	1.84E-02
Gm22009	ENSMUSG00000089417	-2.29	1.11E-04	8.76E-03
Gm26917	ENSMUSG00000097971	-2.81	3.22E-04	1.58E-02
Scarna2	ENSMUSG00000088185	-3.37	6.60E-05	6.23E-03
Hist1h4d	ENSMUSG00000061482	-3.59	5.06E-04	2.00E-02
Rmrp	ENSMUSG00000088088	-3.68	1.87E-03	4.05E-02
Gm23935	ENSMUSG00000076258	-3.71	3.06E-04	1.51E-02
Lars2	ENSMUSG00000035202	-3.72	2.85E-04	1.45E-02
Rn7sk	ENSMUSG00000065037	-3.94	4.07E-04	1.76E-02
Gm24187	ENSMUSG00000088609	-3.96	1.35E-04	1.00E-02
Gm42418	ENSMUSG00000098178	-4.42	3.62E-09	3.42E-06
Gm24270	ENSMUSG00000076281	-4.55	4.02E-05	4.62E-03
Mir6236	ENSMUSG00000098973	-5.32	1.12E-05	2.13E-03
Gm15564	ENSMUSG00000086324	-5.37	6.06E-06	1.61E-03

List of Publications

Riedmayr, L. M., **Hinrichsmeyer, K. S.**, Thalhammer, S. B., Karguth, N., Böhm, S., Mittas, D., Weber, V. J., Otify, D., Splith, V., Brümmer, M., Boon, N., Wijnholds, J., Mehlfeld, V., Michalakis, S., Fenske, S., Biel, M. & Becirovic, E. (2022). mRNA trans-splicing dual AAV vectors for genome editing and gene therapy. Manuscript submitted.

Riedmayr, L. M.*, **Hinrichsmeyer, K. S.***, Karguth, N., Böhm, S., Splith, V., Michalakis, S., & Becirovic, E. (2022). dCas9-VPR-mediated transcriptional activation of functionally equivalent genes for gene therapy. *Nature protocols*, *17*(3), 781–818. https://doi.org/10.1038/s41596-021-00666-3. *: equal contribution

Böhm, S., Splith, V., Riedmayr, L. M., Rötzer, R. D., Gasparoni, G., Nordström, K., Wagner, J. E., **Hinrichsmeyer, K. S.**, Walter, J., Wahl-Schott, C., Fenske, S., Biel, M., Michalakis, S., & Becirovic, E. (2020). A gene therapy for inherited blindness using dCas9-VPR-mediated transcriptional activation. *Science advances, 6*(34), eaba5614. https://doi.org/10.1126/sciadv.aba5614.

Acknowledgements

First, I would like to thank Prof. Dr. Martin Biel for the opportunity to conduct my thesis in his laboratory and his scientific input as a member of my thesis advisory committee.

The biggest thank you goes to my supervisor PD Dr. Elvir Becirovic, who brought me on board, for his amazing scientific ideas and excellent supervision. Thank you for the great support and the freedom you gave me during my doctorate.

I would also like to thank all other members of my thesis advisory committee, Prof. Dr. Stylianos Michalakis and Dr. Irina Solovei for their scientific advice and guidance during this time, and Prof. Dr. Christof Osman for representing my dissertation before the Faculty of Biology.

Thank you to all the collaborators of this work, Dr. Verena Mehlfeld, Nanda Boon, Manuela Brümmer, and Stefan Thalhammer, for their help and the successful collaborations.

I am beyond grateful for the former members of my group who welcomed me with open arms, introduced me to new methods, and were always there for advice. Thank you very much, Vicky, Lisa, Sybille! I would also like to thank all the current members of the Becirovic group, Nina, Johannes, David, and Dina, for the incredible team spirit. As well as Berit Noack for her great technical support.

Thank you to the entire LMU Department of Pharmacology for Natural Sciences, especially René, for making the daily lab work more entertaining, the mutual support, and cheerful evenings.

Furthermore, I want to thank Elena for being an excellent editor, a great friend, and an amazing driver, as well as my family and friends for just being there and supporting my thirst for knowledge.